

Activation of CXCR7 improves hyperlipidemia by increasing cholesterol storage in adipose tissue and limits atherosclerosis

Von der Fakultät für Mathematik, Informatik und Naturwissenschaften der
RWTH Aachen University zur Erlangung des akademischen Grades eines
Doktors der Naturwissenschaften genehmigte Dissertation

vorgelegt von

Xiaofeng Li M. Sc.

aus

Henan, China

Berichter:

Universitätsprofessor Dr. med. Andreas Schober

Universitätsprofessor Dr. rer. nat. Jürgen Bernhagen

Tag der mündlichen Prüfung: 07.10.2013

Diese Dissertation ist auf den Internetseiten der Hochschulbibliothek online
verfügbar.

The results of this work have been submitted for publication:

Li X, Penfold ME, Koenen RR, Thiemann A, Heyll K, Akhtar S, Koyadan S, Wu Z, van Zandvoort M, Weber C, Schober A "Activation of Cxcr7 limits atherosclerosis and improves hyperlipidemia by increasing cholesterol storage in adipose tissue". *Circulation*, 2013 (under revision).

TABLE OF CONTENTS

ABBREVIATIONS	III
1. INTRODUCTION	1
1.1 Atherosclerosis.....	1
1.2 Restenosis	2
1.3 The leukocyte adhesion cascade	3
1.4 Monocytes and macrophages in atherosclerosis and neointima formation	4
1.5 Chemokines and chemokine receptors.....	6
1.5.1 Chemokines.....	6
1.5.2 Chemokine receptors.....	7
1.5.3 CXCL12 and CXCR4	7
1.5.4 CXCR7	11
1.6 Aims of the study	12
2. MATERIALS AND METHODS	14
2.1 Materials	14
2.1.1 Equipment	14
2.1.2 Assay kits.....	15
2.1.3 Buffers and solutions	16
2.1.4 Consumables.....	18
2.1.5 Chemicals, reagents, and cell culture medium	18
2.2 Methods.....	19
2.2.1 Animal experiments	19
2.2.2 Molecular biology techniques	23
2.2.3 Histological staining protocols	27
2.2.4 Immunofluorescence staining protocols	30
2.2.5 Flow cytometry.....	33
2.2.6 Cxcl12 ELISA.....	35
2.2.7 Two-photon laser scanning microscopy	35
2.2.8 Quantification of cholesterol and DiI concentration in murine tissues.....	37
2.2.9 SVEC culture protocol.....	37
2.2.10 Statistical analysis	37
3. RESULTS	38
3.1 Cxcr7 expression patterns	38
3.2 Role of Cxcr7 on neointima formation	44
3.2.1 Conditional Cxcr7 deletion exacerbated neointimal hyperplasia.....	44
3.2.2 Role of Cxcr7 in bone marrow cells on neointima formation	50

ABBREVATIONS

3.3 Pharmacological targeting of Cxcr7 in neointima formation	53
3.3.1 Effect of CCX771 treatment on neointima formation	53
3.3.2 Role of splenic Cxcr7 expression in the effects of CCX771 treatment on neointima formation	59
3.4 CCX771 treatment reduced diet-induced atherosclerosis.....	61
3.5 Effect of CCX771 treatment cholesterol metabolism.....	63
3.6 Endothelial-specific deletion of Cxcr7 and hyperlipidemia	67
4. DISCUSSION.....	68
4.1 Role of Cxcr7 in vascular repair	68
4.1.2 Cxcr7 and hyperlipidemia-induced monocytosis	69
4.1.3 Cxcr7 indirectly modulates the macrophages accumulation in neointima.....	71
4.1.4 Effects of Cxcr7 on SPC mobilization and Cxcl12 levels.....	73
4.2 Effects of CCX771 treatment on the development of atherosclerosis	74
4.3 Effects of CCX771 treatment on the uptake of VLDL into adipose tissue	75
5. SUMMARY.....	81
6. REFERENCES.....	83
7. ACKNOWLEDGEMENT.....	100
8. CURRICULUM VITAE.....	103

ABBREVIATIONS

Ab	antibody
ABCA1	ATP-binding cassette protein A1
ACAT	Acyl-Coenzyme A acyltransferase
Ag	antigen
Apoe	Apolipoprotein E
Arg	arginase
ATP	adenosine triphosphate
A _{II}	angiotensin- II
BMMC	bone marrow-derived mononuclear cell
BMT	bone marrow transplantation
BSA	bovine serum albumin
CVD	Cardiovascular disease
cAMP	cyclic adenosine monophosphate
CCA	common carotid artery
CD	cluster of differentiation
cDNA	complementary DNA
CDP	common dendritic cell precursor
CETP	cholesterol ester transfer protein
CHD	coronary heart disease
CM	chylomicron
CNS	central nervous system
CVD	cardiovascular disease
d	day
DAG	diacylglycerol
DiI	1,1'-dioctadecyl-3,3',3'-tetramethylindocarbocyanine perchlorate
DNA	deoxyribonucleic acid
DAPI	4',6-diamidino-2-phenylindol
DC	dendritic cell
DMSO	dimethylsulfoxide
DRP	Asp-Arg-Tyr
e.g.	for example
EC	endothelial cell
ECA	external carotid artery
ECL	extracellular loop
EDHF	endothelium-derived hyperpolarizing factor
EDTA	ethylenediaminetetraacetic acid
EEL	external elastic lamina
ELISA	enzyme-linked immunosorbent assay
ELR	Glu-Leu-Arg
EPC	endothelial progenitor cell
ER	estrogen receptor
ESAM	endothelial cell-selective adhesion molecule
ESS	endothelial shear stress
ET-1	endothelin-1
EVG	Elastica van Giesson
FACS	fluorescent activated cell sorting

ABBREVATIONS

FC	free cholesterol
FCH	familial combined hyperlipidemia
FCS	fetal calf serum
FDG	fluorescein di- β -Dgalactopyranoside
FITC	fluorescein isothiocyanate
FPLC	fast protein liquid chromatography
GAPDH	glyceraldehyde 3-phosphate dehydrogenase
GEF	guanine nucleotide exchange factor
GPCR	G-protein coupled receptor
Gr-1	granulocyte antigen 1
GRK	G-protein coupled receptor kinase
GTP	guanosine triphosphate
GWAS	genome-wide association study
h	hour
HBSS	hanks' balanced solution
HCD	high cholesterol diet
HDL	high-density lipoprotein
HIC1	hypermethylated in cancer 1
HL	hepatic lipase
HMG-CoA	3-hydroxy-3-methylglutaryl coenzyme A
HSC	hematopoietic stem cell
HUVEC	human umbilical vein endothelial cells
ICA	internal carotid artery
ICAM1	intracellular adhesion molecular 1
ICL	intracellular loop
IDL	intermediate-density lipoprotein
IEL	internal elastic lamina
IP	intraperitoneal injection
IP3	inositol 1,4,5-trisphosphate
I-TAC	Interferon-inducible T-cell alpha chemoattractant
IV	intravenous
JAM	junctional adhesion molecule
LCAT	lecithin-cholesterol acyltransferase
LC-MS	liquid chromatography–mass spectrometry
LDL	low-density lipoprotein
LDLr	LDL receptor
LFA1	lymphocyte function-associated antigen 1
LN	lymph node
LP	common lymphoid progenitor cells
LPA	lysophosphatidic acid
LPL	lipoprotein lipase
LPS	lipopolysaccharide
Ly-6C	lymphocyte antigen 6C
mAb	monoclonal Ab
MAC1	macrophage antigen 1
MAC2	Galectin-3
MADCAM1	mucosal vascular addressin cell-adhesion molecule 1
MAPK	mitogen-activated protein kinase
MCP-1	monocyte chemoattractant protein-1
MCSF	macrophage colony-stimulating factor

MDP	macrophages and dendritic cell precursor
MDSC	myeloid-derived suppressor cell
MI	myocardial infarction
MIF	macrophage inhibitory factor
min	minute
MP	common myeloid progenitor cell
MSC	mesenchymal stem cell
NF- κ B	nuclear factor kappa-light-chain enhancer of activated B cell
NO	nitric oxide
oxLDL	oxidized LDL
PBPC	peripheral blood progenitor cell
PBS	phosphate buffered saline
PCR	polymerase chain reaction
PDGF-BB	platelet derived growth factor-BB
PECAM1	platelet/endothelial-cell adhesion molecule 1
PETG	phenylethyl β -D-thiogalactopyranoside
PFA	paraformaldehyde/platelet activating factor
PGC	primordial germ cell
PGI ₂	prostacyclin
PI3K	phosphoinositide 3-kinase
PIP ₂	phosphatidylinositol 4,5-biphosphate
PKA	protein kinase A
PKC	protein kinase C
PLC	phospholipase L
PLC β	β -isoforms of phospholipase C
PMT	two-photo multiplier tubes
PPAR- γ	peroxisome proliferator-activated receptor-gamma
PSGL1	P-selectin glycoprotein ligand 1
qRT-PCR	quantitative Real-time PCR
RNA	ribonucleotid acid
RT	room temperature
s	second
s.c	subcutaneous injection
Sca-1	stem cell antigen-1
SEM	standard error of mean
SDF-1	stromal cell-derived factor-1
SDS	sodium-dodecylsulfate
SHG	second harmonic generation
SMC	smooth muscle cells
SPC	smooth muscle progenitor cell
SR-BI	scavenger receptor BI
STEMI	ST-elevation myocardial infarction
SVEC	small vessel endothelial cells
TG	triglyceride
Tip-DC	TNF- α /iNOS-producing DC
TLR4	Toll-like receptor
Tm	temperature
TMB	3,3',5,5'-Tetramethylbenzidine
TMX	tamoxifen
TNF- α	tumor necrosis factor- α

ABBREVIATIONS

TPLSM	two-photon laser scanning microscopy
VAT	visceral adipose tissue
VCAM1	vascular cell adhesion molecule 1
VE-Cad	vascular endothelial cadherin
VLA-4	very late antigen 4
VLDL	very-low-density lipoprotein
VLDLr	very-low-density lipoprotein receptor
vWF	van Willebrand factor
wk	week
X-gal	5-bromo-4-chloro-indolyl- β -D-galactopyranoside
β -gal	β -galactosidase

1. INTRODUCTION

1.1 Atherosclerosis

Cardiovascular diseases (CVDs) arising from atherosclerosis are a major clinical problem worldwide (1). More and more persons all over the world suffer from diverse forms of CVDs, including heart attacks, strokes and angina. For instance, approximately 33% of deaths in 2008 in the United States were due to vascular diseases (2).

Atherosclerosis is a chronic inflammatory disorder of arterial blood vessels characterized by hardening of the vessel wall and narrowing of the arterial lumen, resulting from interactions between diverse cytokines, lipoproteins, blood cells, and cellular elements of the arterial wall (3, 4). The multifactorial and multiple-step process of atherosclerosis could be categorized into four phases: the initiation phase, the stable phase, the vulnerable phase, and the rupture phase (3) (Fig. 1).

In the initiation phase (Fig. 1A), several physiological and behavioral risk factors cause dysfunction of ECs, adhesion of leukocytes and platelets, and increased permeability of the vessels (5). In response to a local chemoattractant gradient, adherent monocytes migrate into the subendothelial space, where they differentiate into macrophages. Cholesterol progressively accumulates in macrophages via the uptake of oxLDL by scavenger receptors (*e.g.*, SR-A and CD36) (6). Accumulation of cholesterol-laden macrophages (known as foam cells) leads to formation of the characteristic fatty streak, which is one of the features of the stable phase (3, 4) (Fig. 1B). Over time, these fatty streaks progress into complicated lesions containing a massive accumulation of lipid and necrotic debris. Meanwhile, smooth muscle cells (SMCs) also migrate into the plaque, proliferate, synthesize extracellular matrix proteins, and form a fibrous cap that covers the lipid core of the plaques. Additionally, activated T cells in the lesion express Th1 and Th2 cytokines, initiating a broad range of immune responses. Inflammation and oxLDL cause programmed cell death of lesional cells during the development of plaques, which results in the formation of a necrotic core. In addition, neovascularization and hemorrhage occur in atherosclerotic lesions, which are hallmarks of the vulnerable phase (3, 4) (Fig. 1C). Finally, a combination of factors, such as matrix metalloproteinase secretion, extensive fibrin deposition, increasing neovascularization, and hemorrhage may result in plaque

erosion and rupture, eventually inducing thrombus formation and coagulation via the release of pro-thrombogenic plaque material (3, 4, 7) (Fig. 1D).

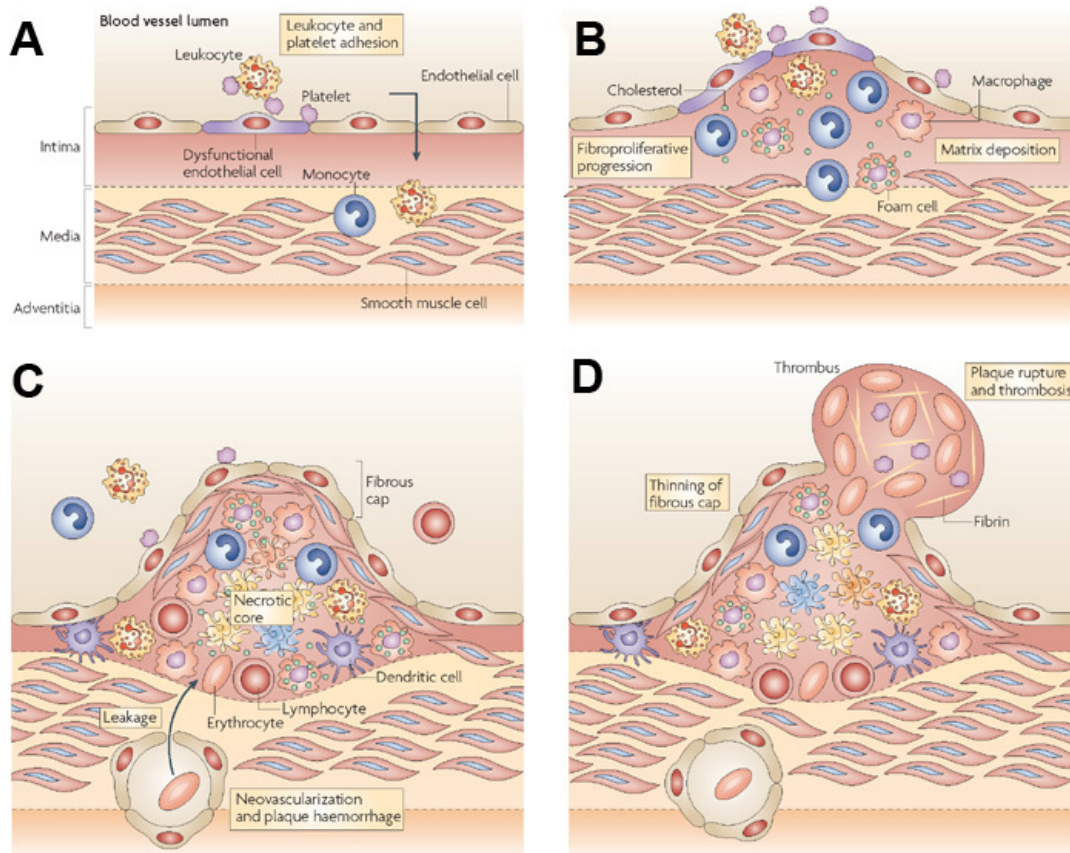


Figure 1. The development of atherosclerosis (A) Pro-inflammatory stimulation by hyperlipidemia causes endothelial-cell dysfunction and activation, the adhesion of platelet and leukocytes, and increased permeability of endothelium. (B) Recruited monocytes accumulate lipids and differentiate into macrophages (foam cells), which constitute fatty streaks. Enhanced mononuclear-cell influx, deposition of matrix components, and the accumulation of SMCs are characteristic for the fibroproliferative progression of atherosclerotic lesions. (C) SMCs migrate into the plaques, proliferate and form a fibrous cap. Apoptosis of mainly plaque macrophages gives rise to a necrotic core. Neovascularization and hemorrhage can occur within the plaque. (D) Through matrix degradation by proteases and thinning of the fibrous cap, unstable plaques ultimately rupture, and elicit the coagulation cascade and thrombosis [adapted from Weber C *et al.* (3)].

1.2 Restenosis

There are several pharmacological and surgical therapies for symptomatic atherosclerotic diseases. Pharmacological management of atherosclerosis consists in statin and antiplatelet drug therapy (8). Interventional therapies include surgical bypass grafting and the implantation of drug-eluting stents by balloon angioplasty (9, 10). Restenosis (recurrent stenosis) is a major limitation of these interventional

therapies, despite significant technical innovations (11). Restenosis is the renarrowing of the target vessel segment following revascularization by excessive neointima formation and medial hypertrophy. It is initiated by an inflammatory response to mechanical injury and eventually evolves into the hypertrophic wound healing, which is predominantly associated with massive macrophage accumulation and SMCs proliferation in the neointima (11, 12).

1.3 The leukocyte adhesion cascade

The leukocyte adhesion cascade is a crucial biological mechanism involved in various physiological and pathological processes (Fig. 2), like the recruitment of leukocytes to sites of inflammation (13). This cascade includes 5 main steps: 1) *Rolling*. Leukocyte rolling along the vessel wall under flow conditions depends on the interaction of selectins with their ligands (13). Selectins, like endothelial P-selectin and E-selectin, bind to P-selectin glycoprotein ligand 1 (PSGL1) or other glycosylated ligands expressed on leukocytes, which enables short term interactions of leukocytes with the endothelium and triggers intracellular signals (14-17). 2) *Arrest*. In response to inflammation, ECs, platelets, and activated mast cells secrete chemokines and chemoattractants, which promote firm arrest of rolling leukocytes by activating integrins (13). Integrins are heterodimeric adhesion receptors consisting of a membrane-spanning α and β subunit that play an essential role in cell-cell, cell-matrix, and matrix (extracellular)-cytoskeleton (intracellular) interactions (18, 19). Chemokines induce firm arrest of rolling leukocytes by activating mainly β 1- (*e.g.*, VLA-4) and β 2-integrins (*e.g.*, LFA-1 and MAC-1) through GPCR-mediated inside-out signaling (13, 20), which increases the avidity of integrins towards their ligands, such as ICAM-1 and VCAM-1 (13). 3) *Adhesion strengthening and spreading*. Integrin binding induces concurrently outside-in signaling, which is required to further enhance adhesion (13). 4) *Intravascular crawling*. ICAM-1 and MAC-1 play a crucial role in leukocyte crawling (21, 22) by which leukocytes find the preferred place for transendothelial migration. 5) *Transmigration*. Transendothelial migration (diapedesis) can occur either via a paracellular or transcellular route and is mainly mediated by junctional molecules, like PECAM-1 and JAM-A (23-25). This leukocyte adhesion cascade has been suggested to provide a basis for novel and combinatorial therapies of atherosclerotic diseases (13).

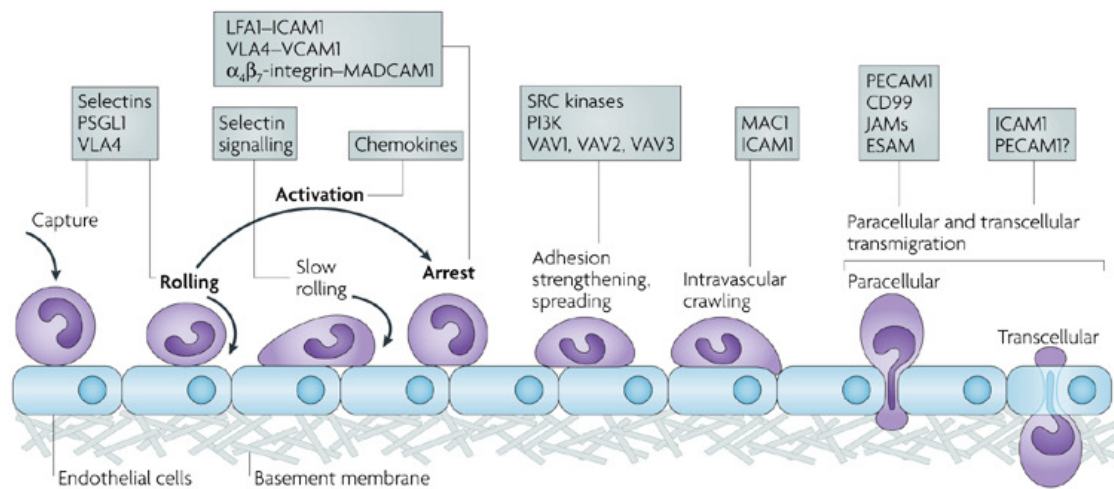


Figure 2. The leukocyte adhesion cascade. The original leukocyte adhesion cascade includes three steps (shown in bold): selectin-mediated rolling, chemokine-mediated activation, and integrin-mediated arrest. This cascade was modified by the discovery of additional steps: capture (or tethering), slow rolling, adhesion strengthening and spreading, intravascular crawling, and paracellular/transcellular transmigration. The chief molecules participating in each step are shown in boxes [adapted from Ley *et al.* (13)] .

1.4 Monocytes and macrophages in atherosclerosis and neointima formation

Monocytes are a leukocyte subtype that plays a central role in the innate immune response, which is essentially involved in multiple steps during atherogenesis (26, 27). In humans, 10% of blood leukocytes are monocytes. In contrast, only 4% of the leukocytes are monocytes in mice (28). Hematopoietic stem cells (HSCs) firstly differentiate into common myeloid progenitor cells (MP) and common lymphoid progenitor cells (LP) (26). MPs can develop into monocytes, macrophages, and dendritic cell precursors (MDPs), which mainly give rise to monocytes and common dendritic cell precursors (CDPs) (26).

Monocyte heterogeneity is well established and human blood monocytes can be categorized into three distinct populations based on the surface receptor expression: $CD14^+CD16^-$, $CD14^-CD16^+$ and $CD14^{dim}CD16^-$ monocytes (29-31). In mice, two subpopulations of blood monocyte, the $CD115^+Ly6C^+$ and the $CD115^+Ly6C^-$ monocytes, were functionally characterized by adoptive transfer and intravital studies (32, 33).

$Ly6C^+$ monocytes play a role in proteolysis, phagocytosis, and inflammation, and can differentiate into classically activated inflammatory macrophages (M1-type),

Tip-DCs (TNF- α /iNOS-producing DCs), and myeloid-derived suppressor cells (MDSCs) (26, 27, 34, 35). Under homeostatic conditions, Ly6C⁻ monocytes patrol along blood vessels to monitor the endothelium and surrounding tissues (32). In response to inflammation, Ly6C⁻ monocytes can differentiate into alternatively activated macrophages (M2-type) and alveolar macrophages, participating in chemokine expression, phagocytosis, wound repair, and tissue remodeling (26, 27, 35).

Monocytes play a key role in the pathogenesis of restenosis and atherosclerosis. Circulating monocytes infiltrate injured or inflamed vessels and subsequently differentiate into macrophages, which is the most abundant cell type in atherosclerotic plaques and neointimal lesions (27). Accordingly, transient depletion of peripheral monocytes by liposomal alendronate inhibits neointima formation after vascular injury (36). Moreover, atherosclerotic plaques in patients with unstable angina or non-Q-wave myocardial infarction contain more macrophages compared to patients with stable angina (37). Furthermore, hypercholesterolemia increases the Ly6C⁺ monocyte population in the circulation during atherosclerosis (38). Ly6C⁺ monocytes preferentially infiltrate into atherosclerotic lesions (39, 40) and also play a decisive role in the progression of transplant atherosclerosis particularly under hyperlipidemic conditions (41). Within atherosclerotic lesions, Ly6C⁻ monocytes tend to develop into CD11c⁺ cells, which contribute to atherosclerosis (40, 42). Following myocardial infarction, Ly-6C⁻ monocytes attenuate inflammation and promote collagen deposition, angiogenesis, and the accumulation of myofibroblasts (35). Altogether, two monocyte subsets with different and complementary functions may participate in the progression of restenosis and atherosclerosis.

Lesional macrophages take up lipid via scavenger receptors and become foam cells, which expand the neointima and atherosclerotic plaques (43). Moreover, accumulated macrophages also produce a series of cytokines, inflammatory mediators, and growth factors, which further modulate the process of neointima formation and atherosclerosis through promoting SMC and EC proliferation, increasing monocyte recruitment, and enhancing the inflammatory response (44-46). Accordingly, monocyte-derived macrophages act as a principal effector cell type in the process of restenosis and atherosclerosis.

1.5 Chemokines and chemokine receptors

1.5.1 Chemokines

Chemokines (short version for chemotactic cytokines) and their heptahelical receptors play a critical role in neointimal remodeling and atherosclerotic plaque progression by orchestrating leukocyte trafficking (47).

Chemokines are small-sized proteins (approximately 8 - 10 kDa), which share a very similar tertiary structure and can be grouped into four families according to the first two of four cysteine residues (CC, XC, CXC, and CX₃C chemokines) (Fig. 3) (48). CXC chemokines are further subdivided into two groups depending on the presence of a Glu-Leu-Arg motif (the ELR) immediately preceding the first cysteine residue. ELR⁺ CXC chemokines are proangiogenic, whereas ELR⁻ CXC chemokines, except CXCL12, are angiostatic (49, 50). Chemokines are usually secreted, but membrane-anchored chemokines, such as CX₃CL1 and CXCL16, have been described (51, 52).

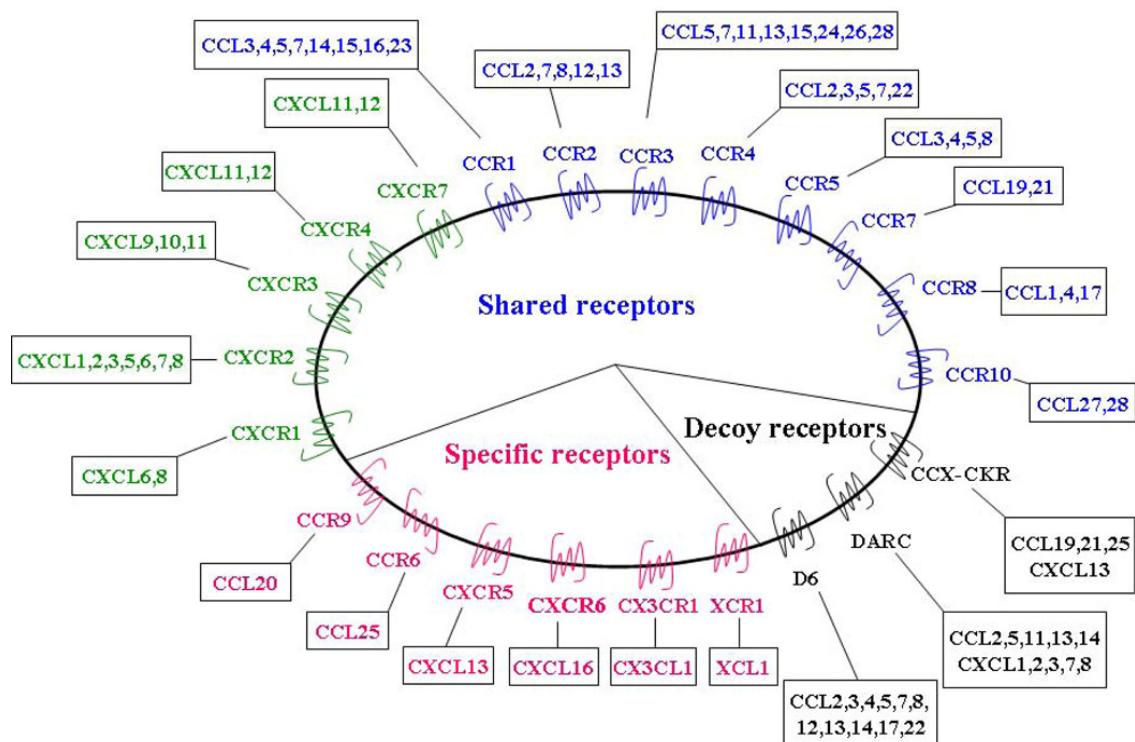


Figure 3. Chemokines and their receptors. A single chemokine (CC, blue; CXC, green) generally binds multiple receptors and one receptor usually can bind more than one chemokine. Decoy receptors (black) engage various chemokines, but do not induce intracellular signaling. However, a minority of chemokine (red)-chemokine receptor interactions are monogamous [adapted from Sun *et al.* (53)].

1.5.2 Chemokine receptors

GPCRs are a superfamily of cell surface signaling proteins (54). These receptors play a pivotal role in various physiological functions and diseases, and are therefore common drug targets (55). Usually, chemokines promiscuously bind to one or more of approximately 23 GPCRs, thus inducing heterogeneous biological functions. Chemokine-induced receptor activation triggers downstream signaling by coupled G proteins. However, 3 non-signaling (decoy) receptors exist, which bind to a number of different chemokines. According to the chemokines that bind to the receptor, chemokine receptors are divided into four groups (*i.e.*, CC receptors, XC receptors, CXC receptors, and CX₃C receptors) (56).

Chemokine receptors are structurally characterized by seven membrane-spanning domains with an extracellular N-terminus, an intracellular C-terminus, 3 intracellular (ICLs), and 3 extracellular loops (ECLs) (57). The conserved amino acid sequence Asp-Arg-Tyr (DRY motif) in the 2nd ICL is responsible for signal transduction (58, 59). Surprisingly, CXCR4-mediated activation of G_i does not require the DRY motif (60).

Like most GPCRs, chemokine receptors can exist in oligomeric complexes, including dimers (homodimers/ heterodimers) and higher-order oligomers (61, 62). Most oligomerizations are constitutive rather than ligand-dependent (63). GPCR oligomerization plays a crucial role in ligand binding, G protein activation, and signal transduction (56, 61).

1.5.3 CXCL12 and CXCR4

The CXCL12/CXCR4 axis has been implicated in the vascularization, progenitor cell trafficking, lymphocyte migration, HIV-1 entry, tumor growth, and metastasis (64-72). CXCL12, also known as pre-B cell growth stimulating factor (PBSF) or stromal-derived factor (SDF-1), is a CXC chemokine that is ubiquitously expressed in vertebrate tissues (73-75). The *CXCL12* cDNA is highly conserved during evolution and encodes two splicing variants, CXCL12 α (89 residues) and CXCL12 β (93 residues), the C-terminal of the latter contains 4 additional amino acids (76).

The high expression of CXCL12 in osteoblasts, stromal cells, and ECs within the bone marrow generates a concentration gradient between the bone marrow and peripheral blood, which retains HSCs in the bone marrow (77, 78). Disturbance of this CXCL12 gradient by either a decrease of CXCL12 in the bone marrow or an increase

of CXCL12 in the peripheral blood can induce the migration of HSCs into the blood circulation (79-81).

Since *Cxcl12*^{-/-} mice display numerous similar phenotypes as *Cxcr4*^{-/-} mice, including defective hematopoiesis, ventricular septum defect, abnormal cerebellum, and prenatal lethality, CXCL12 and CXCR4 have been regarded as an exclusive ligand-receptor pair (82, 83). Accordingly, the effects of CXCL12 have been attributed to its interaction with CXCR4. The CXCL12/CXCR4 axis has been intensively studied in vascular repair after mechanical injury and atherosclerotic lesion formation (84-89).

1.5.3.1 The role of CXCL12 in atherosclerosis

Bone marrow-derived CXCL12 appears to be beneficial in atherosclerosis, because mice in which CXCR4 is inhibited in the bone marrow develop increased atherosclerosis by releasing neutrophils into the circulation (86, 90). Moreover, up-regulation of CXCL12 in atherosclerotic lesion by microparticle-mediated delivery of miR-126 from apoptotic ECs is atheroprotective, probably due to the recruitment of circulating angiogenic cells (91). High plasma CXCL12 concentrations are associated with increased plaque stability most likely due to anti-inflammatory and matrix-stabilizing effects of CXCL12 (92). Plasma CXCL12 levels are decreased in patients with ST-elevation myocardial infarction (STEMI), indicating that CXCL12 maybe protective in patients with acute myocardial infarction (93).

However, CXCL12 may also exert pro-atherogenic effects, because the abundant CXCL12 expression in the atherosclerotic plaque by macrophages, SMCs, and ECs can trigger platelet aggregation via interaction with CXCR4, which may accelerate the development of atherosclerosis (94). Additionally, genome-wide association studies (GWAS) identified a coronary artery disease risk allele (10q11) downstream of the *CXCL12* gene, which is associated with elevated plasma CXCL12 levels (95). During vascular repair, interruption of the CXCL12/CXCR4 interaction by a *Cxcl12* antibody, small molecule *Cxcr4* antagonists, or transplantation of *Cxcr4*^{-/-} bone marrow cells diminishes neointimal hyperplasia due to reduced recruitment of smooth muscle progenitor cells (SPCs) (84, 85, 87, 89). Accordingly, CXCL12 appears to participate in the progression of vascular remodeling and atherosclerosis in a context-dependent manner.

1.5.3.2 The role of the CXCL12/CXCR4 axis in vascular repair by SPCs

During neointima formation, contractile medial SMCs transform into synthetic SMCs, which migrate into the intima, proliferate, and produce extracellular matrix (96-99). This paradigm has been complemented by ample evidence indicating that HSCs and resident stem cells can be recruited to the intimal layer of injured vessels and give rise to intimal SMCs (84, 100, 101). Controversial results exist on the origin of SPCs and the extent of their participation in neointima formation and atherosclerosis, which might be due to the different models used (vascular injury versus graft or diet-induced atherosclerosis), varying staining procedures (like the marker used to define SMCs) and microscope techniques, or the mouse strains (102, 103).

Despite these controversies, it is clear that peripheral blood progenitor cells (PBPCs) contribute much more to neointima formation after mechanical vascular injury than to atherosclerotic plaque formation. PBPCs that express the stem cell antigen (Sca-1⁺) but no hematopoietic lineage markers (Lin⁻) are increased in the circulation after vascular injury, and can be detected in the neointima where they express SMC markers, such as SMMHC (84). These data concur with the results from Simple *et al.*, who reported that bone marrow-derived mononuclear cells (BMMCs) differentiate into SMC-like cells in vitro after treatment with platelet-derived growth factor-BB (PDGF-BB) (104). Furthermore, Sata *et al.* found in mice, which express the reporter gene *lacZ* in bone marrow cells that more than half of all neointimal and medial cells originate from the bone marrow. These *lacZ*⁺ cells express SMC markers, such as α -SMA, suggesting that neointimal SMCs could be derived from the bone marrow (100). Similar results are obtained in a parabiotic model, which avoids unexpected effects of irradiation (105). Furthermore, bone marrow-derived SMCs expressing *lacZ* under the control of the SMC-specific promoter SM22 can be detected in the neointima of mice by two-photon laser scanning microscopy (TPLSM), confirming that circulating SPCs differentiate into neointimal SMC cells (106). TPLSM provides 3D-dimensional fluorescent images of viable arteries at a single-cell resolution avoiding false-positive signals from adjacent cells and fixation artifacts. Additionally, bone marrow-derived smooth muscle-like cells promote atherosclerosis by secreting proinflammatory cytokines and mitogens (107). In summary, SPCs are mobilized from the bone marrow into the blood after mechanical vascular injury and are recruited into neointimal lesions, thus contributing to

neointimal hyperplasia. Remaining questions regarding the definition of SPCs and of differentiated SMCs, the origin of SPCs, and the potential contribution of SPCs under specific conditions need to be further addressed.

The interaction of CXCR12 and CXCR4 maintains hematopoietic progenitor and stem cells within the bone marrow niches under homeostatic conditions and the disruption of the CXCL12 gradient leads to the mobilization of stem cells to the peripheral circulation (Fig. 4) (79, 80, 108). Following vascular injury, the apoptotic medial SMCs secrete apoptotic bodies, which induce the expression of CXCL12 in uninjured SMCs (84, 85). Moreover, activated platelets not only secrete CXCL12, but also present CXCL12 at the site of injury (85, 109). Plasma CXCL12 levels are elevated at 1 d and return back to baseline levels at 2 wks after injury (85). However, the expression of CXCL12 in the injured arteries is abundant throughout neointima formation (84). Elevated CXCL12 levels in the circulation disturb the gradient of CXCL12 between bone marrow and peripheral circulation, and consequently mobilize CXCR4⁺ SPCs, which contribute to neointimal hyperplasia (84, 85). Neointima formation is ameliorated by treatment with a CXCL12 antibody or a CXCR4 antagonist, confirming the critical role of the CXCL12/CXCR4 axis (85, 87, 95). Understanding the exact mechanism of SMCs recruitment in vascular diseases will pave the way for novel preventive and therapeutic strategies against restenosis (96).

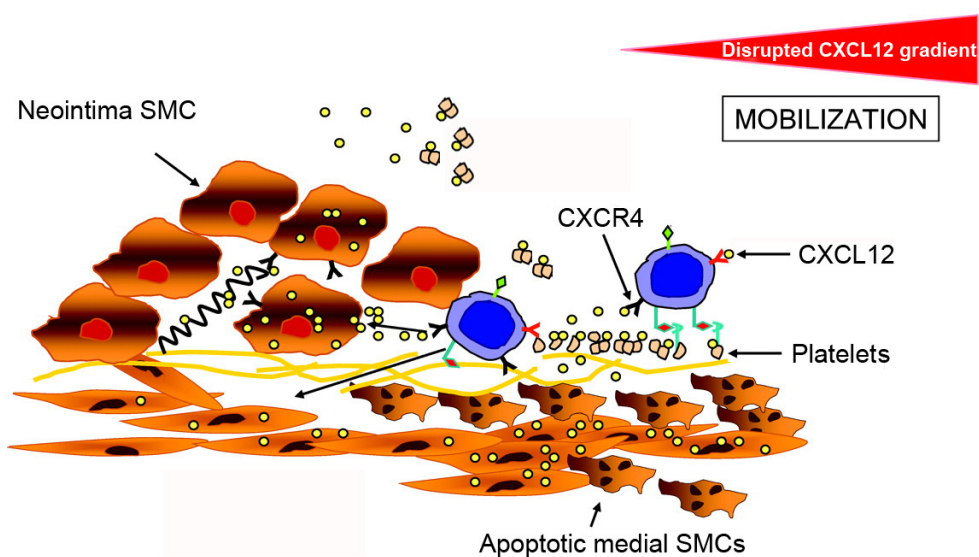


Figure 4. The CXCL12/CXCR4 axis recruits SPCs during vascular repair. Medial and neointimal SMCs produce CXCL12, which is released into the circulation and thus alters the CXCL12 gradient between the bone marrow and circulation. The

disrupted CXCL12 gradient results in the mobilization of SPCs, which are subsequently recruited to injury site via CXCL12 bound on the platelet surface [adapted from Schober *et al.* (108)].

1.5.4 CXCR7

CXCR7 (formerly known as RDC1) is an alternative receptor for CXCL12, which additionally binds to CXCL11 (110, 111). Two research groups independently reported a high rate of postnatal death and dilated ventricles in *Cxcr7*^{-/-} mice (112, 113). Sierro *et al.* also detected thickened cardiac valve leaflets due to chondrification in *Cxcr7*^{-/-} mice (113). In contrast to *Cxcl12*^{-/-} and *Cxcr4*^{-/-} mice, hematopoiesis is not impaired in *Cxcr7*^{-/-} mice (113). Furthermore, endothelial cell-specific deletion of *Cxcr7* recapitulated the phenotype of mice with a ubiquitous *Cxcr7* deletion (112, 113). Although the majority of *Cxcr7*^{-/-} mice develop dilated right ventricles in the study by Sierro *et al.* (113), Gerrits *et al.* found dilatation of both ventricles and cardiomyocyte hyperplasia in some *Cxcr7*^{-/-} mice (112).

CXCR7 mRNA is ubiquitously expressed in diverse tissues and cell types and promoter activity of the *Cxcr7* gene is detectable in the cardiovascular and nervous system as well as in the bones (112). CXCR7 protein is expressed on the surface of various malignant cell types, haematopoietic cells, and activated ECs, but not on leukocytes (110, 114-118). Moreover, CXCR7 expression is directly repressed by hypermethylated in cancer 1 (HIC1) in U2OS cells (119) and is downregulated by estrogens (E2) in breast cancer cells (120). In HUVECs, stimulation with pro-inflammatory cytokines, such as TNF- α and interleukin-1 β (IL-1 β), or hypoxic conditions increase CXCR7 mRNA expression (110, 121, 122). Furthermore, CXCR7 expression is upregulated by activated NF- κ B in tumor cells, such as Jurkat cells and rhabdomyosarcomas (116, 118, 123).

Ligand binding to CXCR7 affects cell adhesion, cell proliferation and survival, and leukocyte infiltration (110, 113, 124). However, CXCR7 activation fails to induce heterotrimeric G α i protein activation and subsequent intracellular calcium mobilization (110), although it shows homology with conserved domains of GPCRs and may constitutively interact with G proteins (125, 126). One possible explanation is that CXCR7 contains a DRYLSIT-sequence instead of the conserved DRYLAIV domain, which is coupling to G proteins (127, 128). However, replacement of the DRYLSIT motif of CXCR7 with DRYLAIV does not result in chemotaxis and

calcium mobilization upon stimulation with CXCL12 (128). Additionally, CXCR7 forms heterodimers with CXCR4, which can either activate or inhibit the signaling of CXCR4 (113, 126). Co-expression of CXCR7 and CXCR4 reduces CXCR4-mediated calcium response in HEK-293T cells by altering conformational rearrangement between CXCR4 and G proteins (126). In contrast, a potentiated calcium response is induced in HEK293 cells expressing both CXCR7 and CXCR4 (113). The intracellular crosstalk of CXCR7 and CXCR4 enhances rapid integrin activation induced by CXCL12 (129). Moreover, CXCR7 mediates the recruitment of β -arrestins leading to MAP kinases activation (130). This β -arrestin-linked signaling pathway is promoted by CXCR7/CXCR4 heterodimers compared to the signaling by G protein coupling (131). Furthermore, CXCR7 has important functions as a non-signaling decoy receptor that continuously scavenges and degrades its ligands through internalization (128, 132). This scavenging function of CXCR7 shapes the extracellular gradients of its ligands, such as CXCL12, and thus modulates the effects of CXCL12 in mammalian cells and zebrafish (128, 132). Taken together, CXCR7 may play a key role in the modulation of CXCL12/CXCR4 axis.

CCX771 is a small molecule with high affinity and selectivity for CXCR7, and it competes with CXCL12 and CXCL11 for the binding to CXCR7 (110, 124). However, CCX771 does not only antagonize the binding of CXCL12 and CXCL11 to CXCR7, but induces β -arrestin recruitment to CXCR7 more strongly than the endogenous CXCR7 ligands (133).

1.6 Aims of the study

Chemokines and their receptors govern atherosclerosis and vascular remodeling by a complex and fine-tuning network (1, 47). Compelling evidence demonstrated that the CXCL12/CXCR4 axis is essentially involved in restenosis and atherosclerosis by modulating SPC mobilization and neutrophils homeostasis, respectively; however, relatively little is known about the role of CXCR7 in these processes (84, 85, 108). This study tests the hypothesis that CXCR7 modulates the effect of the CXCL12/CXCR4 axis in vascular repair and atherosclerosis.

Widespread *Cxcr7* expression has been previously reported (112, 129, 134, 135), but little is known about the expression of *Cxcr7* in the arteries during atherosclerotic diseases. Therefore, the first aim of this study was to determine the

transcriptional and translational expression pattern of *Cxcr7* in *Apoe*^{-/-} mice during atherosclerosis and neointima formation.

Secondly, this study aimed to identify the role of *Cxcr7* on neointima formation after vascular injury, on the mobilization of SPCs, and on the alteration of *Cxcl12* levels in *Apoe*^{-/-} mice with an inducible *Cxcr7* knockout.

The third aim of the study was to assess the effects of the synthetic CXCR7-ligand CCX771 on neointima formation after vascular injury, the mobilization of SPCs, and the alteration of *Cxcl12* levels. Moreover, the role of CCX771 in diet-induced atherosclerosis was examined.

Finally, the mechanism of the effect of *Cxcr7* and CCX771 on neointima formation and atherosclerosis was studied.

2. MATERIALS AND METHODS

2.1 Materials

2.1.1 Equipment

Table1: List of general laboratory equipment

Equipment	Company
7900HT Fast Real-Time PCR System	Applied Biosystems, Darmstadt, Germany
Aladdin-1000	World Precision Instruments, Inc.USA
Balance	Sartorius, Göttingen, Germany
Biosprint 15 system	Qiagen, Hilden, Germany
CCD camera	JVC, USA
CO2-Incubator HERA cell 240	Fisher Scientific GmbH, Schwerte, Germany
CUT 6062	SLEE MAINZ, Germany
DNA engine opticon	Bio-Rad laboratories GmbH, Munich Germany
GenoPlex system	VWR International, LLC, Germany
Eppendorf 5417C	Eppendorf, Hamburg, Germany
FACSCanto™ II	BD Biosciences, San Jose, CA, USA
Hematology analyzer MEK-6450K	Nihon Kohden, Rosbach v.d.H., Germany
Heraeus Labofuge 400	Heraeus, Osterode,Germany
Heraeus Multifuge 3 S-R	Heraeus, Osterode,Germany
Infinite M200	Tecan, Crailsheim, Germany
Laminar flow hood	Heraeus, Osterode, Germany
Leica CM3050 S cryostats	Leica, Wetzlar, Germany
Leica DM 2500	Leica, Wetzlar, Germany
Leica DMLB	Leica, Wetzlar, Germany
Leica EG 1160	Leica, Wetzlar, Germany
Milli Q	Millipore, Schwalbach, Germany
Mini-sub cell GT	Bio-Rad, Hercules, USA
MyCycler	Bio-Rad, Hercules,USA
NanoDrop	Peqlab, Erlangen, Germany
Olympus BX61WI	Olympus Optical, Hamburg,Germany
Olympus CK30-F200	Olympus Optical, Hamburg,Germany
Olympus CK31RBSF	Olympus Optical, Hamburg,Germany
Olympus SZX10	Olympus Optical, Hamburg,Germany
Opticon Real-Time PCR System	Bio-Rad Laboratories GmbH, Munich, Germany
pH meter InoLab level 1	WTW, Weilheim, Germany
Systec 2540EL	Systec, Wetztenberg, Germany
Tissuelyser LT	Qiagen, Germany

2.1.2 Assay kits

Table 2: Assay kits

Kit	Company
BioSprint 15 DNA Blood Kit	Qiagen, Germany
Cell Lysis Buffer (10×)	Cell signaling, MA, USA
Cholesterol assay kit	Cayman Europe, Germany
DC Protein Assay Kit	Bio-Rad, USA
DiI-VLDL	Kalen Biomedical, USA
Elastic van Gieson kit	Merck, Germany
GAPDH primer set	Qiagen, Germany
ImaGene Green C12 FDG lacZ Gene Expression Kit	Invitrogen, Karlsruhe, Germany
Mouse Cxcl12 Elisa kit	Ray biotech, Inc., GA, USA
Murine Cxcr4 primer set	Qiagen, Germany
Murine Cxcr7 primer set	Qiagen, Germany
Murine Ldlr primer set	Qiagen, Germany
Murine rpl13a primer set	Qiagen, Germany
Murine Vldlr primer set	Sigma-Aldrich, Munich, Germany
Murine β -actin primer set	Qiagen, Germany
Qproteome Mammalian Protein Prep Kit	Qiagen, Germany
Quantitect SYBR green PCR kit	Qiagen, Germany
Quick-Load 100 bp DNA Ladder	Biolabs, USA
Reverse Transcription M-MLV Reverse Transcriptase	Promega, Madison, USA
RNA isolation RNeasy Mini/Micro Kit	Qiagen, Hilden, Germany
SYBR Green qPCR Master Mix	Fermentas, St. Leon-Rot, Germany

2.1.3 Buffers and solutions

Table 3: List of buffers and solutions

Buffer/Solution	Composition
Agarose gel	2 g agarose, 6 µl ethidium bromide, 100 ml 1× TBE.
Anesthesia solution	0.1 ml of ketamine hydrochloride (80 mg/kg), 0.05 ml of xylazine (5 mg/kg), and 0.85 ml of 0.9% sodium chloride.
Tamoxifen solution	Tamoxifen (Sigma-Aldrich, USA) was dissolved in neutral oil at the concentration of 15 mg/ml or 20mg/ml.
FACS staining buffer	1.6% mouse serum; 1.6% rabbit serum; 1.6% human serum; 1.6% bovine serum albumin (BSA); dissolved in PBS.
Hank's complete solution	1× HBSS, 0.3 mM EDTA, 0.1% BSA.
HBSS 1× solution	1:10 diluted 10× HBSS (Calcium, Magnesium).
Blocking solution	PBS containing 1% BSA and 2.5% blocking serum, or PBS containing 10% blocking serum (option: 0.2% Triton X-100 for permeabilization).
Paraformaldehyde	4% paraformaldehyde dissolved in PBS, pH 7.4 - 8.
Primary antibody buffer	PBS containing 10% blocking solution
Red blood cell lysis buffer	150 mM NH ₄ Cl; 10 mM KHCO ₃ ; 0.1 mM EDTA, pH 7.4
Sodium Citrate Cooking Buffer	12.6 ml of 0.1 M citric acid; 57.4 ml of 0.1 M NaCitrate dehydrate; 0.35 ml Tween20, and 630 ml distilled water. (Adjust pH to 6.0 with 5 M NaOH).
X-gal washing solution	PBS containing 2 mM MgCl ₂ .
X-gal staining solution	5 mM potassium ferrocyanide, 5 mM potassium ferricyanide, 2 mM MgCl ₂ , 0.02% Nonidet P-40 (was diluted from 10% stock), 0.01% Na deoxycholate (diluted from 10% stock), and 1 mg/ml X-gal (was dissolved in dimethylformamide, Invitrogen), were dissolved in PBS.
X-gal stock solution	40 mg/ml X-gal in dimethylformamide (store at -20°C in foil covered glass contain).
Vitro-Clud mounting medium	Vitro-Clud (Angenbrinck, Emmendingen, Germany) diluted into xylene.
1% Alcian blue solution	1 g Alcian blue (Sigma A5268), 100 ml milipore water, and 1 ml acetic acid (filtration).
Alkaline ethanol	5 ml ammonium hydroxide was mixed with 95 ml of 96% ethanol.
Orcein-Verhoeffschem Hematoxylin solution A	1 g Orcein (Merck, 1071000025), 98 ml 70% ethanol, 1 ml 25% HCL (filtration).
Orcein-Verhoeffschem Hematoxylin solution B	8 g Hematoxylin (Sigma, H3136), 160 ml 100% ethanol.

Buffer/Solution	Composition
Orcein-Verhoeffschem Hematoxylin solution C	9.6 g Iron(III)-Chloride (Merck, 8039450500), 90 ml Millipore water.
Orcein-Verhoeffschem Hematoxylin solution D	1 g Iodine, 2 g Potassium iodide, and 97 ml Millipore water.
Orcein-Verhoeffschem Hematoxylin working solution	25 ml of Orcein-Verhoeffschem Hematoxylin solution A; 20 ml of Orcein-Verhoeffschem Hematoxylin solution B; 8 ml of Orcein-Verhoeffschem Hematoxylin solution C; 8 ml of Orcein-Verhoeffschem Hematoxylin solution D.
Acidic alcohol	1 ml of 25% HCL and 100 ml of 95% ethanol.
Brilliant Crocein Scarlet MOO solution A	0.1 g Brilliant Crocein Scarlet, 0.5 ml Acetic acid, and 99.5 ml Millipore water.
Brilliant Crocein Scarlet MOO solution B	0.1 g Acid fuchsin (Merck, 105231), 0.5 ml Acetic acid, and 99.5 ml Millipore water.
Brilliant Crocein Scarlet MOO working solution	40 ml Brilliant Crocein Scarlet MOO solution A and 10 ml Brilliant Crocein Scarlet MOO solution B.
0.5% acetic acid	1 ml of acetic acid and 200 ml of milipore water.
6% alcoholic saffron	6 g of saffron was dissolved in 94 ml of absolute ethanol and stored at 56 °C for 48 hours before use.
Oil red O stock	1 g oil red O (Sigma-Aldrich, St. Louis, USA) in 200 ml 99% isopropanol.
Oil red O working solution	Dilute Oil red O stock with distilled water in a ration 3:2, stand for 1 h and through filter paper.
Glycerine mounting Medium	10 g gelatin, 70 ml glycerol, 0.25 g phenol in 60 ml distilled water.

2.1.4 Consumables

Table 4: Consumables

Consumables	Company
96-well plates	Nunc, Denmark
EDTA-coated tubes	Sarstedt, Germany
FACS-tubes	BD Biosciences, USA
Microhematocrit capillary tube	Hilgenberg, Germany
SuperFrost [®] Plus slides	Thermo Scientific, Germany
Polysine [™] slides	Thermo Scientific, Germany
PAXgene tissue containers	Qiagen, Germany
QIAshredder homogenizer	Qiagen, Germany
SERAFLEX suture (USP 5/0, EP 0.5)	SERAG WIESSNER, Germany
SERAFLEX suture (USP 7/0, EP 1)	SERAG WIESSNER, Germany
Serological pipettes (5 ml, 10 ml, 25 ml)	Corning, USA
Serum-separating tubes	Sarstedt, Germany
Sterile filter-tips	Starlab, Germany
Superose 6 10/300 colum	GE healthcare, USA
Syringes (2 ml, 5 ml, 10 ml, 20 ml)	Terumo, Belgium

2.1.5 Chemicals, reagents, and cell culture medium

Table 5: Chemicals, reagents, and cell culture medium

Chemical, reagents, medium	Company
Bovine serum albumin	Serva, Heidelberg, Germany
Collagen Type I, Rat Tail	Millipore, USA
Collagenase Type II	Invitrogen, Germany
cOmplete, Mini Protease Inhibitor	Roche, Swiss
DiI-VLDL	Kalen Biomedical, Montgomery Village, USA
Endothelial cell growth medium	Promocell, Germany
Gibco [®] HBSS (10×)	Life Technologies, Inc., USA
Gibco [®] HBSS (10×, Calcium, Magnesium)	Life Technologies, Inc., USA
Human serum	Sigma-Aldrich, St. Louis, USA
IL-1 β	Pepro Tech, USA
Isofluran	Abbott, Germany
MIGLYOL [®] 812	Germany GmbH, Hamburg, Germany
Mouse serum	Sigma-Aldrich, St. Louis, USA
Nuclear Fast Red	Vector Laboratories Inc., Burlingame, CA, USA
Rabbit serum	Innovative Research, Research, Novi, USA
Tissue-Tek [®] O.C.T. compound	Sakura Finetek Germany GmbH, Staufen, Germany
TNF- α	Pepro Tech, USA
Mounting medium with DAPI	Vector Laboratories Inc., Burlingame, CA, USA
X-gal	Invitrogen, USA

2.2 Methods

2.2.1 Animal experiments

2.2.1.1 Animals

Cxcr7^{lacZ/+} (136) and *Cxcr7^{fllox}* mice (manuscript in preparation) were generated by ChemoCentryx, Inc. *CAG-CreERTM* (137) and *Apoe^{-/-}* mice were obtained from The Jackson Laboratory (Bar Harbor, Maine, USA). *VE-Cad-Cre^{T2}* mice were kindly provided by Dr. Iruela-Arispe (UCLA, Los Angeles, USA) (138). *CAG-CreERTM* mice were crossed with *Cxcr7^{fllox}* mice to generate *CAG-CreERTMCxcr7^{fllox}Apoe^{+/+}* mice, then *Apoe^{-/-}* mice with a ubiquitous TMX-inducible *Cxcr7* knockout (*CAG-Cre⁺Cxcr7^{fllox}Apoe^{-/-}*) were generated by breeding *CAG-CreERTMCxcr7^{fllox}Apoe^{+/+}* and *Apoe^{-/-}* mice. Additionally, *VE-Cad-Cre^{T2}* mice were crossed with *Cxcr7^{fllox}* mice to generate *VE-Cad-Cre⁺Cxcr7^{fllox}Apoe^{+/+}* mice. To generate *Apoe^{-/-}* mice with an endothelial TMX-inducible *Cxcr7* knockout *VE-Cad-Cre⁺Cxcr7^{fllox}Apoe^{+/+}* were crossed with *Cxcr7^{fllox}Apoe^{-/-}* mice.

In *CAG-Cre⁺Cxcr7^{fllox}Apoe^{-/-}* mice, Cre recombinase is fused to a mutated ligand-binding domain of the murine estrogen receptor (Cre-ERTM), which does not bind to its natural ligands, but binds to TMX. Upon TMX binding, Cre-ERTM translocates into the nucleus and initiates the recombination of loxP-flanked genes, like the *Cxcr7^{fllox}* gene. A chicken β -actin promoter and cytomegalovirus enhancer drive the expression of the Cre-ERTM fusion protein (137).

In *VE-Cad-Cre⁺Cxcr7^{fllox}Apoe^{-/-}* mice, Cre-ERTM expression is under the control of the vascular endothelial cadherin promoter (138). Accordingly, TMX-induced Cre-recombinase mediates the recombination of floxed genes in ECs.

Of note, the background of mice used in this project is C57BL/6, which contains a natural null mutant of *Cxcl11*, excluding the involvement of *Cxcl11* in the *Cxcr7*-mediated signal pathways (113).

All animal experiments were reviewed and approved by the local authorities (LANUV NRW) in accordance with the German animal protection laws.

2.2.1.2 Wire-induced injury of carotid arteries

In the wire injury model, mechanically-induced endothelial denudation simulates restenosis after angioplasty without disturbing normal blood flow (102, 139). *Apoe^{-/-}*

mice are characterized by severe hypercholesterolemia and a compromised immune response. These mice develop enhanced neointimal hyperplasia following vascular injury and are susceptible to diet-induced atherosclerosis (102, 140). Therefore, *Apoe*^{-/-} mice may provide a model for neointima formation that is more closely related to clinical restenosis, because in patients the already atherosclerotic artery is mechanically injured by the stent implantation or angioplasty.

Wire injury was performed in *Apoe*^{-/-} mice after 1 wk of HCD feeding (HCD; 21% fat and 0.15% cholesterol; Altromin, Lage, Germany) (84). Mice were anesthetized with ketamine (100 mg/kg) and xylazin (10 mg/kg) via intraperitoneal injection (IP) and then fixed backside down on the operating table. The operating area was shaved and swabbed with 70% isopropanol. A skin incision was made at the left lateral side of neck, and then the common carotid artery (CCA) and the bifurcation area were exposed using a dissecting microscope. Ligatures were placed around the proximal part of the CCA, the external carotid artery (ECA), and the internal carotid artery (ICA). The distal ligature around ECA was tied off while the ligatures around CCA and ICA were pulled and fixed on the operating table, thus suspending blood flow locally in the artery. A transverse incision was made in the ECA between the proximal and distal ligatures using fine scissors. A 0.36-mm flexible angioplasty guidewire was introduced into the arterial lumen through the incision and passed through the CCA with rolling movement, thus achieving endothelial denudation. The proximal ligature of ECA was permanently ligated following withdrawal of the wire. The ligatures of the ICA and CCA were removed and blood flow re-established. Skin incisions were closed with clips.

2.2.1.3 Diet-induced atherosclerosis model

The diet-induced atherosclerosis model is a commonly used method to aggravate the development of atherosclerosis in mice by feeding a diet with high cholesterol content (141). Animals were fed a HCD for 3 months until sacrifice.

2.2.1.4 Splenectomy

In anesthetized *Apoe*^{-/-} mice, the left hypochondrium was surgically opened. Then, the spleen was dissected from adjacent tissues and removed after the ligation of the

vessels of the spleen (142). Wire injury of the carotid artery was performed in these mice 2 wks after the splenectomy.

2.2.1.5 Bone marrow transplantation

Bone marrow cells were harvested from femurs of *CAG-Cre⁺Cxcr7^{fllox}Apoe^{-/-}* or *CAG-Cre⁻Cxcr7^{fllox}Apoe^{-/-}* and delivered (4×10^6 /mouse) into irradiated recipient *Apoe^{-/-}* mice (2×6 Gray, 4 h interval, Faxitron's CP160) via tail vein injection. Three wks later, the recipient *Apoe^{-/-}* mice were treated with TMX for 5 consecutive days. One wk after the final TMX injection, the mice were fed a HCD for 1 wk before wire injury of the carotid artery was performed. Tissues and blood were harvested 4 wks after vascular injury.

2.2.1.6 Sacrifice, blood collection, and tissue fixation

Mice were sacrificed by injection of an overdose of ketamine and xylazine (250 mg/kg Ketamine with Xylazine 25 mg/kg administered, IP). Whole blood was collected from mice by cardiac puncture and further processed to plasma and serum samples (Table 6). In some mice, blood was obtained by puncturing the retro-orbital sinus with microhematocrit capillary tubes during short-time anesthesia using isofluran inhalation.

To assess the plasma concentration of CCX771, blood samples were obtained 1 h and 12 h after a subcutaneous injection of CCX771 (2 mg/ml, dissolved in 10% Captisol; 100 μ l/mouse). The plasma concentrations of CCX771 were measured using liquid chromatography–mass spectrometry (LC-MS) by ChemoCentryx, Inc.

Table 6: Blood collection

Samples	Tubes	Treatment	Centrifuge
Serum	Serum-separating tubes	Satisfactory clot retraction for at least 30 min	2000g, 15 min, 4°C
Plasma	EDTA-coated tubes	Mix thoroughly, centrifuge as soon as possible	1000g, 10 min, 4°C

For perfusion fixation, a catheter was inserted into the apex of the left ventricle and the right atrium was cut to allow outflow of PBS and the fixation solution. Then, the circulatory system was flushed with pre-cooled PBS (5 ml) and subsequently

perfusion fixation was performed with 4% paraformaldehyde (PFA, 5 ml) using a roller pump (1 ml/min, Aladdin-1000). Some mice were fixed by PAXgene Tissue Fix (PAXgene Tissue Containers, 500 µl) using a syringe (2 ml) equipped with a 23G needle after completing PBS perfusion.

After incubated in 10% formalin or PAXgene Tissue Stabilizer overnight at 4°C, tissues were embedded in paraffin (Leica EG1160) after dehydration (Tissue processors). Sections were made by a microtome (CUT 6062). For cryosections, tissues were embedded into OCT solution, transferred to liquid nitrogen, and stored at -80°C. Sections were made using a cryotome (Leica CM3050 S).

2.2.1.7 Blood biochemistry

Serum samples were analyzed by dry chemistry using a Vitros 250 Analyzer to determine the total cholesterol, creatinine, alanine transaminase (ALT), or aspartate transaminase (AST) levels. Increased levels of AST or ALT indicate hepatic injury. Elevated creatinine levels indicate impaired kidney function (143). The EDTA-anticoagulated blood was analyzed by a hematology analyzer (MEK-6450K). The percentage of the leukocyte subtypes was determined by a blood smear.

Plasma lipoprotein fractions (VLDL, LDL, and HDL) were separated using fast protein liquid chromatography (FPLC) by size (144). A Superose 6 10/300GL column was first equilibrated with PBS. After loading 200 µl diluted blood plasma solution (1:1 diluted in PBS) to a 100-µl injection loop, the system was running with PBS as a running buffer at a constant flow rate of 0.5 ml/min. Fractions containing the plasma lipoproteins (0.25 mL) were collected and cholesterol was further measured in the different fractions using a cholesterol fluorometric assay (Table 2).

2.2.1.8 CCX771 and tamoxifen administration

Treatment with CCX771 was performed by daily subcutaneous injections [5 ml/kg of CCX771 (2 mg/ml) dissolved in 10% Captisol]. In the control group, mice were injected with vehicle alone (5 ml/kg, 10% Captisol, s.c.). Injections were started 1 h before injury and continued for 4 wks after vascular injury. In the diet-induced atherosclerosis model, the CCX771 treatment was performed daily for 3 months.

TMX was dissolved in neutral oil (MIGLYOL[®] 812) at a concentration of 15 mg/ml or 20 mg/ml. TMX (75 mg/kg, body weight) was injected intraperitoneally for

5 consecutive days in *CAG-Cre⁺ Cxcr7^{fllox} Apoe^{-/-}* and *CAG-Cre⁻ Cxcr7^{fllox} Apoe^{-/-}* mice. TMX (100 mg/kg, body weight) was injected intraperitoneally for 5 consecutive days in *VE-Cad-Cre⁺ Cxcr7^{fllox} Apoe^{-/-}* and *VE-Cad-Cre⁺ Cxcr7^{+/+} Apoe^{-/-}* mice. HCD feeding was started 7 d and arterial injury was performed 14 d after the last injection of TMX (137).

2.2.2 Molecular biology techniques

2.2.2.1 Isolation and quantification of DNA and RNA

The BioSprint 15 DNA Blood Kit was used to purify DNA from murine tails. These tails were digested by proteinase K (more than 4 h, 56°C) and the lysates mixed with buffer AL (lysis), isopropanol, and Magattract Suspension G were transferred to the first well of 5-tube trip. Buffer AW1 (washing), AW2 (washing) and AE (elution) were separately added to the other wells. DNA was harvested after running the protocol “BS15 DNA Tissue” in the BioSprint 15 workstation.

Total RNA was extracted using RNeasy micro or mini kit (Qiagen) dependent on the weight of tissues or the number of cells. Tissues were lysed and homogenized by TissueLyser LT, and cells by QIAshredder homogenizer. The RNA was isolated using RNeasy/RNeasy MinElute spin columns.

DNA/RNA concentrations were measured using a spectrophotometer (NanoDrop). The purity of DNA/RNA was determined by the ratio of the absorbance at 260 nm and 280 nm. DNA and RNA with an approx. Ratio_{260/280} of 1.8 and 2, respectively, were used for further downstream analysis.

2.2.2.2 cDNA synthesis

Reverse transcription was carried out according to Quantitect Reverse Transcription kit protocol (Qiagen). Following elimination of genomic DNA by gDNA wipeout buffer (Table 7), a certain amount of RNA was mixed with reverse transcriptase, reverse transcription buffer, primer mix, and water in a 20-μl reaction mixture and then incubated for 30 min at 42°C (Table 8). Finally, the reverse transcriptase was inactivated by incubation at 95°C for 3 min.

Table 7: The first step of reverse transcription

Component	Volume
gDNA Wipeout Buffer, 7×	2 μ l
RNA	Less than 1 μ g
RNase-free water	Up to total volume 14 μ l

Table 8: The second step of reverse transcription

Component	Volume (μ l)
Quantiscript Reverse Transcriptase	1
Quantiscript RT Buffer, 5×	4
Primer Mix (reverse transcription)	1
RNA (from first step)	14

2.2.2.3 Polymerase chain reaction (PCR) and electrophoresis

PCR was performed using DNA isolated from mouse tissue to genotype the mice. Amplification of the DNA by PCR includes three steps: denaturation, cycling, and extension (Table 9). Gene specific primer pairs (Table 10) were used to amplify DNA. PCR products of the DNA samples were loaded into a 2% agarose gel containing 0.03 μ g/ml ethidium bromide (Table 3) and the bands were visualized after electrophoresis by UV transillumination and photographed using the GenoPlex system.

Table 9: PCR protocol for genotyping

Component	Volume (μ l)
H ₂ O	12.75
Buffer 5X	5
Mgcl ₂ (25 mM)	2
dNTP (10 mM)	0.5
Forward Primer (10 μ M)	1.25
Reverse primer (10 μ M)	1.25
Taq polymerase (units/ μ l)	0.25
Template	2
Final volume	25

Table 10: Primers for the genotyping of the mouse lines

Sequence	Annealing	Result	Application
5'-CTAGGCCACAGAATTGAAAGATCT-3'	55 °C, 30 s	lox/WT: 396 bp and 362 bp; lox/lox:	Genotyping for Cxcr7 loxp mice
5'-GTAGGTGGAAATTCTAGCATCATCC-3'	55°C, 30 s	396 bp only; WT/WT: 362 bp only	Genotyping for Cxcr7 loxp mice
5'-AGCCTGGCAACTACTCTGACATC-3'	60°C, 45 s	WT: CXCR7 458 bp, lacZ no band Het: Cxcr7 458 bp, lacZ 404 bp KO: Cxcr7 no band, LacZ 404 bp	Genotyping for Cxcr7/lacZ
5'-CACGGCGTACCATCTTCTTCTTAT-3'	60°C, 45 s		Genotyping for Cxcr7/lacZ
5'-AGGGCCGCAAGAAACTATCC-3'	60°C, 45 s		Genotyping for Cxcr7/lacZ
5'-ACTTCGGCACCTTACGCTTCTTCT-3'	60°C, 45 s		Genotyping for Cxcr7/lacZ
5'-CTAGGCCACAGAATTGAAAGATCT-3'	55°C, 30 s	This will not distinguish Cre homozygous from heterozygous mice. Internal control = ~324 bp Cre fragment = ~100 bp	Genotyping for Cre mice
5'-GTAGGTGGAAATTCTAGCATCATCC-3'	55°C, 30 s		Genotyping for Cre mice
5'-GCGGTCTGGCAGTAAAACTATC-3'	55°C, 30 s		Genotyping for Cre mice
5'-GTGAAACAGCATTGCTGTCACTT-3'	55°C, 30 s		Genotyping for Cre mice
5'-GCAAGTTTGGGGTACAGTCC-3'	55°C, 30 s	2209 bp, without recombination 521 bp, with recombination	Genotyping for Cxcr7 deletion
5'-ACAACAGCCTTACACCTCCC-3'	55°C, 30 s		Genotyping for Cxcr7 deletion
5'-CCATCTTACACTACATCCCG-3'	55°C, 30 s		Genotyping for Cxcr7 deletion

2.2.2.4 Quantitative real-time PCR

Quantitative real-time PCR (qRT-PCR) is a reliable and sensitive technique to quantify mRNA expression following reverse transcription into cDNA by determination of the crossing points of the amplification curve obtained from incorporated fluorescent probes, such as SYBR green. All qRT-PCR runs were carried out by Opticon Real-Time PCR System or 7900HT Fast Real-Time PCR System according to a general protocol (Table 11) using a specific cycler program (Table 12).

Primer pairs for *Cxcr7*, *Cxcr4*, *Vldlr*, and *Ldlr* (Table 2) were used for PCR amplification in a real-time cycler. *Gapdh*, β -actin, and *rpl13a* (Table 2) were used as reference genes. The relative values were calculated by Qbase^{PLUS} software (Biogazelle) and were further log₂ transformed for data analysis (145).

Table 11: Protocol of the qRT-PCR runs

Component	Volume (μl)
2× Quantitect SYBR Green PCR Master Mix	12.5
10× QuantiTect Primer Assay	2.5
Template cDNA (diluted)	2
RNase-free water	up to 25

Table 12: Program of the qRT-PCR runs

Step	Tm	Time
Initial activation step	95°C	15 min
Cycling steps (40 cycles)	94°C	15 s
	60°C	30 s
	72°C	30 s
Plate reading		

2.2.3 Histological staining protocols

2.2.3.1 Movat's pentachrome staining

After deparaffinization, slides were stained successively with alcian blue, Orcein-Verhoeff's Hematoxylin, Brilliant Crocein Scarlet MOO, and alcoholic saffron (Table 13). The pentachrome staining allows differential analysis of nuclei/elastic fibers (black), collagen/reticular fibers (yellow), ground substance/mucin (blue), and fibrinoid/fibrin intense (red) (146).

Table 13: Procedure of Movat' pentachrome staining

Staining procedure	Time	Tm
Xylene	30 min	RT
100% isopropanol	5 min x 2	RT
96% isopropanol	5 min	RT
70% isopropanol	5 min	RT
Millipore water	5 min	RT
PBS	5 min	RT
Alcian blue solution (1%)	20 min	RT
Tap water	5 min	RT
Alkaline alcohol	10 min	56°C
Running water	2 min	RT
Millipore water (dip several times)	—	RT
Orcein-Verhoeff's Hematoxylin	30 min	37°C
Running water	3 min	RT
Iron (III)-Chloride solution (2%)	2 min	RT
Acidic alcohol	2 min	RT
Brilliant Crocein Scarlet MOO solution	10 min	RT
Acetic acid (0.5%)	30 s	RT
Phosphor-tungstic acid (5%)	4 min	RT
Acetic acid (0.5%)	30 s	RT
100% ethanol	1 min x 3	RT
Alcoholic saffron (6%, sealed container)	8 to 15 min	RT
Absolute ethanol	3 min x 2	RT
Xylene (dip several times)	—	RT
Vitrocloud solution	—	RT

2.2.3.2 Elastic van Gieson staining

Elastic van Gieson (EVG) staining was performed according the manual of Elastic van Gieson kit (Table 14) using Weigert's hematoxylin, picrofuchsin, and the resorcinol-fuchsin solution. Elastic fibers (black), nuclei (black-brown), collagen (red), and muscle (yellow) can be differentially analyzed by the EVG staining (147).

Table 14: Protocol of EVG staining

Staining procedure	Time	Tm
Xylene	30 min	RT
100% isopropanol	5 min x 2	RT
96% isopropanol	5 min	RT
70% isopropanol	5 min	RT
Millipore water	5 min	RT
PBS	5 min	RT
Resorcinol-Fuchsine-solution (Roth, X877.1)	15 min	56°C
Tap water (dip twice)	—	RT
80% ethanol (dip once)	—	RT
Tap water (dip once)	—	RT
Millipore water	—	RT
Solution A + B (refer to table 3)	5 min	RT
0.5% HCL-alcohol (dip once)	—	RT
Tap water (dip once)	5 min	RT
Picrofuchsin	1 min	RT
Tap water (dip once)	—	RT
70% ethanol (dip once)	—	RT
96% ethanol (dip once)	—	RT
100% ethanol (dip once)	—	RT
Xylene	5 min	RT
Vitrocloud solution	—	RT

2.2.3.3 Oil red O staining

Lipid deposition in the aorta can be quantified by oil red O staining (148). After an overnight incubation in 4% PFA, the adventitia and adipose tissues of the thoracoabdominal aorta were gently and completely removed. The aorta was dissected, cut longitudinally, and finally *en face* pinned onto a black rubber plate. After washing with running tap water, the aorta was rinsed with 60% isopropanol (10 dips), followed by staining with the oil red O solution (Table 3) for 15 min. The

stained aorta was rinsed by 60% isopropanol (10 tips) and running tap water. The *en face* prepared aorta was transferred on a glass slide and coverslipped with glycerin mounting solution (Table 3). Digital images of aorta were recorded using a microscope (Leica DM 2500) equipped with a CCD camera (JVC) and Diskus software (Hilgers, Bonn). The lesional area (oil red O positive) was quantified by Image J software (National Institute of Health, USA), and expressed as the percentage of the positive area relative to the whole aortic area.

2.2.3.4 Histomorphometry

Histomorphometry is a useful technique to measure and characterize the microscopical images including quantification and comparison of target geometric areas and perimeters.

Cross-sections (4 μm thickness, 6 sections/mouse) of the left common carotid arteries were selected within a standardized distance (80 to 320 μm) from the bifurcation and subsequently stained with modified Movat's pentachrome or EVG stain. Cross-sections (4 μm thickness, 4 sections/mouse) of the aortic roots were selected within a standardized distance (40 to 160 μm) from the first section in which three leaflets were visible and subsequently stained with modified Movat's pentachrome or EVG stain. Lumen area, lumen area inside the internal elastic lamina (IEL), lumen area inside the external elastic lamina (EEL), and the aortic root plaques were determined using image analysis software (Diskus, Hilgers, Bonn). These data were used to calculate neointimal and medial areas as follows: neointimal area = IEL area – lumen area; medial area = EEL area – IEL area.

2.2.3.5 β -galactosidase activity assay

A β -galactosidase (β -gal) activity assay is commonly used to analyze expression of the reporter gene lacZ, which encodes for β -gal from *E. coli*. In the X-gal assay, the activity of β -gal is visualized using the β -gal substrate 5-bromo-4-chloro-indolyl- β -D-galactopyranoside (X-gal), which is converted to 5,5'-dibromo-4,4'-dichloro-indigo (an insoluble blue dye) (149).

To determine the *Cxcr7* promoter activity in different tissues, *Cxcr7*^{+/*lacZ*} and *Cxcr7*^{+/+} mice were perfused with 10 ml of ice-cold 2% PFA. Tissues were harvested

and post-fixed in 2% PFA for 15 min on ice. Following a washing step (PBS containing 2 mM MgCl₂), tissues were incubated in the staining solution (Table 3) overnight at 37°C (149). Subsequently, the stained tissues were frozen and embedded in Tissue-Tek[®] O.C.T. compound for cryosectioning by cryostats (Leica CM3050 S). Cryosections (5-10 µm thickness) were re-stained with the staining solution overnight at 37°C and nuclei were counterstained with Nuclear Fast Red. The sections were coverslipped with Vitro-Clud mounting medium.

2.2.4 Immunofluorescence staining protocols

Immunofluorescence staining is a technique to identify proteins in tissues or cells using specific primary antibodies. Staining was carried out on cryosections or paraffin embedded sections. All stainings were performed according to specific protocols (Table 15). Corresponding secondary antibodies (Abs) conjugated to a fluorescence dye were used to visualize the primary Abs. Nuclei were counterstained with 4', 6-diamidino-2-phenylindole (DAPI).

For Cxcr7 immunostaining, cryosections (fixed in 4% PFA) from wild type mice were used and compared to sections from *Cxcr7^{lacZ/lacZ}* mice, which served as negative controls (Table 14). After antigen retrieval and a blocking step (10% horse serum in PBS containing 0.2% Triton X-100), slides were incubated with a monoclonal anti-human CXCR7 Ab (10 µg/ml, 4°C, and overnight), followed by incubation with a donkey-anti-mouse IgG-FITC-conjugated Ab (1:100, RT, and 1 h). Murine isotype IgG was used for negative control stainings on sections of the carotid artery with neointima.

Several sections of the carotid arteries or aortic roots (4 per mouse, fixed in 4% PFA, and paraffin-embedded) were used for α-SMA, SM22, and Mac-2 staining (Table 15 and 16). Slides were blocked with PBS containing 10% goat serum (for SM22 staining) or 1% BSA and 2.5% horse serum (for α-SMA and Mac-2 staining). After the blocking step, slides were incubated with a monoclonal anti-mouse α-SMA Ab (1:200, 4°C, and overnight), a rabbit polyclonal anti-SM22 Ab (1:200, 4°C, and overnight), or a monoclonal anti-mouse Mac-2 Ab (1:400, 4°C, and overnight). Subsequently, the Mac-2 Ab was visualized by a donkey-anti-rat IgG-FITC-conjugated Ab (1:100, RT, and 30 min) or a donkey-anti-rat IgG-cy3-conjugated Ab (1:300, RT, and 30 min). The α-SMA Ab was detected by a donkey-anti-mouse IgG-FITC-conjugated Ab (1:100, RT, and 30 min), and the SM22 Ab was visualized by a

goat-anti-rabbit IgG-Dylight549-conjugated Ab (1:200, RT, and 30 min). Appropriate non-specific control Abs in the same concentration as the primary Abs were used as negative controls (Table 16).

Digital images were recorded using a fluorescence microscope (Leica DM 2500) equipped with a CCD camera (JVC) and Diskus image acquisition software. The positively stained area per neointima was quantified with Image J (National Institute of Health, USA); the relative SMCs content was evaluated by dividing the α -SMA- or SM22-positive area by the whole neointimal or plaque area. The macrophage number per lesion was determined by counting the DAPI-stained nuclei in the Mac-2 positive area.

Table 15: Immunostaining protocols

Procedure	Method and material
Deparaffinization	Xylene: 2 × 15 min 100% ethanol: 2 × 5 min 96% ethanol: 1 × 5 min 70 % ethanol: 1 × 5 min PBS: 1 × 5 min
Antigen retrieval	Cooking in Sodium Citrate Buffer for 15 min
Blocking	PBS containing 10% goat serum or 1% BSA and 2.5% horse serum
Primary antibody incubation	Appropriate antibody (Table 16)
Second antibody incubation	Appropriate antibody (Table 16)
Counterstaining and mounting	Vectashield Mounting Medium with DAPI

Table 16: Antibodies for immunostaining

Antibody	Clone	Ig type	Conjugate	Manufacturer
Monoclonal anti-human alpha-SMA Ab	1A4	Mouse IgG2a, κ	Purified	Dako
Monoclonal anti-mouse MAC-2 Ab	M3/38	Rat Ig2a	Purified	Cedarlane
Monoclonal anti-human CXCR7/RDC1 Ab	11G8	Mouse IgG1	Purified	ChemoCentryx. Inc/R&D
Rabbit polyclonal anti-SM22 Ab	—	—	Purified	Abcam
Mouse IgG	—	—	Purified	SANTA CRUZ
Rat IgG	—	—	Purified	SANTA CRUZ
Donkey anti-mouse IgG (H+L) Ab	—	—	cy3	Jackson ImmunoReserch
Donkey-anti-mouse IgG (H+L) Ab	—	—	FITC	Jackson ImmunoReserch
Donkey-anti-rat (H+L) Ab	—	—	cy3	Jackson ImmunoReserch
Goat-anti-rabbit IgG (H+L) Ab	—	—	Dylight549	KPL

2.2.5 Flow cytometry

Flow cytometry is a biophysical technology for counting, sorting, and biomarker analysis of cells or particles. The advantage of flow cytometry is the rapid and simultaneous multi-parametric analysis (size, granularity and fluorescent intensity) of a cell suspension on a single cell level dependent on light scatter and fluorescence.

Blood (approximately 100 μ l) was obtained from the retro-orbital sinus and collected in EDTA-coated tubes before adding erythrocyte lysis buffer (3 ml, at RT for 10 min).

To quantify murine Sca-1⁺lin⁻ peripheral blood progenitor cells (SPCs) (Fig. 5), blood cells were incubated with phycoerythrin (PE)-conjugated anti-mouse Sca-1 (1:50 dilution; Table 17) and the biotinylated anti-mouse hematopoietic lineage Ab panel (CD3, CD45R, CD11b, Ter-119, and Ly-6G, 1:50 dilution of each Ab; Table 17) on ice for 30 min followed by streptavidin phycoerythrin-Cy7 (1:500 dilution, for 30 min on ice; Table 17). The same gating strategy was applied to identify Sca-1⁺lin⁻ cells in all experiments (Fig. 5).

Table 17: Antibodies for flow cytometry

Antibody	Clone	Ig type	Conjugate	Manufacturer
Monoclonal anti-human/mouse CXCR7 Ab	8F11-M16	Mouse IgG2b	PE	Biolegend
Monoclonal anti-human/mouse IgG2b Ab	MPC11	Mouse IgG2b	PE	Biolegend
Mouse IgG2b	—	—	Biotinylated	eBioscience
Monoclonal anti-mouse Ly-6A/E (Sca-1) Ab	D7	Rat IgG2a, κ	PE	eBioscience
Monoclonal anti-mouse CD115 Ab	AFS98	Rat IgG2a, κ	PE	eBioscience
Monoclonal anti-mouse Gr-1 Ab	RB6-8C5	Rat IgG2a, κ	PerCP-Cy*5.5	BD Biosciences
Mouse hematopoietic lineage flow panel	—	—	Biotinylated	eBioscience
Streptavidin phycoerythrin-cy7	—	—	cy7	eBioscience

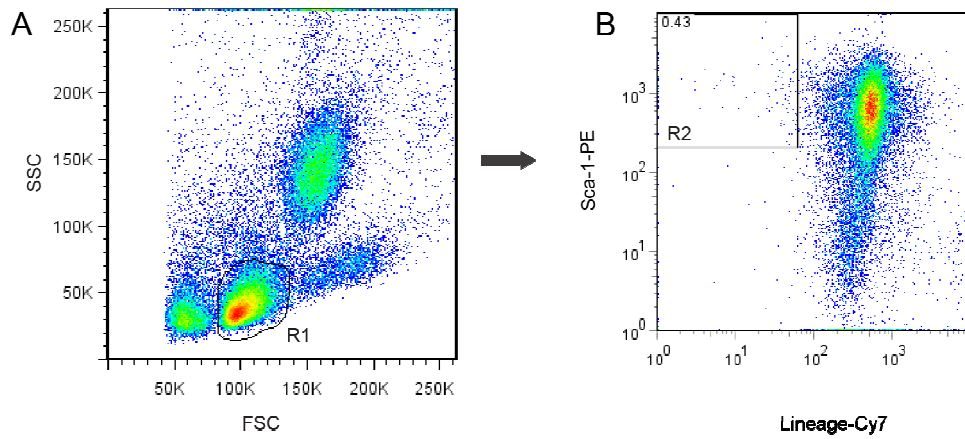


Figure 5. Gating strategy of Sca-1⁺lin^{-/lo} peripheral blood progenitor cells (PBPCs) by flow cytometry. (A) The cell population of interest (R1) excluding platelets, cell debris, monocytes, and neutrophils was gated in a forward (FSC) vs. side scatter (SSC) dot plot. (B) The cell population in the R1 gate was further analyzed for the expression of Sca-1 (stem cell marker) and hematopoietic lineage markers (Lineage), including CD3 (T cell marker), Ter-119 (erythroid cells), CD45R (lymphocytes), CD11b (monocytes/neutrophils), and Ly-6G (monocytes/neutrophils). Sca-1⁺lin^{-/lo} cells were quantified in the R2 gate.

To quantify murine monocyte subtypes (Fig. 6), blood cells were treated with biotinylated anti-mouse CD3, CD45R, and Ter-119 antibodies (1:50 dilution of each Ab) on ice for 30 min, followed by incubation with streptavidin phycoerythrin-Cy7 (1:500 dilution), PE-conjugated Ab against CD115 (1:100) and an PerCP-Cy*5.5-conjugated Gr-1 Ab (1:100) on ice for 30 min

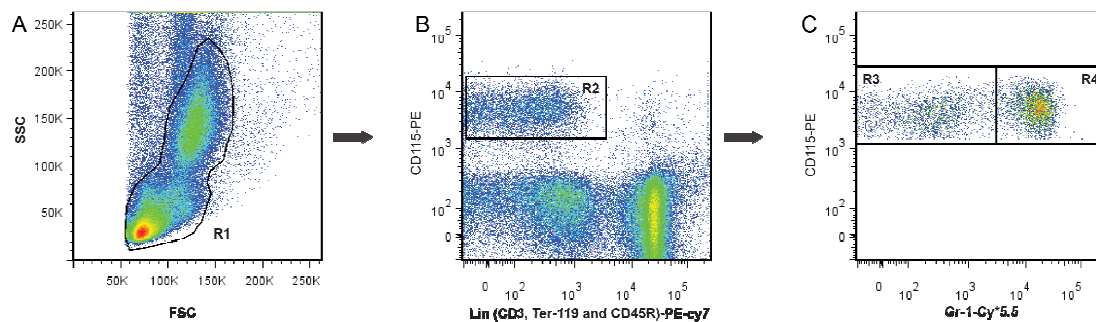


Figure 6. Gating strategy of monocyte subtypes by flow cytometry. (A) The leukocyte population (R1) was gated in a FSC vs. SSC dot plot. (B) The monocyte population (R2) was identified as CD115⁺ and CD3^{-/lo}Ter-119^{-/lo}CD45R^{-/lo}. (C) Monocytes were divided into two subtypes defined as CD115⁺ Gr-1⁺ (R4) and CD115⁺ Gr-1^{-/lo} (R3).

To analyze Cxcr7 protein expression on the cell surface, different cell suspensions were stained with an anti-human/mouse CXCR7 Ab (Table 17) conjugated with phycoerythrin. Cells from *Cxcr7*^{-/-} mice or a PE-conjugated anti-human/mouse IgG2b Ab were used as negative controls.

Data were collected using a flow cytometry (FACSCantoTM II) and analyzed using FlowJo software (TreeStar, Inc., Ashland, USA).

2.2.6 Cxcl12 ELISA

Cxcl12 plasma concentrations were measured following centrifugation (10000g, 4°C, and 15 min). Bone marrow extracellular fluid of femurs was flushed with pre-cold PBS (500 µl), and then the supernatant was obtained after centrifugation (300g, 5 min). Plasma, bone marrow supernatant, and a series of standards were incubated in wells of a microplate coated with anti-mouse Cxcl12 (2.5 h, RT, and gentle shaking). After thoroughly washing, the plate was incubated with a biotinylated anti-mouse Cxcl12 Ab (1 h, RT, and gentle shaking). Following the second washing step, the streptavidin solution was added to the wells (45 min, RT, and gentle shaking). After the third washing step, TMB one-step substrate reagent was added to the wells (30 min, RT, and gentle shaking in the dark). The absorbance in each well was read at 450 nm (Infinite M200) after quenching the reaction using the stop solution. The standard curve created by the standard concentration and absorbance was used to determine the Cxcl12 concentration in the samples. Additionally, the Cxcl12 concentration in the bone marrow was standardized to the protein concentration measured with DC Protein Assay Kit. Absorbance was measured at 450 nm using a plate reader (Infinite M200).

2.2.7 Two-photon laser scanning microscopy

Two-photon laser scanning microscopy (TPLSM) is a novel three-dimensional fluorescence imaging technique based on the excitation of fluorophores by the non-linear absorption of two photons (150, 151). This technology could investigate viable tissues with enhanced penetration depth and imaging resolution, and decreased background and phototoxicity (150, 151).

2.2.7.1 LacZ staining of the carotid artery

Intact arteries were first incubated with chloroquine reagent (300 µM in HBBS, ImaGene Green C12 FDG lacZ Gene Expression Kit) for 30 min at 37°C to inhibit endogenous lysosomal β-D-galactosidase activity. For imaging, arteries were mounted in a perfusion chamber that was then filled with HBSS (GIBCOTM, 10×, 1:10 diluted) and the temperature of artery was constantly maintained at 37°C by a heating platform. To assess the lacZ reporter gene activity, C12 fluorescein di-β-D-

galactopyranoside (C12 FDG, ImaGene Green, Invitrogen, 33 μ M in HBBS) was administered intraluminally with a pressure of 60 mmHg for 90 min. Phenylethyl β -D-thiogalactopyranoside (PETG, ImaGene Green, 1mM in HBBS) was applied to stop the β -gal reaction. Dead cells were excluded by propidium iodide staining to assure that the lacZ signal was only derived from viable cells. Prior to imaging, intraluminal pressure was restored. Arteries were imaged with a multi-photon system (TriM Scope, LaVision Biotec GMBH, Bielefeld, Germany) in single beam mode coupled to a motorized up-right microscope (Olympus BX61WI with a 20 \times NA 0.95 water immersion objective; Olympus GmbH, Hamburg, Germany). For two-photon excitation, the pulsed Ti-Sapphire laser (MaiTai HP, Spectra Physics, Mountain View, US) was tuned to 830 nm for visualization of SHG (second harmonic generation) signals of collagen, C12 FDG, and autofluorescence signals originating from the elastic lamina. Emitted fluorescent signals were detected with PMTs (two-photo multiplier tubes) tuned to corresponding parts of the emission spectra: SHG, 453-497 nm (PMT 1); C12 FDG, 500-550 nm (PMT 2); autofluorescence signals of elastin were detected in both in PMT 1 and PMT 2. Series of x-y plane images were obtained at successive depth (z-stack) using ImSpector Pro 4.0.43 acquisition software (LaVision Biotec GMBH). Further image processing was performed using Image-Pro 3D analyzer 7.0 (Media Cybernetics, Silver Spring, USA)

2.2.7.2 DiI-VLDL uptake into adipose tissues

Intact adipose tissue that was still connected to the circulation was mounted in a perfusion chamber. The chamber was filled with HBSS and the temperature was constantly maintained at 37°C. Adipose tissues were embedded in agarose gels (3% agarose in HBSS), covered with a coverslip (0.17 mm thick), and imaged using the Fluoview FV1000-MPE multi-photon system (Olympus Deutschland GmbH, Hamburg, Germany) coupled to a MaiTai[®] DeepSee[™] HP-DS laser (Newport Spectra-Physics GmbH, Darmstadt, Germany). To determine the autofluorescence of the adipose tissues, images were taken at 730 nm before dye injection. The mice were perfused with PBS to remove DiI-VLDL from the vascular lumen 1 h after IV injection of 1,1'-dioctadecyl-3,3,3',3'-tetramethylindocarbocyanine perchlorate-labeled VLDL (50 μ g/ 20 g, DiI-VLDL; Kalen Biomedical, Montgomery Village, USA). To detect the emitted fluorescent signals, two ultra-sensitive external non-

descanned PMT detectors were tuned to the emission spectra of tissue autofluorescence (495–540 nm) and the DiI dye (575–630 nm). Images (1024 × 1024 pixels) were obtained in the x–y plane using image acquisition software (FV10-ASW Ver3.0; Olympus).

2.2.8 Quantification of cholesterol and DiI concentration in murine tissues

The VAT (approximately 30 µg) was homogenized in 1 ml cell lysis buffer by using TissueLyser LT homogenizer. The cholesterol concentration was determined using a cholesterol assay kit (as described in chapter 2.1.2) and normalized to the protein concentration in the samples, which was measured with DC Protein Assay Kit. Absorbance was measured at 450 nm using a plate reader (Infinite M200).

The VAT and liver were harvested from mice injected with DiI-VLDL after perfusion with PBS. The harvested tissues were homogenized in cell lysis buffer (Table 2) using a TissueLyser LT homogenizer and tissue lysates were obtained after centrifugation (14000 g, 4°C, and 10 min). The DiI fluorescence intensity was measured in the tissue lysates (excitation wavelength: 514 nm; emission wavelength: 565 nm) using a microplate reader (Infinite M200). A standard curve was created using a series of known concentrations of DiI-VLDL. DiI concentration in the lysates was normalized to the protein concentration in the corresponding samples.

2.2.9 SVEC culture protocol

SVEC is a murine lymphoid EC line transfected with virus-40 (152). SVECs were grown to approximately 70% confluence in 6-well plastic tissue culture plates. Then, these cells were treated with medium alone or medium containing TNF- α (10 ng/ml) and IL-1 β (10 ng/ml) for 5 h. Finally, cells were harvested for flow cytometry analysis (110).

2.2.10 Statistical analysis

Data represent the mean \pm SEM. The Student's t-test or 1-way ANOVA followed by Newman-Keuls posttest were used for statistical comparison between groups (Prism, GraphPad Software, La Jolla, USA). *P* values ≤ 0.05 were considered statistically significant.

3. RESULTS

3.1 *Cxcr7* expression patterns

Firstly, the *Cxcr4* and *Cxcr7* mRNA expression levels were compared between leukocytes and different murine tissues by qRT-PCR. *Cxcr7* mRNA was ubiquitously and abundantly expressed in most of the tissues studied, such as arteries, heart, kidney, lung, spleen, and adipose tissue (Fig. 7); however, compared to these tissues, the *Cxcr7* mRNA expression was significantly lower in the bone marrow, liver, and leukocytes. Conversely, *Cxcr4* mRNA expression was lower in the arteries, heart, and kidney compared to bone marrow and leukocytes. In addition, increased expression of *Cxcr4* was found in the lung, spleen, and adipose tissue (Fig. 7). Following vascular injury of the carotid artery in *Apoe*^{-/-} mice, the mRNA expression of *Cxcr4* was significantly increased after 1 and 2 wks, while the *Cxcr7* expression was unaltered compared to uninjured carotid arteries (Fig. 8). In summary, the transcriptional expression pattern of *Cxcr7* differs substantially from that of *Cxcr4* except in the lung, spleen, and adipose tissue, where both *Cxcr7* and *Cxcr4* are highly expressed.

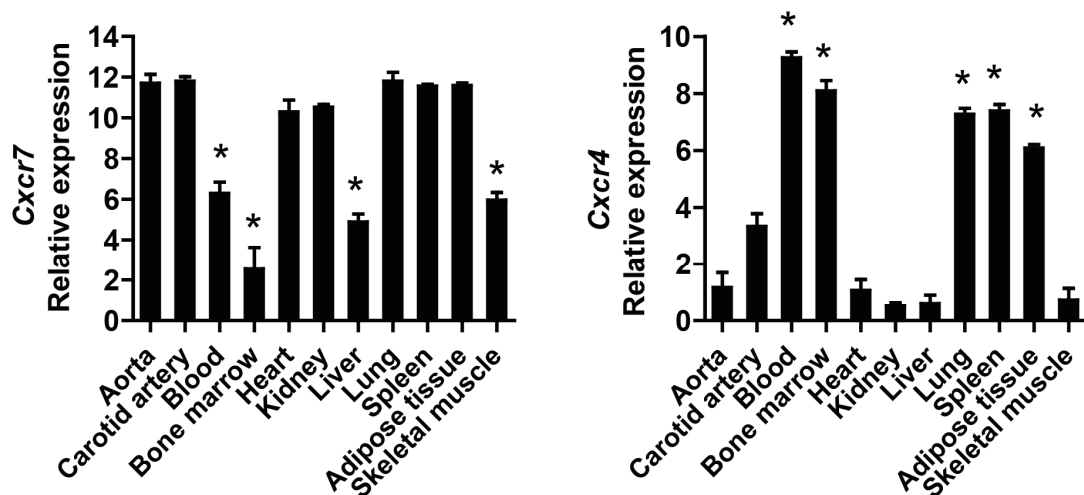


Figure 7. *Cxcr7* and *Cxcr4* mRNA expression pattern in *Apoe*^{-/-} mice. Transcripts for *Cxcr7* and *Cxcr4* were quantified in leukocytes and various tissues of mice by qRT-PCR (n = 3 mice per group). **P* < 0.0001 versus carotid artery.

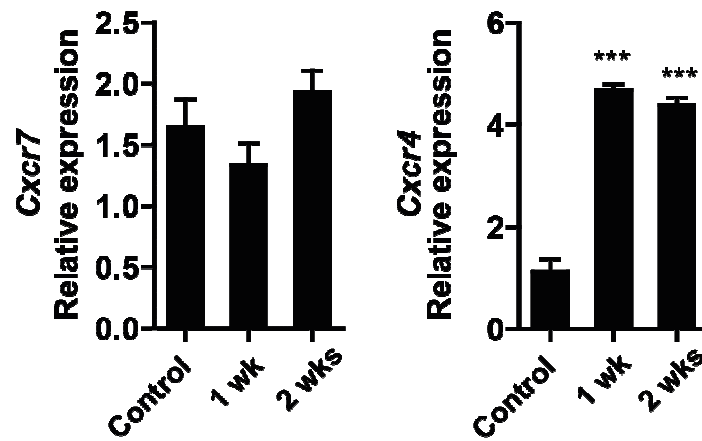


Figure 8. *Cxcr7* and *Cxcr4* mRNA expression after carotid injury in *Apoe*^{-/-} mice. Quantification of *Cxcr7* and *Cxcr4* mRNA levels in normal (control, n = 11) and injured carotid arteries (n = 5 to 6 mice per group). ****P* < 0.0001, versus normal carotid arteries at the indicated time points after vascular injury.

To study the cellular localization of the *Cxcr7* expression, *Cxcr7* promoter activity was studied in different tissues of *Cxcr7*^{lacZ/+} mice by X-gal staining. Activity of the reporter protein, β-gal, indicating *Cxcr7* transcription, was detectable in the marginal and/or sinusoidal zones of the spleen, in epithelial cells of kidney, lung, spleen, and in cardiomyocytes, but not in hepatocytes (Fig. 9). In the kidney, intensive X-gal staining was also detectable in the glomeruli. Moreover, X-gal staining was observed in the endothelial and adventitial cells of the aorta, and in the endothelium covering the aortic valves.

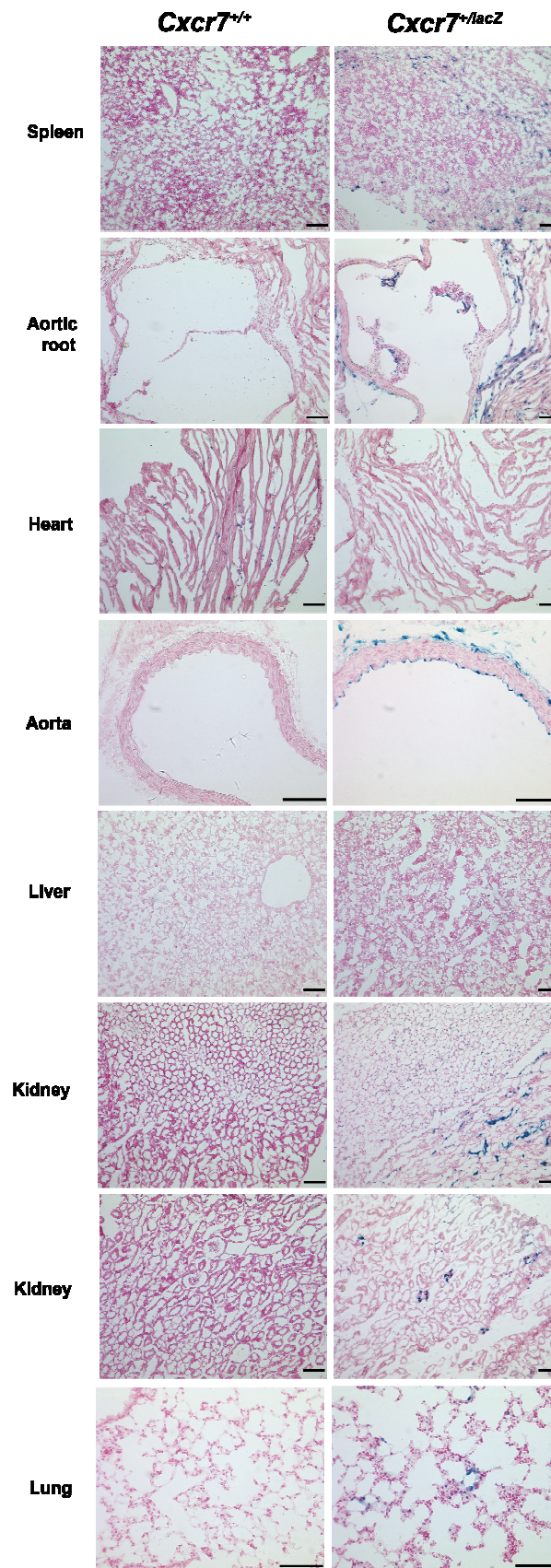


Figure 9. X-gal staining in tissues from *Cxcr7*^{+/lacZ} and *Cxcr7*^{+/+} mice. Representative images of X-gal staining are shown (n = 3 mice per mouse). Scale bars, 200 μ m.

The cellular localization of *Cxcr7* expression in the carotid arteries was further studied by TPLSM in *ex vivo* perfused carotid arteries of *Cxcr7^{+/lacZ}* and *Cxcr7^{+/+}* mice using a β -gal substrate that is converted to a fluorescent dye by β -gal. *Cxcr7* reporter expression was detectable in the ECs but not in the SMCs of carotid arteries by TPLSM (Fig. 10). Thus, *Cxcr7* transcription was primarily found in the endothelium of arterial vessels.

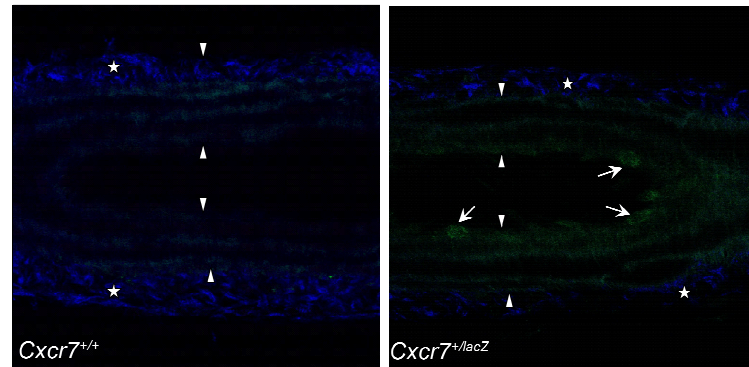


Figure 10. β -gal activity in the endothelium of carotid arteries from *Cxcr7^{+/lacZ}* and *Cxcr7^{+/+}* mice. Representative images of *lacZ⁺* cells (green) obtained by TPLSM in the viable carotid arteries (n = 3 mice per group). Arrows indicate positive staining. Arrowheads indicate internal and external elastic membranes. Stars represent collagen (blue autofluorescence).

Next, *Cxcr7* protein expression was investigated in different murine tissues by immunostaining. *Cxcr7* protein expression was not detectable in the liver and carotid arteries by immunostaining. In accordance with the *Cxcr7* promoter activity, *Cxcr7* positive immunostaining was found in the spleen, kidney, and endothelium of the aortic valves (Fig. 11). Co-staining for *Cxcr7* and CD31 further confirmed that *Cxcr7* expression was restricted to the CD31⁺ ECs in the leaflets of the aortic valve (Fig. 12). However, *Cxcr7* immunostaining was absent in neointimal macrophages, SMCs, and ECs of the carotid artery (Fig. 11 and 13).

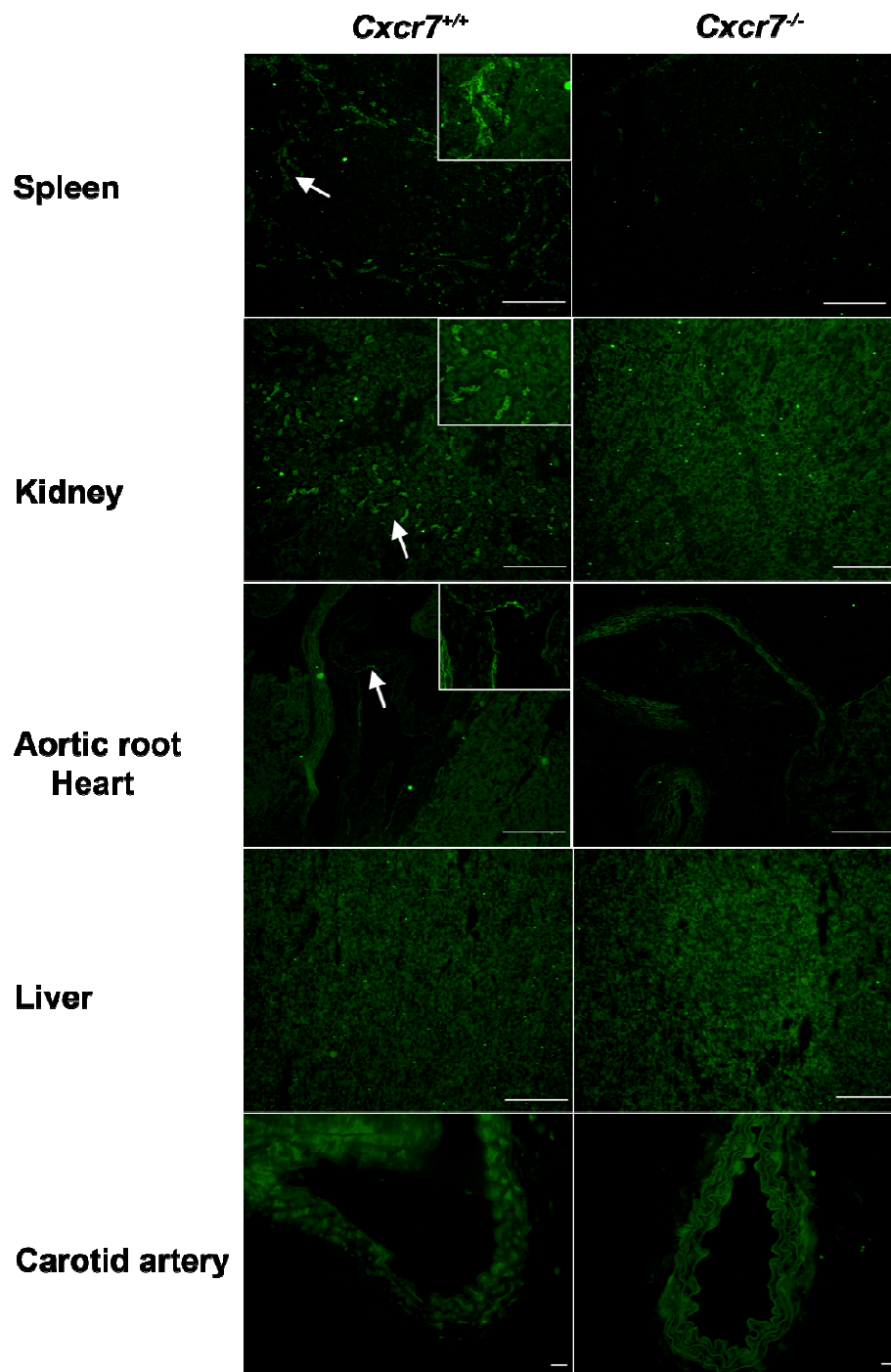


Figure 11. Cxcr7 protein expression patterns. (A) Immunostaining of Cxcr7 in the spleen, kidney, the aortic root, liver, and carotid artery from *Cxcr7*^{+/+} was performed. *Cxcr7*^{-/-} mice served as negative controls (n = 3 mice per group). Scale bars, 200 μm. The rectangle shows a high magnification view of the positive area indicated by the arrows.

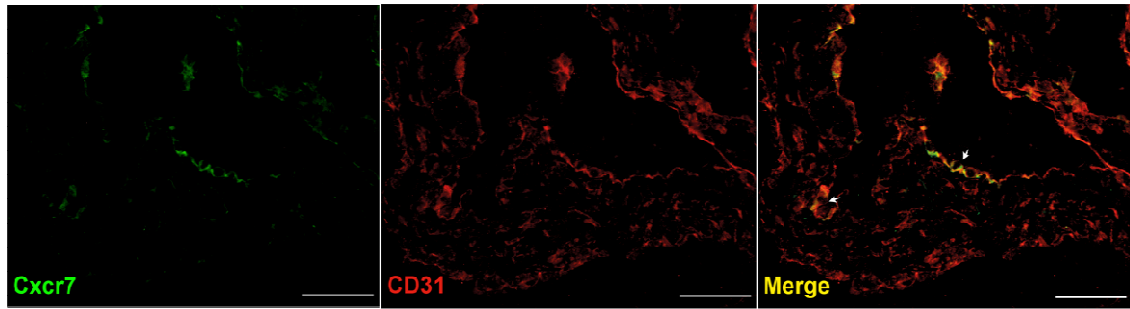


Figure 12. Endothelial expression of Cxcr7. Double-immunostaining of Cxcr7 and CD31 in aortic valves (n = 3 mice per group). Arrows point to the co-stained area. Scale bars, 200 μ m.

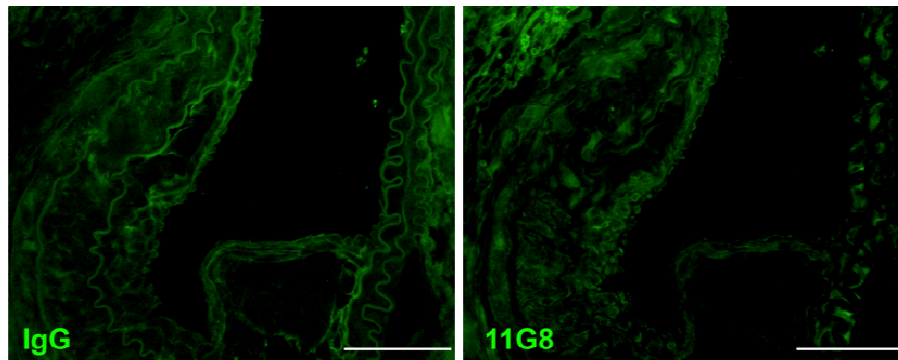


Figure 13. Absence of Cxcr7 protein expression in the neointima of carotid artery. (A) Immunostaining of Cxcr7 (11G8 antibody) was performed in the neointima of carotid arteries from *Apoe*^{-/-} mice. Negative control stainings were performed using isotype IgG (n = 3 mice per group). Scale bars, 50 μ m.

In addition, Cxcr7 protein expression was analyzed on hematopoietic cells by flow cytometry (Fig. 14). Cxcr7 was not detectable in murine peripheral leukocytes, bone marrow cells, or platelets. Expression of Cxcr7 was found on unstimulated SVECs, and on SVECs activated with TNF- α and IL-1 β .

In summary, *Cxcr7* promoter activity and expression at the mRNA and protein level were consistently present in the spleen and in ECs of aortic valves.

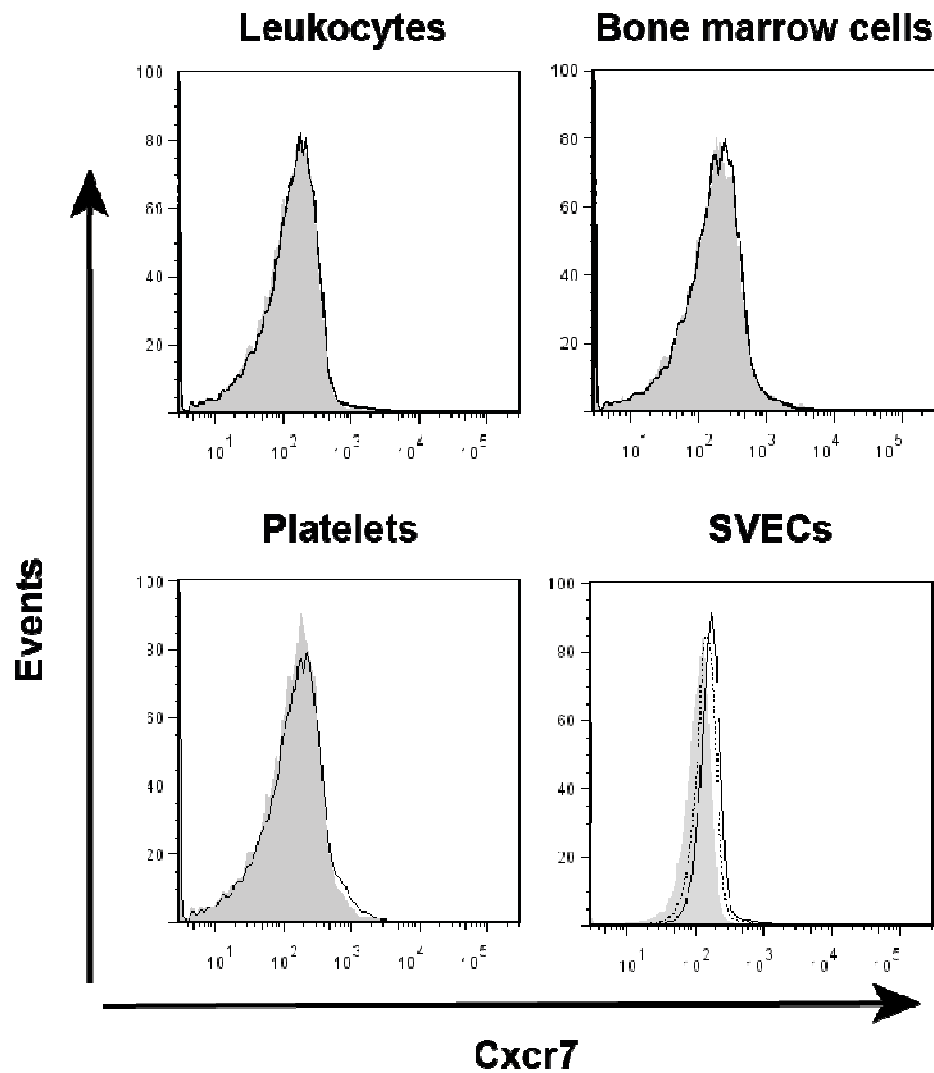


Figure 14. Cxcr7 protein expression on murine hematopoietic cells and ECs. Cxcr7 expression on leukocytes, bone marrow cells, or platelets from *Cxcr7*^{+/+} (open histogram) and *Cxcr7*^{-/-} mice (shaded histogram) was studied by flow cytometry (n = 3 per group). SVECs (isotype control antibody, shaded histogram; Cxcr7 antibody, dotted histogram) and activated SVEC (treated with 10 ng/ml TNF- α and 10 ng/ml IL-1 β for 5 h, open histogram with solid line) served as positive control. Representative data from three independent experiments are shown.

3.2 Role of Cxcr7 on neointima formation

3.2.1 Conditional Cxcr7 deletion exacerbated neointimal hyperplasia

To explore the function of Cxcr7, an inducible *Cxcr7* knockout model was established by using *CAG-Cre*⁺*Cxcr7*^{fllox}*Apoe*^{-/-} mice in which Cxcr7 is deleted following activation of a ubiquitously expressed Cre-recombinase by TMX. *CAG-Cre*⁻*Cxcr7*^{fllox}*Apoe*^{-/-} mice served as controls. Firstly, *Cxcr7* deletion was confirmed by Cxcr7 immunostaining and semi-quantitative PCR with Cxcr7-specific primers. In contrast to *CAG-Cre*⁻*Cxcr7*^{fllox}*Apoe*^{-/-}

mice, *Cxcr7* immunostaining was no longer observed in the spleen at 2 wks after TMX treatment (Fig. 15). Moreover, the band intensity of the *Cxcr7* product amplified from genomic DNA of *CAG-Cre⁺Cxcr7^{fllox}Apoe^{-/-}* mice was substantially reduced compared to *CAG-Cre⁻Cxcr7^{fllox}Apoe^{-/-}* mice at 2 wks after TMX treatment (Fig. 16). Therefore, knockdown of *Cxcr7* in *CAG-Cre⁺Cxcr7^{fllox}Apoe^{-/-}* mice was verified at the protein level in the spleen and deletion of the *Cxcr7* gene was detected at the DNA level.

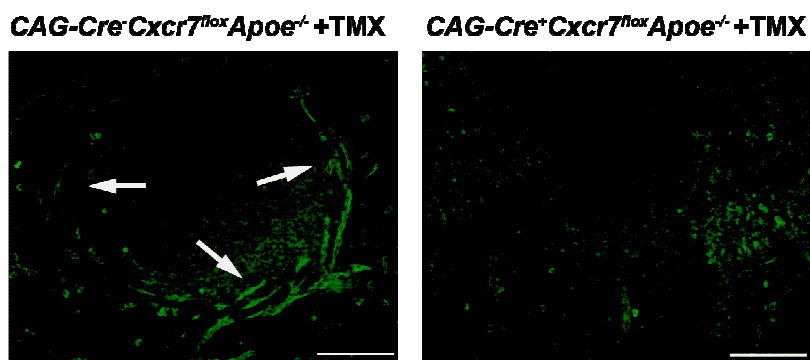


Figure 15. *Cxcr7* was efficiently deleted by Cre-recombinase in the spleen. *Cxcr7* immunostaining (green) was performed in spleen sections from *CAG-Cre⁻Cxcr7^{fllox}Apoe^{-/-}* and *CAG-Cre⁺Cxcr7^{fllox}Apoe^{-/-}* mice at 2 wks after TMX treatment (n = 4 mice per group). Representative images are shown. Arrows indicate the *Cxcr7* positive staining. Scale bars, 200 μ m.



Figure 16. The *Cxcr7* gene was deleted by Cre-recombinase activation. Semi-quantitative PCR with specific primers for *Cxcr7*, Cre-recombinase, and an internal control was performed on genomic DNA samples, which were isolated from the tails of *CAG-Cre⁻Cxcr7^{fllox}Apoe^{-/-}* and *CAG-Cre⁺Cxcr7^{fllox}Apoe^{-/-}* mice 2 wks after TMX treatment (n = 2 mice per group). A representative gel is shown.

To evaluate the function of *Cxcr7* in the neointima formation, vascular injury was carried out in *CAG-Cre⁺Cxcr7^{fllox}Apoe^{-/-}* mice and *CAG-Cre⁻Cxcr7^{fllox}Apoe^{-/-}* mice 2 wks after TMX treatment. The neointimal area was increased in the carotid arteries of TMX-treated *CAG-Cre⁺Cxcr7^{fllox}Apoe^{-/-}* mice fed a HCD at 4 wks after vascular injury

compared to TMX-treated *CAG-Cre⁻Cxcr7^{fllox}Apoe^{-/-}* mice (Fig. 17). However, the medial area was not significantly different between these two groups (Fig. 17).

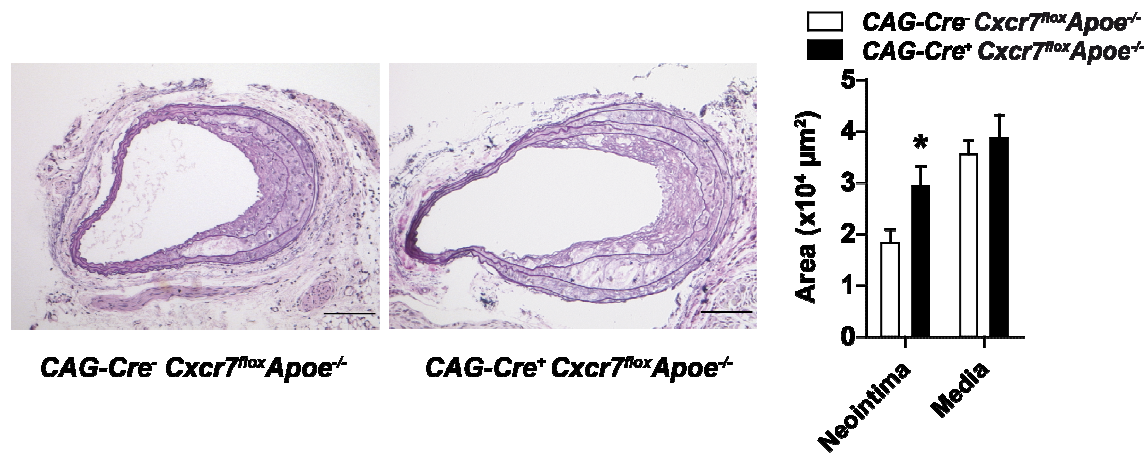


Figure 17. Effect of *Cxcr7* deficiency on neointima formation. The neointimal and medial areas were quantified by planimetry in EVG-stained sections of carotid arteries 4 wks after wire injury in *Apoe^{-/-}* mice in which *Cxcr7* was deleted by an ubiquitously expressed Cre-recombinase after TMX treatment (*CAG-Cre⁺Cxcr7^{fllox}Apoe^{-/-}* mice). TMX-treated *CAG-Cre⁻Cxcr7^{fllox}Apoe^{-/-}* mice that do not express Cre-recombinase were used as controls (n = 8 mice per group). Representative images of the EVG-stained carotid sections are shown. Scale bars, 100 μm; **P* < 0.05.

The effects of *Cxcr7* deficiency on the cellular composition of the neointima were determined by immunostaining of macrophage-specific Mac-2 or SMC-specific α -SMA. The number of Mac-2 immunopositive cells in the neointima was significantly higher in *CAG-Cre⁺Cxcr7^{fllox}Apoe^{-/-}* than in *CAG-Cre⁻Cxcr7^{fllox}Apoe^{-/-}* mice (Fig. 18A). In contrast, the α -SMA immunopositive area in the neointima was not significantly different between *Cre⁺Cxcr7^{fllox}Apoe^{-/-}* and *CAG-Cre⁻Cxcr7^{fllox}Apoe^{-/-}* mice (Fig. 18B). These results indicate that *Cxcr7* deficiency increases the accumulation of macrophages in the neointimal lesions, whereas *Cxcr7* does not affect the relative neointimal SMC content.

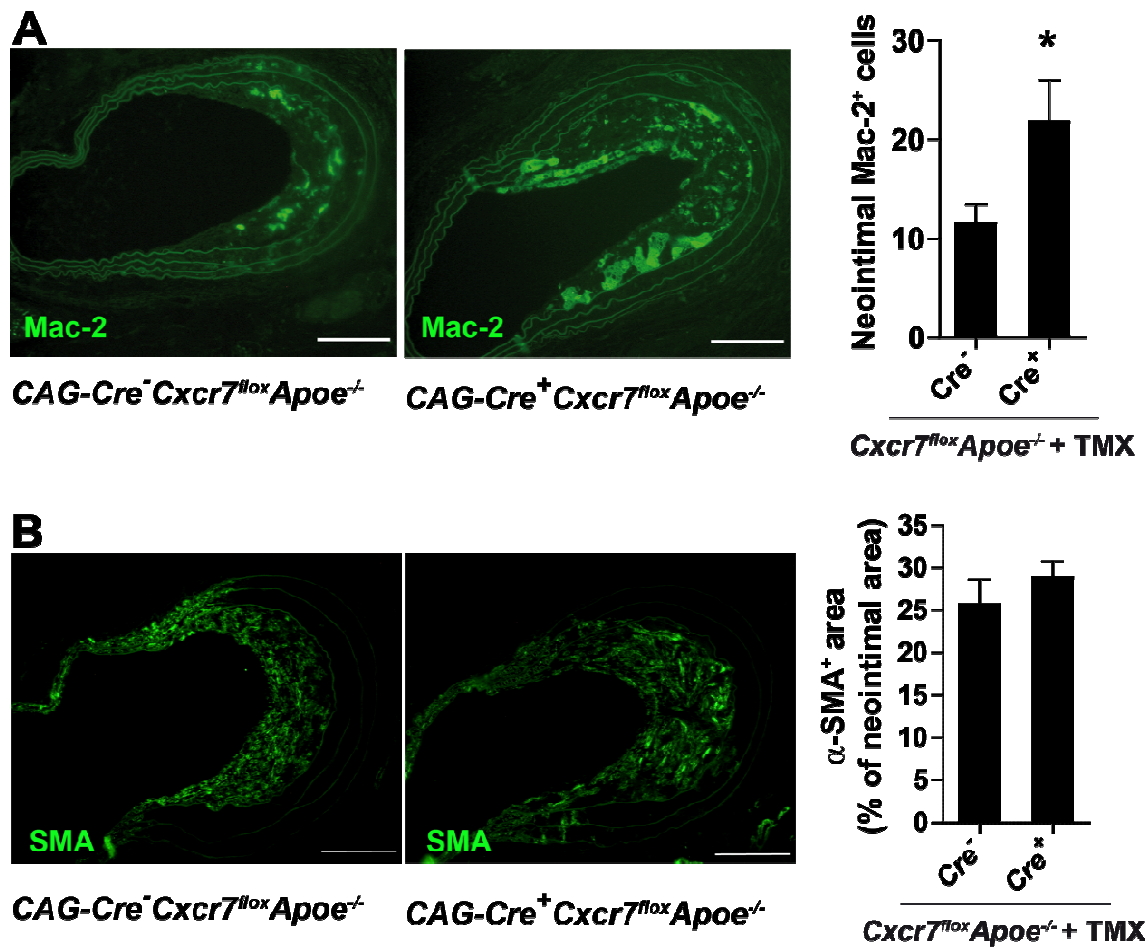


Figure 18. Effects of *Cxcr7* deficiency on the cellular composition of the neointima. Quantification of the neointimal macrophage cell number (A) and the relative SMC content (B) was performed by Mac-2 and α -SMA immunostaining, respectively. Representative images of Mac-2 and α -SMA immunostainings are shown ($n = 6$ to 8 , $*P < 0.05$). Scale bars, $100\ \mu\text{m}$.

The Cxcl12/Cxcr4 axis plays a crucial role in neointima formation via mobilization of SPCs after vascular injury (88, 89, 153). To test whether *Cxcr7* affects the Cxcl12-mediated SPC mobilization following vascular injury, circulating levels of Sca-1⁺Lin⁻ cells were measured 1 d before and 1 d after vascular injury. The injury-induced increase of Sca-1⁺Lin⁻ cells at 1 d after injury was similar in *CAG-Cre⁺Cxcr7^{flox}Apoe^{-/-}* and *CAG-Cre⁻Cxcr7^{flox}Apoe^{-/-}* mice (Fig. 19), suggesting that *Cxcr7* is not involved in the mobilization of SPCs after vascular injury.

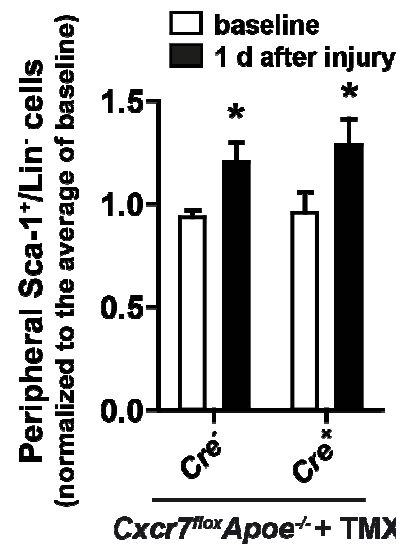


Figure 19. Effects of Cxcr7 deficiency on injury-induced SPC mobilization. The Sca-1⁺/Lin⁻ cell population was measured at 1 d before (baseline) and 1 d after carotid injury in *CAG-Cre⁺Cxcr7^{lox}Apoe^{-/-}* and *CAG-Cre⁻Cxcr7^{lox}Apoe^{-/-}* mice (n = 7 to 8, **P* < 0.05, the values after injury versus the corresponding baseline).

Cxcr7 can internalize and degrade Cxcl12, thus modulating the extracellular availability of Cxcl12 (132, 134). To study whether Cxcr7 affects the levels of Cxcl12 in the plasma and bone marrow after vascular injury, Cxcl12 concentrations were determined by ELISA. The Cxcl12 levels in the plasma and in the bone marrow of *CAG-Cre⁺Cxcr7^{lox}Apoe^{-/-}* mice were higher than in *CAG-Cre⁻Cxcr7^{lox}Apoe^{-/-}* mice at 4 wks after injury (Fig. 20), suggesting that Cxcr7 might regulate the Cxcl12 concentration in the plasma and bone marrow in a similar way.

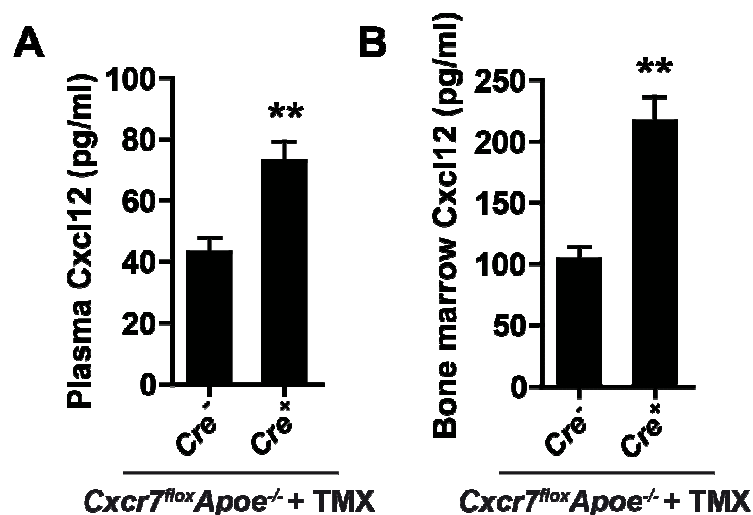


Figure 20. Effects of Cxcr7 deficiency on Cxcl12 concentrations. Cxcl12 levels were quantified in the plasma (A, n = 9, ***P* < 0.01) and bone marrow (B, n = 5, ***P* < 0.01) of *CAG-Cre⁺Cxcr7^{lox}Apoe^{-/-}* and *CAG-Cre⁻Cxcr7^{lox}Apoe^{-/-}* mice 4 wks after carotid injury by ELISA.

The role of hypercholesterolemia in the protective effects of *Cxcr7* on neointima formation was investigated in *CAG-Cre⁺Cxcr7^{fllox}Apoe^{+/+}* and *CAG-Cre⁻Cxcr7^{fllox}Apoe^{+/+}* mice, which develop only a mild hyperlipidemia in response to a HCD. Interestingly, the neointima formation was not significantly different between *CAG-Cre⁺Cxcr7^{fllox}Apoe^{+/+}* and *CAG-Cre⁻Cxcr7^{fllox}Apoe^{+/+}* mice (Fig. 21). The medial area was also similar between these groups (Fig. 21). Thus, these data indicate that hypercholesterolemia in *Apoe^{-/-}* mice crucially determines the effect of *Cxcr7* on the neointima formation.

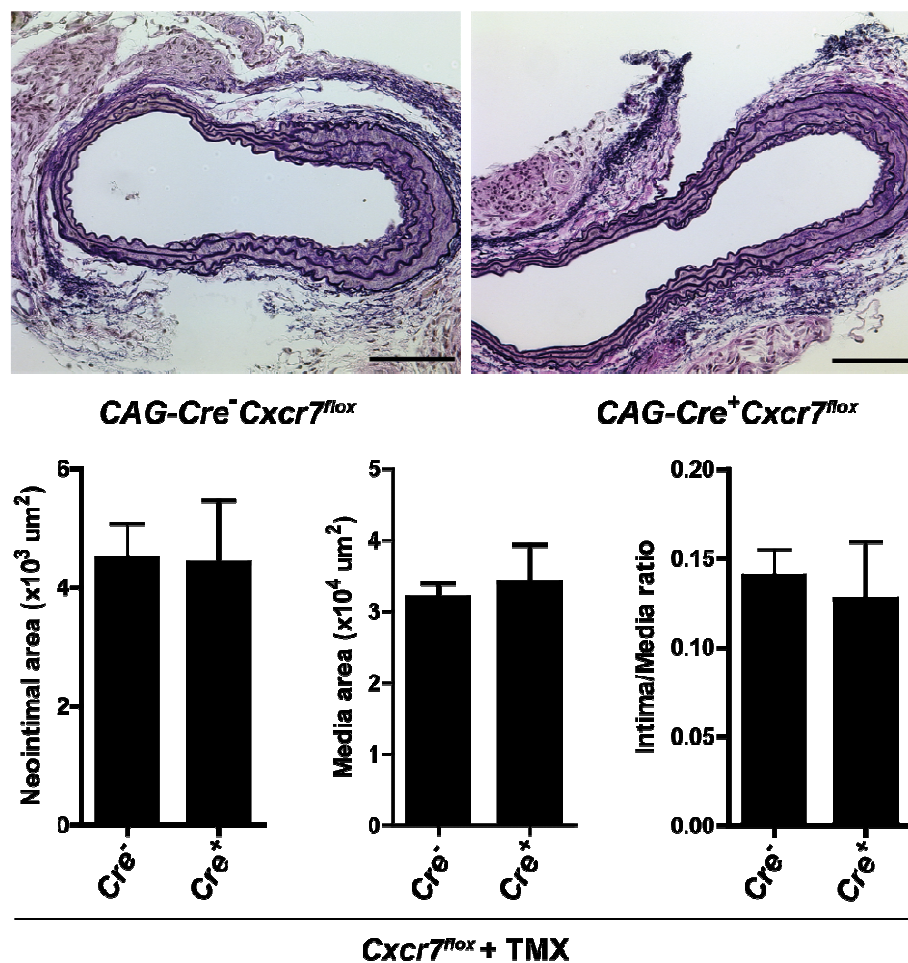


Figure 21. *Cxcr7* deficiency in *Apoe^{+/+}* mice did not affect neointima formation. Quantification of the neointimal and medial areas in carotid arteries 4 wks after wire injury in *Apoe^{+/+}* mice fed a HCD in which *Cxcr7* was deleted by activation of ubiquitously expressed Cre-recombinase via TMX (*CAG-Cre⁺Cxcr7^{fllox}Apoe^{+/+}* mice). TMX-treated *CAG-Cre⁺Cxcr7^{fllox}Apoe^{+/+}* mice that do not express Cre-recombinase served as control. Representative images of EVG-stained carotid sections are shown (n = 7 to 8 mice per group). Scale bars, 100 μm.

To identify the cause for the aggravated neointimal hyperplasia in severe hyperlipidemic *Cxcr7*^{-/-} mice, lipid levels and peripheral monocyte counts were analyzed following vascular injury. The serum cholesterol and triglyceride levels were significantly increased in *Apoe*^{-/-} mice compared with *Apoe*^{+/+} mice fed a HCD (Figs. 22A and B). Notably, the serum cholesterol and triglyceride levels were higher in *CAG-Cre*⁺*Cxcr7*^{fllox}*Apoe*^{-/-} than in *CAG-Cre*⁻*Cxcr7*^{fllox}*Apoe*^{-/-} mice after 4 wks of a HCD (Figs. 22A and B), whereas no significant difference in the serum cholesterol and triglyceride levels were observed between *CAG-Cre*⁺*Cxcr7*^{fllox}*Apoe*^{+/+} mice and *CAG-Cre*⁻*Cxcr7*^{fllox}*Apoe*^{+/+} mice. In parallel to the changes of the lipid levels, peripheral monocyte counts were also higher in *Apoe*^{-/-} than in *Apoe*^{+/+} mice (Fig. 22C). Moreover, absence of *Cxcr7* increased the peripheral monocyte count in *Apoe*^{-/-} but not in *Apoe*^{+/+} mice (Fig. 22C). Despite the differences in the serum lipid levels, body weights were not altered in *CAG-Cre*⁺*Cxcr7*^{fllox}*Apoe*^{-/-} compared with *CAG-Cre*⁻*Cxcr7*^{fllox}*Apoe*^{-/-} mice after 4 wks of a HCD (Fig. 22D). These findings indicate that *Cxcr7* limits severe hyperlipidemia and monocytosis in *Apoe*^{-/-} mice.

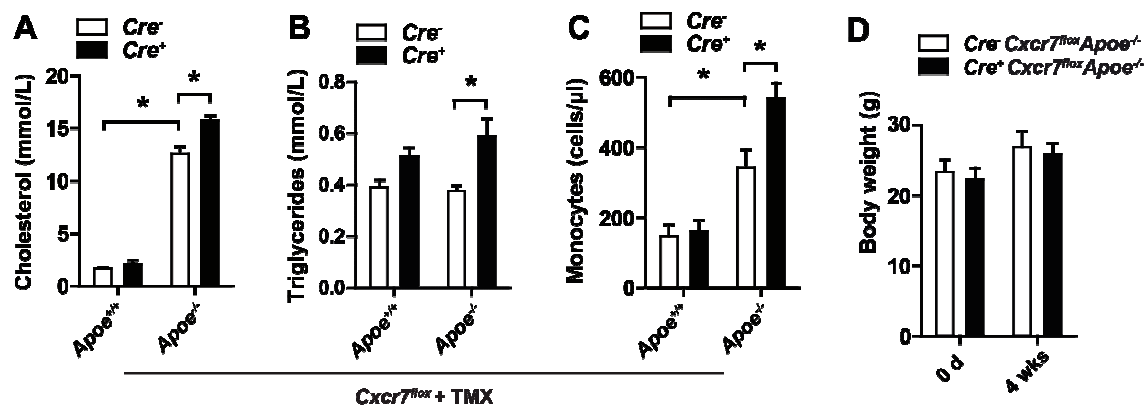


Figure 22. Effect of *Cxcr7* deficiency on hyperlipidemia and hyperlipidemia-induced monocytosis. The serum cholesterol levels (A), triglyceride levels (B), and peripheral monocyte counts (C) were measured in TMX-treated *CAG-Cre*⁻*Cxcr7*^{fllox} and *CAG-Cre*⁺*Cxcr7*^{fllox} mice (either *Apoe*^{+/+} or *Apoe*^{-/-} mice) fed a HCD 4 wks after injury (n = 4 to 10 mice per group). **P* < 0.05. (D) The body weight of *CAG-Cre*⁻*Cxcr7*^{fllox}*Apoe*^{-/-} and *CAG-Cre*⁺*Cxcr7*^{fllox}*Apoe*^{-/-} mice was determined before (0 d) and 4 wks after injury (n = 8 mice per group).

3.2.2 Role of *Cxcr7* in bone marrow cells on neointima formation

To evaluate the role of *Cxcr7* expressed in bone marrow cells on neointima formation, vascular injury was carried out in *Apoe*^{-/-} mice, which were repopulated with bone marrow cells from *CAG-Cre*⁺*Cxcr7*^{fllox}*Apoe*^{-/-} or *CAG-Cre*⁻*Cxcr7*^{fllox}*Apoe*^{-/-} mice and

subsequently treated with TMX. Deletion of the *Cxcr7* gene in bone marrow cells did neither affect neointima formation (Fig. 23), macrophage accumulation (Fig. 24), the relative SMCs content (Fig. 24), serum cholesterol levels, triglycerides levels, nor the peripheral blood cell counts (Fig. 25) significantly.

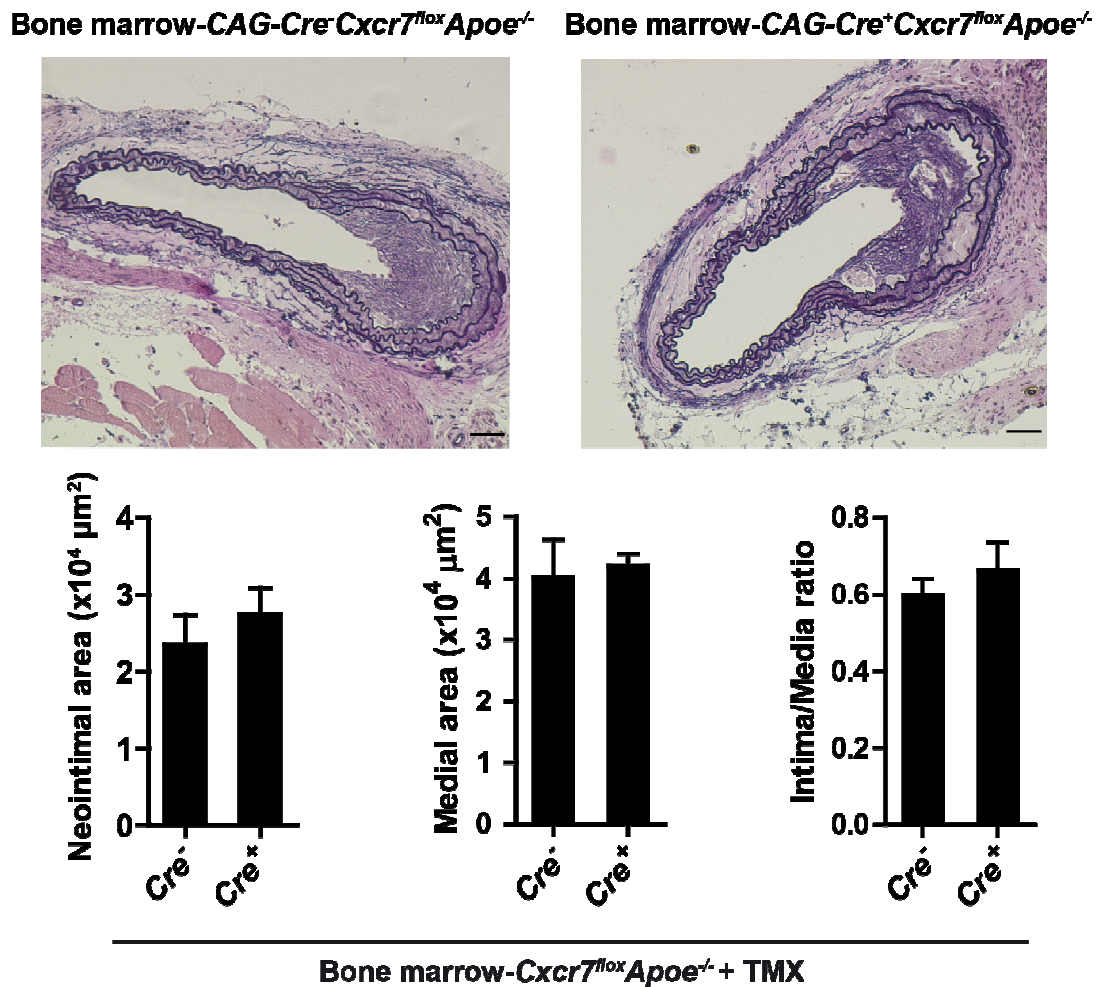


Figure 23. *Cxcr7* deficient bone marrow did not affect neointima formation. Quantification of the neointimal and medial areas in carotid arteries 4 wks after wire injury in *Apoe*^{-/-} mice, which were treated with TMX after repopulation with bone marrow from *CAG-Cre⁻CXCR7^{fllox}Apoe^{-/-}* or *CAG-Cre⁺CXCR7^{fllox}Apoe^{-/-}* mice. Representative images of EVG-stained carotid sections are shown (n = 4 mice per group). Scale bars, 100 μm.

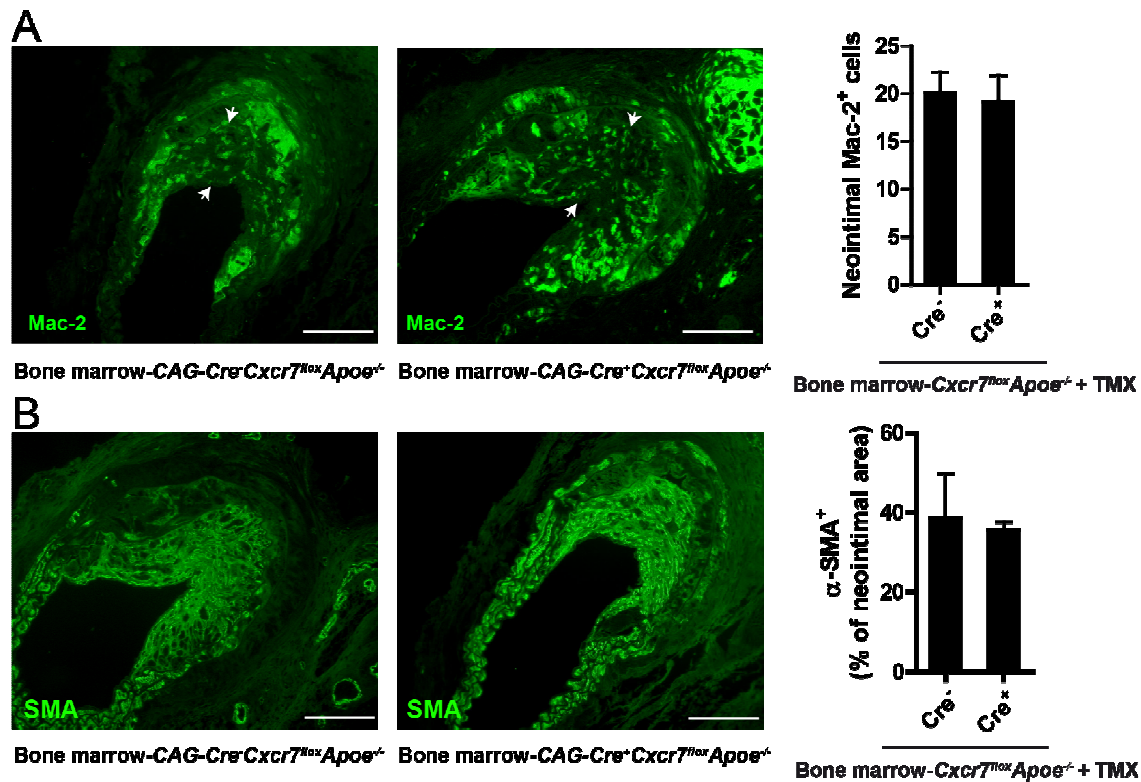


Figure 24. *Cxcr7* deficient bone marrow did not affect the cellular composition of the neointima. Quantification of the neointimal Mac-2 immunopositive cell number (A) and the relative SMC content (B) was performed in Mac-2 and α-SMA immunostained carotid section 4 wks after wire injury in *Apoe*^{-/-} mice harboring bone marrow from CAG-Cre⁻CXCR7^{fllox}Apoe^{-/-} or CAG-Cre⁺CXCR7^{fllox}Apoe^{-/-} mice. Mice were treated with TMX after BMT. Arrows delineate the neointima. Representative images of Mac-2 immunostaining are shown (n = 4 mice per group). Scale bars, 100 μm.

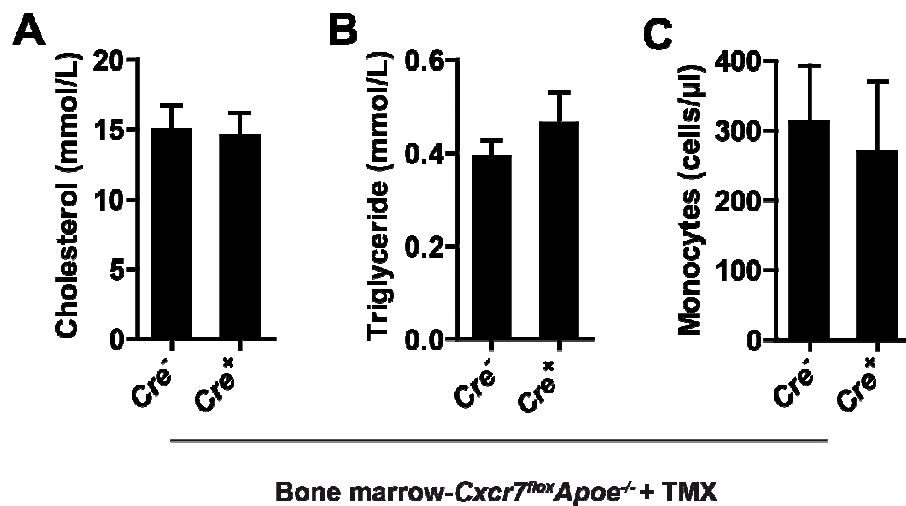


Figure 25. *Cxcr7* deficient bone marrow did not affect lipid levels and monocytosis. The serum cholesterol levels (A), triglyceride levels (B), and peripheral monocyte counts (C) were measured in *Apoe*^{-/-} mice, which were repopulated with bone marrow from CAG-Cre⁻CXCR7^{fllox}Apoe^{-/-} or CAG-Cre⁺CXCR7^{fllox}Apoe^{-/-} mice 4 wks after injury and feeding a HCD. Mice were treated with TMX after the BMT (n = 3 to 4 mice per group).

3.3 Pharmacological targeting of Cxcr7 in neointima formation

3.3.1 Effect of CCX771 treatment on neointima formation

The effect of the synthetic Cxcr7 ligand CCX771 on neointima formation was studied in hyperlipidemic *Apoe*^{-/-} mice following vascular injury. Subcutaneous injection of CCX771 (10 mg/kg) to *Apoe*^{-/-} mice resulted in mean CCX771 plasma levels of 336 ± 13 ng/ml after 1 h and 106 ± 5 ng/ml after 12 h as assessed by LC-MS (Fig. 26).

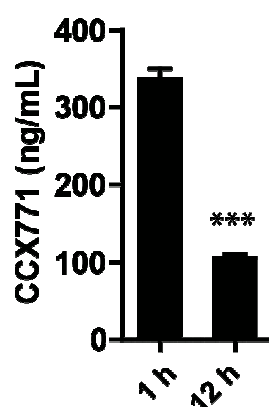


Figure 26. Plasma concentrations of CCX771. CCX771 (10 mg/kg) dissolved in vehicle (10% Captisol) was subcutaneously injected to *Apoe*^{-/-} and the plasma concentrations were determined at 1 h and 12 h after injection by LC-MS (n = 9 mice per group; ****P* < 0.0001 versus 1 h).

To study the effect of CCX771 on neointima formation, *Apoe*^{-/-} mice fed a HCD were treated daily with CCX771 (10 mg/kg, s.c.) or vehicle (10% Captisol) after wire-induced carotid injury. In contrast to the effect of *Cxcr7* deficiency, CCX771 treatment reduced the neointimal area by 39% compared with vehicle treatment at 4 wks after vascular injury. However, the medial area of the carotid arteries was not different between the CCX771- and vehicle-treated mice (Fig. 27).

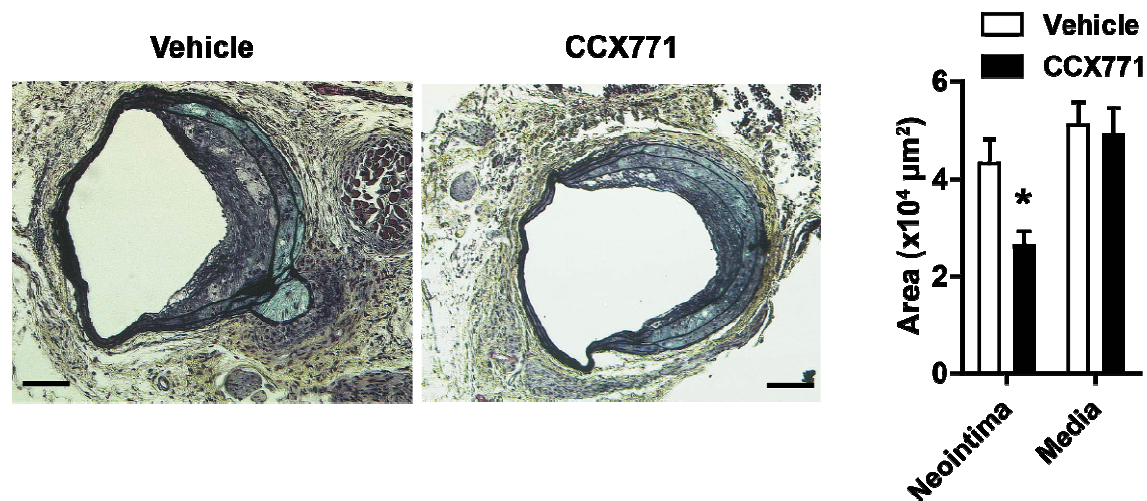


Figure 27. Effects of CCX771 treatment on neointima formation after vascular injury in *Apoe*^{-/-} mice. The neointimal and medial areas were quantified by planimetry in Movat-stained sections of carotid arteries 4 wks after vascular injury in *Apoe*^{-/-} mice (n= 7 to 8 mice per group). Representative images of Movat-stained carotid sections are shown. Scale bars, 100 μm; **P* < 0.05 versus vehicle.

The effects of CCX771 treatment on the cellular composition of the neointima were studied by immunostaining of macrophage-specific Mac-2 antibody or SMC-specific α -SMA antibody. Treatment with CCX771 reduced the number of Mac-2 immunopositive cells in neointima (Fig. 28A); however, the relative neointimal α -SMA immunopositive area was not significantly different between CCX771- and vehicle-treated mice (Fig. 28B). These results indicate that CCX771 treatment decreases the accumulation of macrophages in the neointima, whereas the relative SMC content in the neointima is not altered by CCX771-treatment.

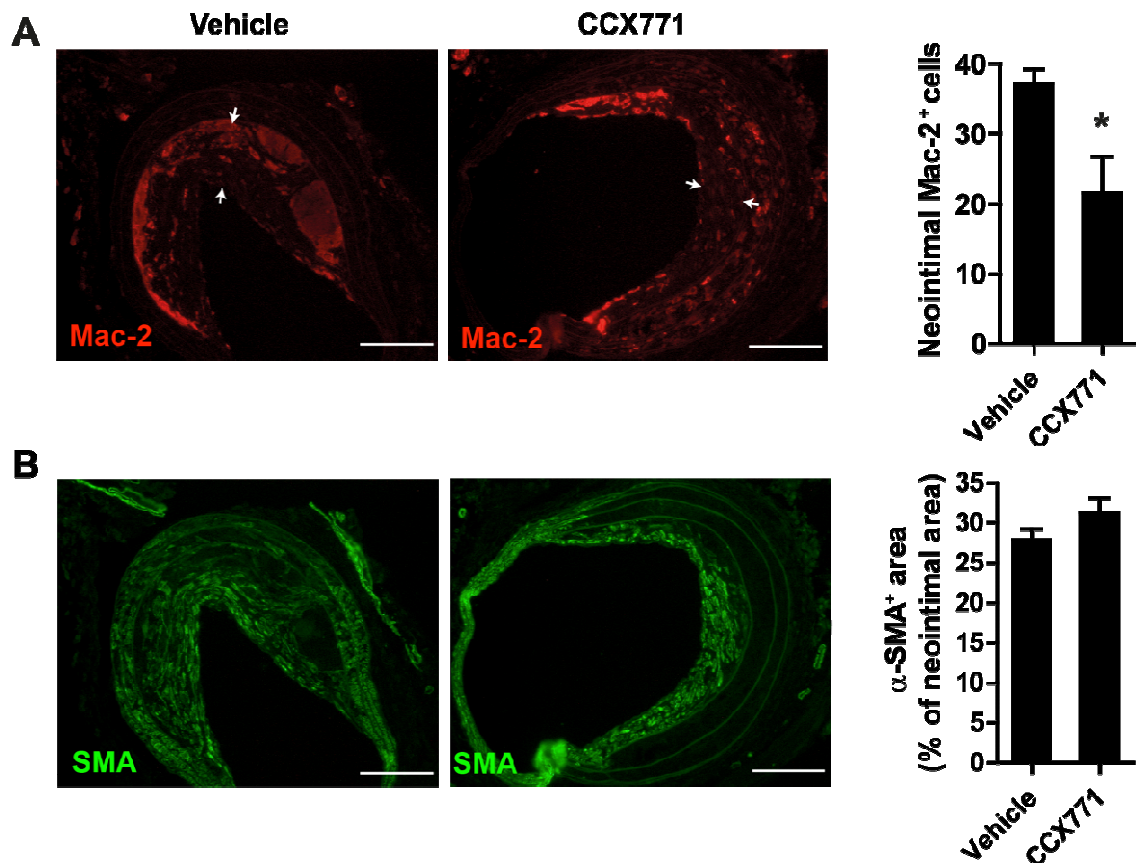


Figure 28. Effects of CCX771 treatment on the cellular composition of the neointima. Quantification of the neointimal Mac-2-immunopositive cell number (A) and the neointimal α -SMA-immunopositive area (B) 4 wks after wire injury in carotid sections of *Apoe*^{-/-} mice treated with vehicle or CCX771 (n= 7 to 8 mice per group). Arrows delineate the neointima. Representative images of Mac-2 and α -SMA immunostainings are shown (n= 7 to 8 mice per group). Scale bars, 100 μ m; **P* < 0.05.

To test whether CCX771 treatment affects the Cxcl12-mediated mobilization of SPCs, circulating Sca-1⁺/Lin⁻ cells were quantified 1 d before and 1 d after vascular injury by flow cytometry. Similar to the results obtained in mice with a conditional *Cxcr7* knockout, treatment with CCX771 did not affect the injury-induced increase of Sca-1⁺/Lin⁻ cells (Fig. 29), suggesting that CCX771 treatment does not interfere with the SPC mobilization after vascular injury.

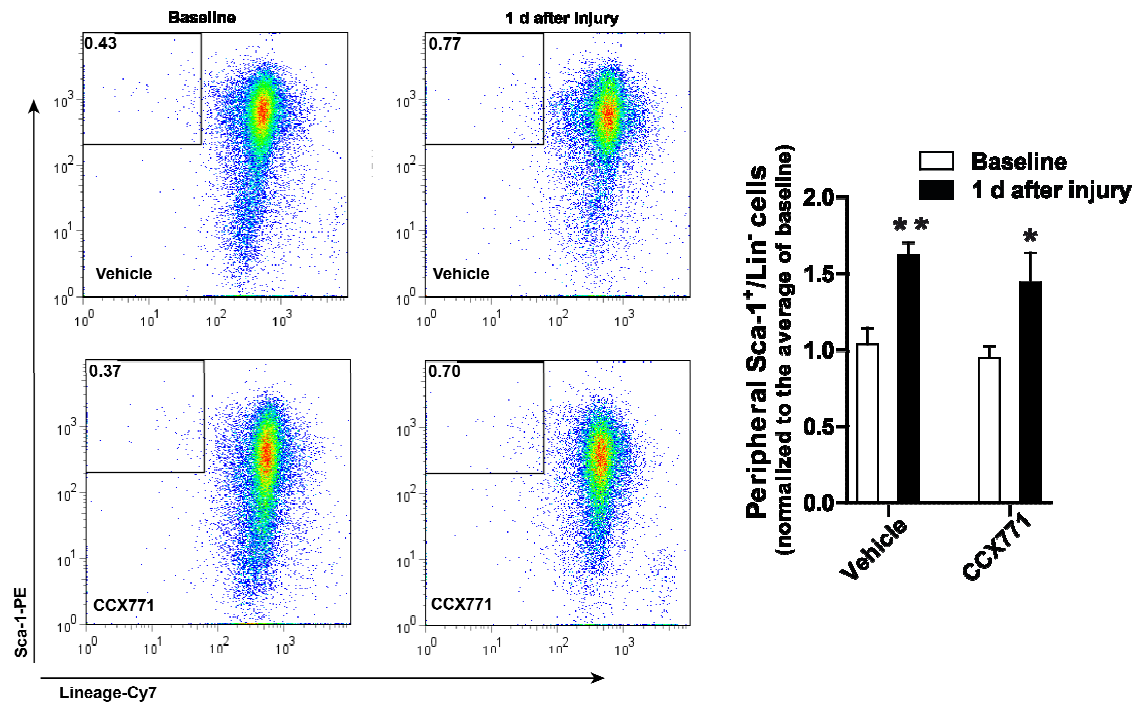


Figure 29. Effects of CCX771 treatment on the injury-induced mobilization of Sca-1⁺/Lin⁻ cells. The circulating Sca-1⁺/Lin⁻ cell population at 1 d before (baseline) and at 1 d after vascular injury in *Apoe*^{-/-} mice treated with vehicle or CCX771 (n = 8 to 9 mice per group). Representative flow cytometric dot plots are shown. ***P* < 0.01, **P* < 0.05 versus the corresponding baseline.

To explore whether CCX771 treatment alters Cxcl12 levels in the circulation and bone marrow, the Cxcl12 concentration was quantified by ELISA at 4 wks after vascular injury in *Apoe*^{-/-} mice that were daily treated with vehicle or CCX771. The Cxcl12 levels in the plasma and in the bone marrow were simultaneously increased in CCX771-treated compared with vehicle-treated *Apoe*^{-/-} mice (Fig. 30). Similar to the results obtained in *CAG-Cre*⁺*Cxcr7*^{fllox}*Apoe*^{-/-} mice, treatment with CCX771 increased the Cxcl12 concentrations.

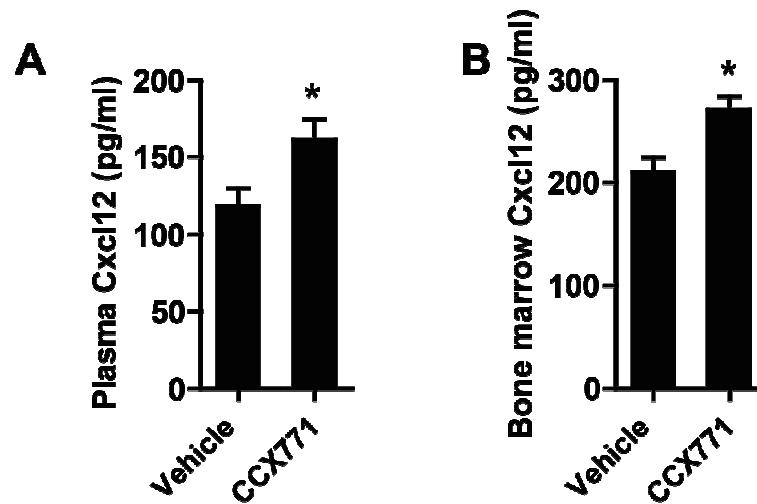


Figure 30. Effect of CCX771 treatment on the Cxcl12 concentrations. (A) The plasma Cxcl12 levels were quantified at 4 wks after vascular injury in *Apoe*^{-/-} mice treated with vehicle or CCX771 (n = 6 to 7 mice per group). **P* < 0.05. (B) The Cxcl12 levels were quantified at 4 wks after vascular injury in the bone marrow of *Apoe*^{-/-} mice injected with vehicle or CCX771 (n = 3 mice per group). **P* < 0.05.

To identify the cause for the reduced neointimal hyperplasia after CCX771 treatment in severe hyperlipidemic *Apoe*^{-/-} mice, the lipid levels and peripheral monocyte counts were analyzed at 4 wks after vascular injury in *Apoe*^{-/-} mice treated daily with vehicle or CCX771. The blood cholesterol and triglyceride levels, and the peripheral monocyte counts were substantially reduced in CCX771-treated mice compared with vehicle-treated mice after 4 wks of a HCD (Fig. 31). To further test whether CCX771 injection differentially affects the monocyte subpopulations, the number of Gr-1^{high} and Gr-1^{low} monocytes were assessed by flow cytometry. Following vascular injury, the number of Gr-1^{high} monocytes was increased, whereas the number of Gr-1^{low} monocytes was decreased in the hyperlipidemic *Apoe*^{-/-} mice after 4 wks of a HCD compared to baseline (before injury) (Fig. 31). No significant difference of the Gr-1^{high} or Gr-1^{low} monocyte cell counts was observed between CCX771- and vehicle-treated mice 4 wks after vascular injury (Fig. 31). These data suggest that CCX771 treatment ameliorates severe hyperlipidemia and monocytosis in *Apoe*^{-/-} mice irrespective of the monocyte subpopulations.

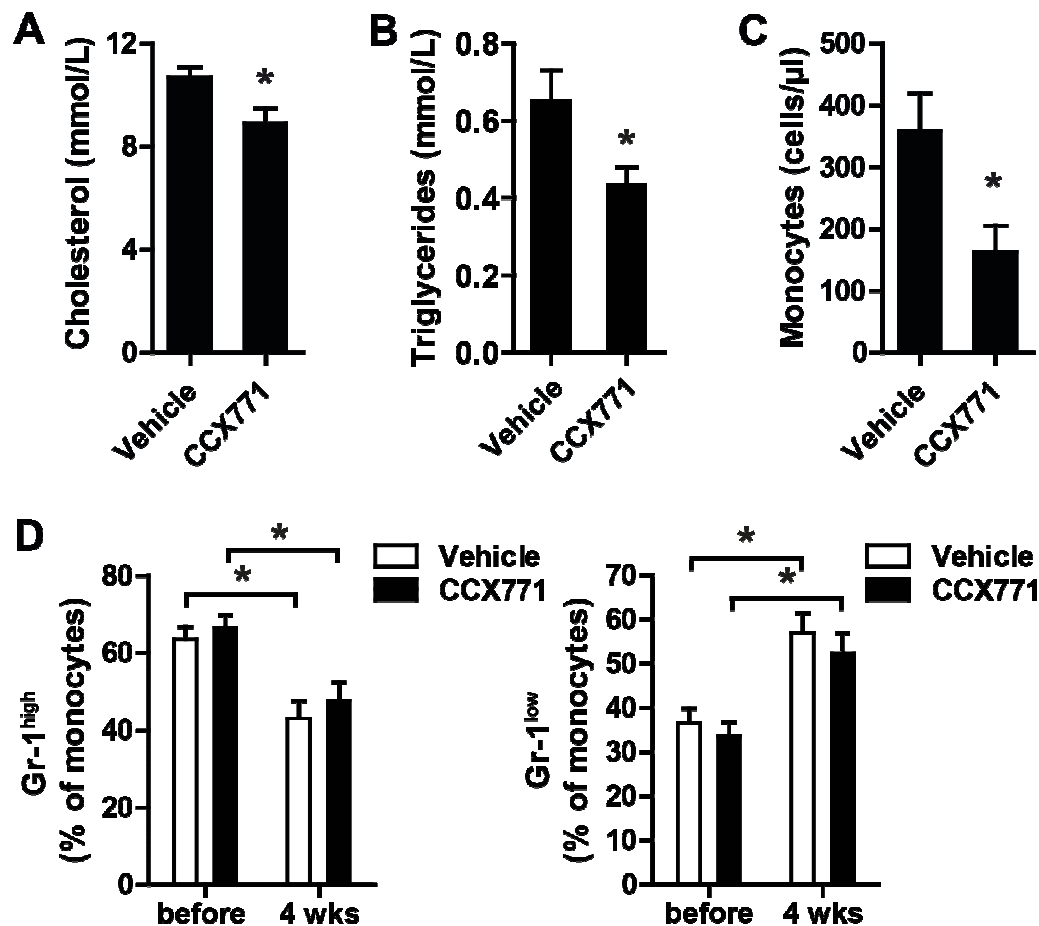


Figure 31. Effects of CCX771 treatment on hyperlipidemia and hyperlipidemia-induced monocytosis. The serum cholesterol levels (A), triglyceride levels (B), and peripheral monocyte counts (C) were quantified 4 wks after vascular injury and treatment with CCX771 or vehicle in *Apoe*^{-/-} mice fed a HCD (n = 5 to 7 mice per group). * $P < 0.05$. (D) The percentage of Gr-1^{high} or Gr-1^{low} monocytes before and 4 wks after vascular injury was studied by flow cytometry (n = 4 mice per group). * $P < 0.05$.

To determine potential side effects of CCX771 on liver and kidney, serum AST and creatinine levels were assessed. The AST and creatinine levels in *Apoe*^{-/-} mice at 4 wks after vascular injury (Fig. 32A and B) were not significantly altered after CCX771 compared with vehicle treatment, suggesting that short-term treatment with CCX771 is not associated with hepatotoxicity and does not impair renal function. Moreover, the body weights and weight gain of mice treated with CCX771 for 4 wks were not significantly different from vehicle-treated mice (Fig. 32C), indicating that CCX771 treatment for 4 wks is not associated with a severe toxicity that affects food intake and weight gain.

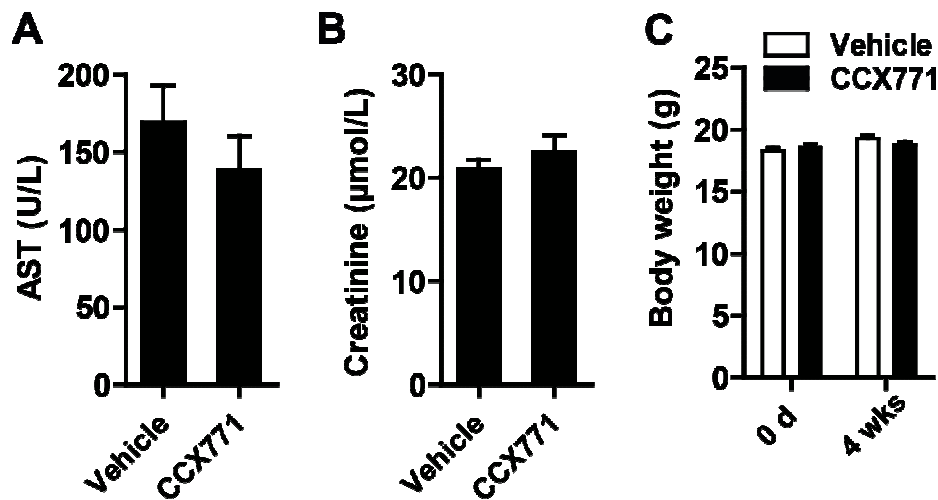


Figure 32. Assessment of toxicities of the CCX771 treatment. The serum AST (A) and serum creatinine levels (B) were quantified in *Apoe*^{-/-} mice on a HCD after treatment with CCX771 or vehicle for 4 wks (n = 6 to 7 mice per group). (C) The body weights of *Apoe*^{-/-} mice treated with CCX771 or vehicle was measured before (0 d) and 4 wks after vascular injury (n = 4 mice per group).

3.3.2 Role of splenic Cxcr7 expression in the effects of CCX771 treatment on neointima formation

The spleen is involved in lipid metabolism under hyperlipidemic conditions and is a major reservoir of monocytes (154-156). Because Cxcr7 is highly expressed in the spleen, the hypothesis that the splenic Cxcr7 expression is required for the effects of CCX771 on neointima formation and hyperlipidemia was studied in splenectomized *Apoe*^{-/-} mice. Treatment with CCX771 reduced the neointimal area of *Apoe*^{-/-} mice at 4 wks after vascular injury also in the absence of the spleen (Fig. 33), suggesting that the splenic Cxcr7 expression is dispensable for the role of CCX771 treatment on neointima formation.

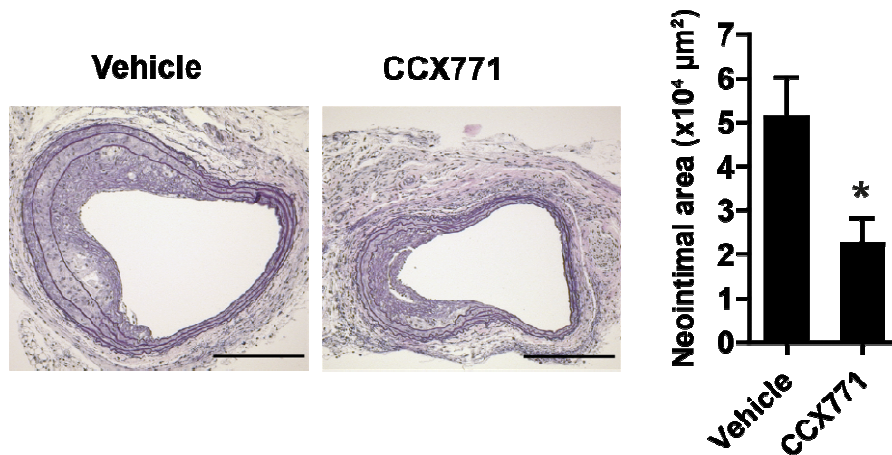


Figure 33. Effects of CCX771 treatment on neointima formation in splenectomized *Apoe*^{-/-} mice. Splenectomized *Apoe*^{-/-} mice fed a HCD were treated with vehicle or CCX771 for 4 wks after vascular injury. The neointimal area was measured in EVG-stained sections of the carotid artery by planimetry (n = 4 mice per group). Representative images of EVG-stained carotid sections are shown. **P* < 0.05; Scale bars, 200 μm.

To analyze whether the effects of CCX771 treatment on the lipid levels and monocyte count are mediated by the splenic *Cxcr7* expression, cholesterol levels and circulating monocytes were measured in the splenectomized *Apoe*^{-/-} mice treated with CCX771 or vehicle at 4 wks after vascular injury. The serum cholesterol levels and peripheral monocyte counts were reduced in the splenectomized *Apoe*^{-/-} mice injected with CCX771 compared with vehicle-treated mice (Fig. 34). These results indicate that the effect of CCX771 on hyperlipidemia and hyperlipidemia-induced monocytosis is not mediated by splenic *Cxcr7* expression, because CCX771 treatment reduced serum cholesterol and peripheral monocytes also in mice without spleens.

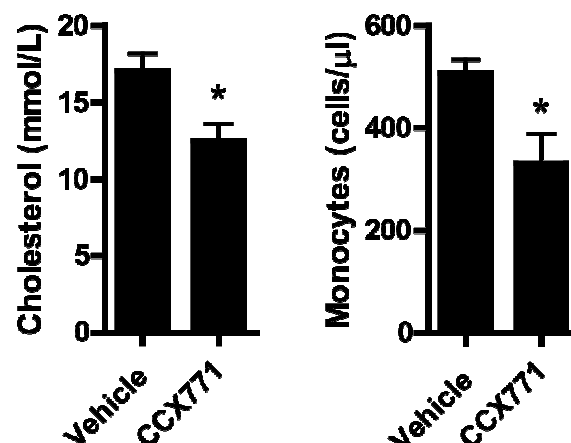


Figure 34. Effects of CCX771 treatment on serum cholesterol levels and peripheral monocyte counts in splenectomized *Apoe*^{-/-} mice. The serum cholesterol levels and peripheral monocyte counts were determined at 4 wks after vascular injury in splenectomized *Apoe*^{-/-} mice treated with vehicle or CCX771 and fed a HCD (n = 4 to 5 mice per group). **P* < 0.05.

3.4 CCX771 treatment reduced diet-induced atherosclerosis

To investigate the role for CCX771 in diet-induced atherosclerosis, *Apoe*^{-/-} mice fed a HCD were daily treated with CCX771 (10 mg/kg, s.c.) or vehicle (10% Captisol) for 3 months. To visualize and quantify the extent of atherosclerosis, cross-sections of the aortic roots were stained with Movat's stain and *en face* prepared aortas were stained with oil red O. The size of atherosclerotic lesions in the aortic roots and the relative oil red O-positive area in the aorta were reduced by CCX771 treatment (Fig. 35), suggesting that CCX771 plays a protective role in the development of atherosclerosis.

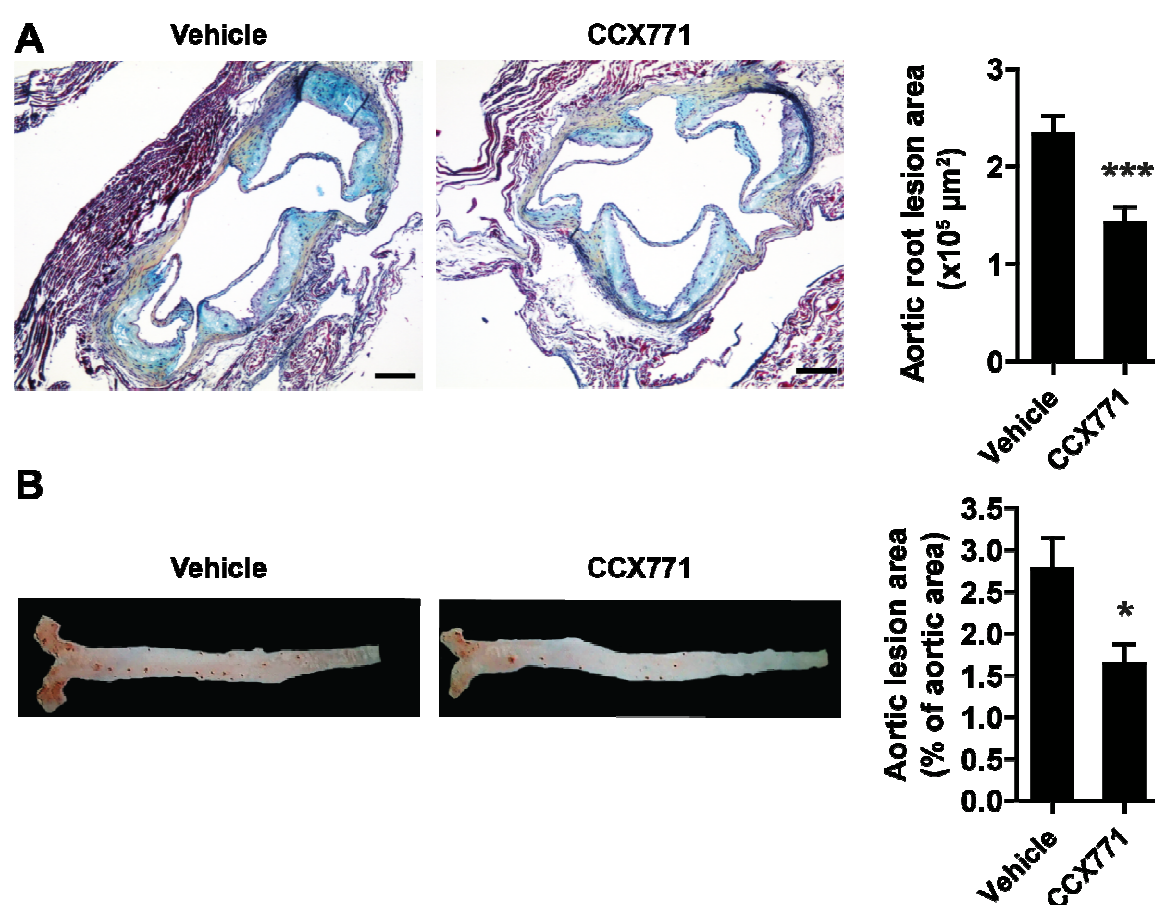


Figure 35: Effects of CCX771 treatment on diet-induced atherosclerosis in *Apoe*^{-/-} mice. (A) The area of atherosclerotic lesions was quantified by planimetry in Movat-stained sections of aortic roots from *Apoe*^{-/-} mice treated with vehicle or CCX771 after 3 months on a HCD (n = 10 mice per group). Scale bars, 200 μm; ****P* < 0.001 versus vehicle treatment. (B) The relative oil red O-stained area was studied in *en face* prepared thoracoabdominal aortas of *Apoe*^{-/-} mice after treatment with vehicle or CCX771 (n = 10 mice per group). **P* < 0.05 versus vehicle treatment.

The effects of long-term CCX771 treatment on the cellular composition of atherosclerotic lesions were determined by immunostaining of macrophage-specific Mac-

2 or SMC-specific SM22. The number of Mac-2 immunopositive cells in the lesions was reduced by CCX771 treatment compared to vehicle treatment (Fig. 36A). The relative SM22 immunopositive area in the lesions of CCX771-treated mice was not significantly different from that in vehicle-treated mice (Fig. 36B). These results indicate that CCX771 treatment reduces the accumulation of macrophages in aortic plaques, whereas the lesional SMC content is not affected by CCX771 treatment.

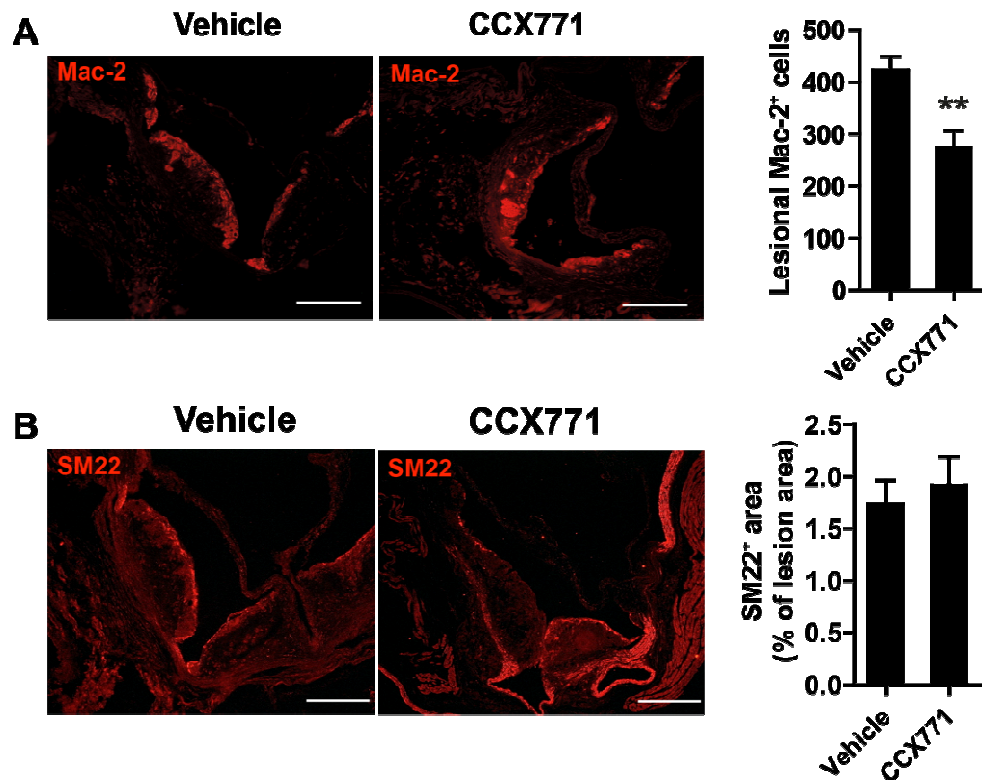


Figure 36. Effects of CCX771 treatment on the cellular composition of aortic root lesions in *Apoe*^{-/-} mice. The number of Mac-2 immunopositive cells (A) and the relative SM22 immunopositive area were analyzed in aortic roots of *Apoe*^{-/-} mice treated with vehicle or CCX771 after feeding a HCD for 3 months (n = 10 mice per group). Scale bars, 200 μ m; ***P* < 0.01 versus vehicle treatment.

To investigate whether long-term CCX771 treatment also affects hyperlipidemia and hyperlipidemia-induced monocytosis in diet-induced atherosclerosis, lipid levels and peripheral monocyte counts were measured in CCX771- or vehicle-treated *Apoe*^{-/-} mice after 3 months of a HCD. The serum cholesterol and triglyceride levels were lower in *Apoe*^{-/-} mice treated with CCX771 than with vehicle (Fig. 37A and 37B). Moreover, the peripheral monocyte counts were markedly reduced in mice treated with CCX771 compared to vehicle (Fig. 37C). However, body weights, creatinine levels, and ALT levels were not significantly different between CCX771- and vehicle-treated mice (Fig. 38). These findings indicate that CCX771 treatment limits monocytosis and severe

hypercholesterolemia during diet-induced atherosclerosis in *Apoe*^{-/-} mice without causing relevant hepatic and renal toxicities.

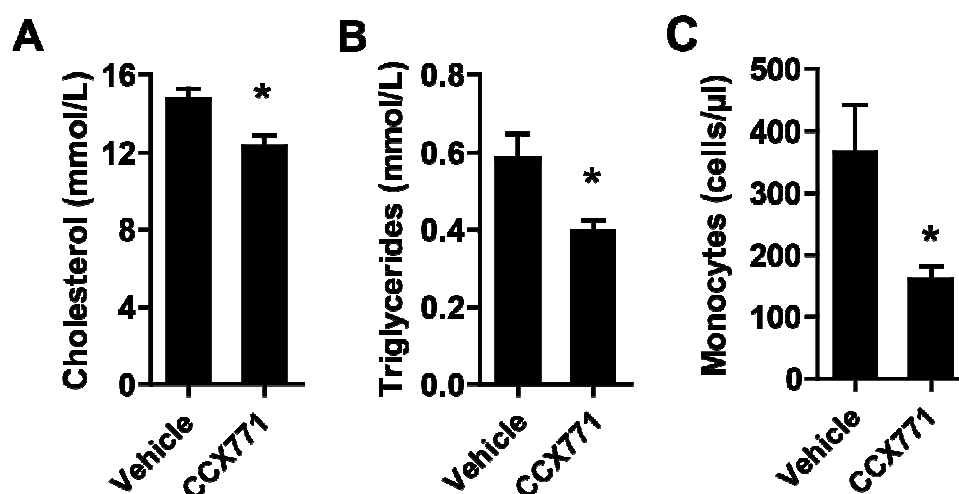


Figure 37. Effects of CCX771 treatment on hyperlipidemia and hyperlipidemia-induced monocytosis in *Apoe*^{-/-} mice. The serum cholesterol levels (A), triglyceride levels (B), and peripheral monocyte counts (C) were determined in *Apoe*^{-/-} mice treated with vehicle or CCX771 after 3 months of a HCD (n = 9 to 10 mice per group). **P* < 0.05 versus vehicle treatment.

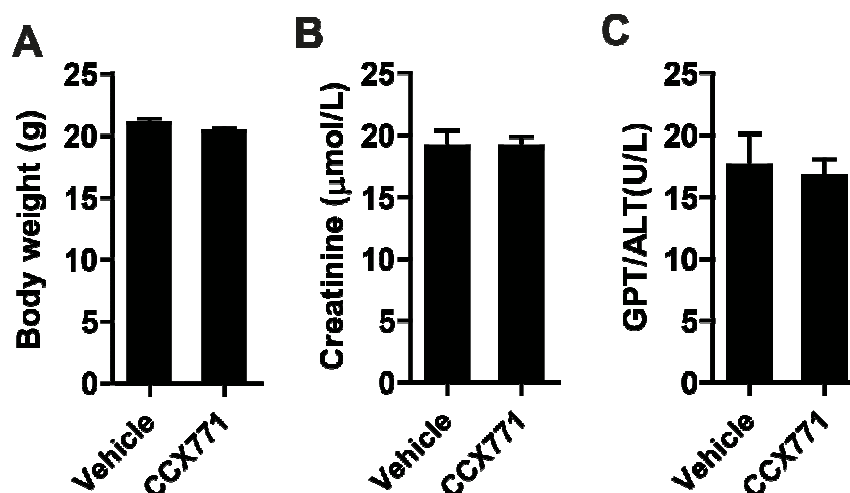


Figure 38. Assessment of CCX771 treatment related toxicities. The body weights (A), serum creatinine levels (B), and serum ALT levels (C) were measured in *Apoe*^{-/-} mice treated with vehicle or CCX771 after 3 months on a HCD (n = 10 mice per group).

3.5 Effect of CCX771 treatment cholesterol metabolism

To study the mechanism of the effects of CCX771 treatment on hyperlipidemia, *Apoe*^{-/-} mice fed a HCD were treated with CCX771 or vehicle for 4 wks and lipoprotein profiles

of these mice were assessed by a cholesterol fluorometric assay following fractionation by FPLC. The total plasma cholesterol and the VLDL-cholesterol levels, but not the LDL-cholesterol and HDL-cholesterol levels were reduced by CCX771 administration (Fig. 39), indicating that CCX771 treatment specifically reduces the circulating VLDL-cholesterol.

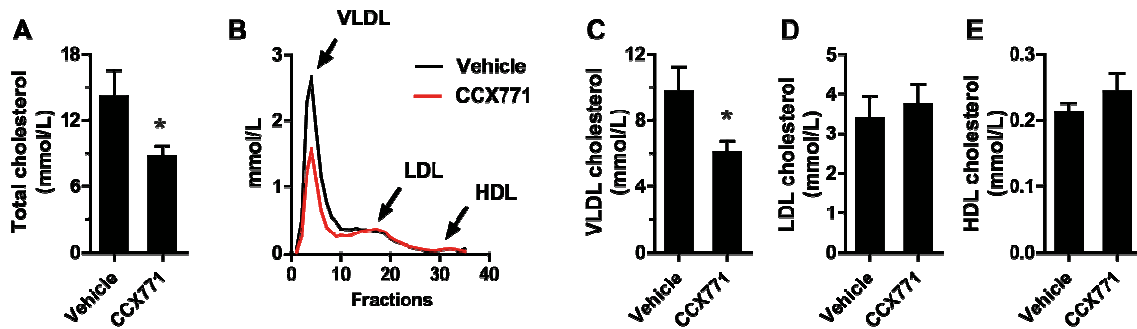


Figure 39. Effects of CCX771 treatment on different lipoprotein fractions. (A) Total cholesterol levels were measured in uninjured *Apoe*^{-/-} mice fed a HCD after 4 wks of CCX771 or vehicle treatment (n = 5 to 7 mice per group). (B-E) Lipoprotein fractions from the plasma of *Apoe*^{-/-} mice fed a HCD after 4 wks of CCX771 or vehicle treatment were separated by FPLC and the cholesterol concentrations in these lipoprotein fractions was further determined by a cholesterol fluorometric assay. (B) A representative result of the cholesterol concentrations in the different lipoprotein fractions is shown. (C-E) The cholesterol concentrations in the VLDL, LDL, and HDL fractions are shown. (n = 5 to 7 mice per group). **P* < 0.05 versus vehicle treatment.

To study the mechanism underlying the cholesterol-lowering effect of CCX771, *Apoe*^{-/-} mice were treated with CCX771 or vehicle for 4 wks and the uptake of injected DiI-labeled VLDL into the visceral adipose tissue (VAT) and liver was analyzed. The concentration of DiI was significantly increased in the VAT, but not in the liver of CCX771-treated compared to vehicle-treated mice (Fig. 40A). Moreover, cholesterol levels were increased in the VAT, but not in the liver from CCX771-treated mice (Fig. 40B). Accordingly, the DiI fluorescence signal in adipocytes determined by multi-photon microscopy *in vivo* was enhanced in CCX771-treated mice (Fig. 40C). Thus, these data indicate that CCX771 administration decreases the blood VLDL levels by enhancing the uptake of VLDL to adipose tissue.

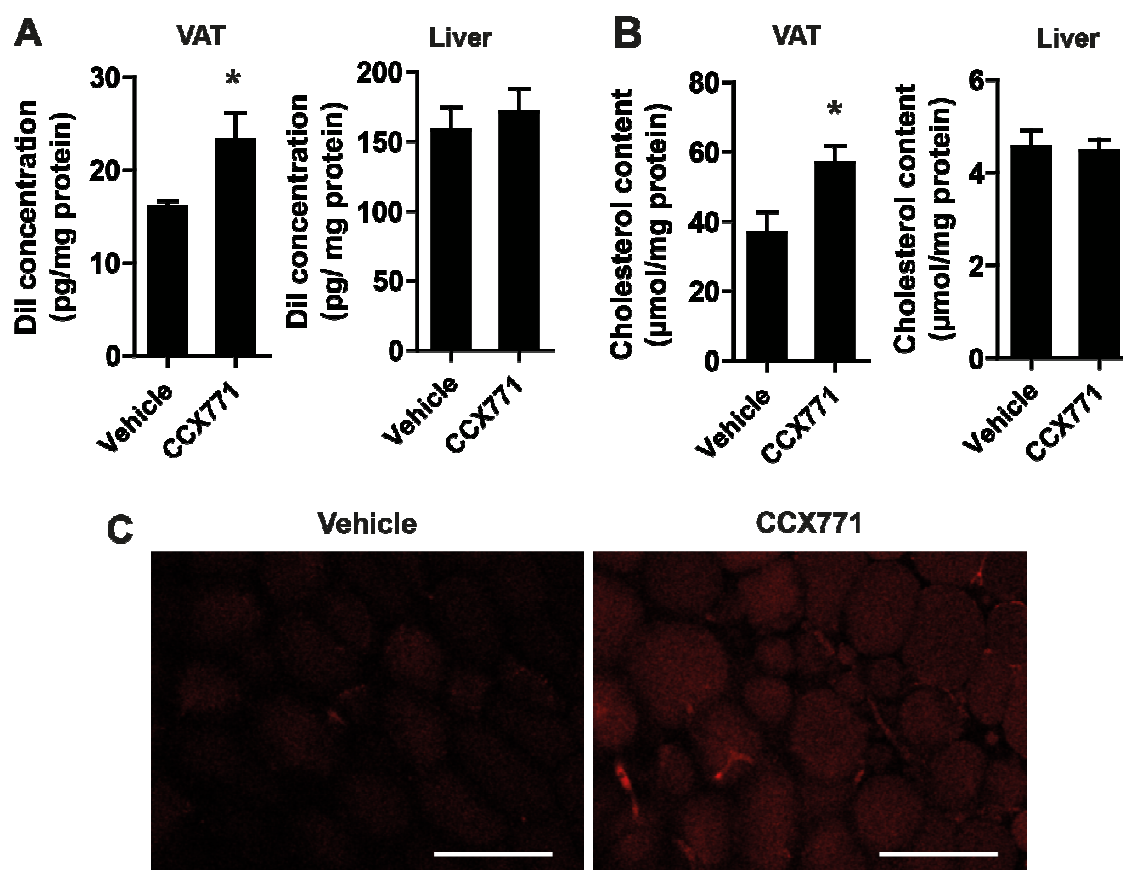


Figure 40. Effects of CCX771 treatment on the uptake of VLDL to adipose tissues in *Apoe*^{-/-} mice. (A) Uptake of VLDL in the VAT and liver was quantified by measuring the DiI fluorescence intensity after injection of DiI-labeled VLDL into *Apoe*^{-/-} mice fed a HCD and treated with vehicle or CCX771 (n = 4 mice per group). (B) Cholesterol levels were quantified in the VAT and in the liver of *Apoe*^{-/-} mice treated with vehicle or CCX771 by a cholesterol fluorometric assay (n = 4 mice per group). (C) DiI-labeled VLDL (red) was detected in the VAT from *Apoe*^{-/-} mice treated with vehicle or CCX771 by multi-photon microscopy (n = 4 mice per group). Scale bars, 100 μm.

Since VLDL can be internalized by VLDLR or LDLR (157), the mRNA expression of *Vldlr* and *Ldlr* in the VAT was studied after CCX771 treatment. However, CCX771 treatment did not substantially change the *Vldlr* and *Ldlr* mRNA expression in the VAT (Fig. 41), suggesting that CCX771 treatment promotes internalization of VLDL without altering the mRNA expression of *Vldlr* and *Ldlr*.

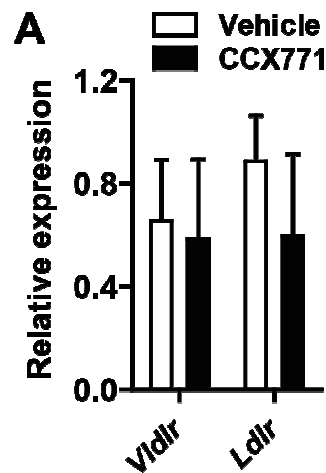


Figure 41. Effect of CCX771 on the *Vldlr* and *Ldlr* mRNA expression in the VAT. The *Vldlr* and *Ldlr* mRNA expression levels were determined by qRT-PCR in the VAT from *Apoe*^{-/-} mice fed a HCD and treated with vehicle or CCX771 for 4 wks (n = 3 mice per group).

Furthermore, the mRNA expression and promoter activity of *Cxcr7* in VATs were investigated by qRT-PCR and X-gal staining in *Apoe*^{-/-} mice and *Cxcr7*^{lacZ/+} mice, respectively. In contrast to *Cxcr4*, the expression of *Cxcr7* mRNA in the different VATs was as high as in the spleen (Fig. 42A). X-gal positive staining indicating *Cxcr7* promoter activity was detectable in the vasculature and adipocytes of *Cxcr7*^{+/lacZ} mice (Fig. 42B). *Cxcr7*^{+/+} mice served as control for the X-gal staining. Thus, *Cxcr7* is highly expressed in the endothelium of adipose tissue and in adipocytes.

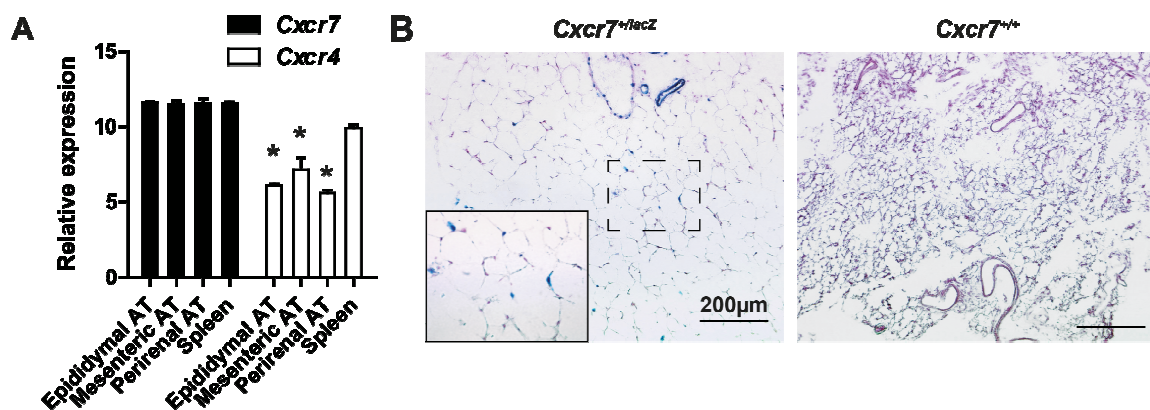


Figure 42. Expression of *Cxcr7* and *Cxcr4* in VATs. (A) Expression of *Cxcr7* and *Cxcr4* mRNA was studied in various VATs and spleen (n = 3 mice per group). **P* < 0.05 versus spleen. (B) X-gal staining (*Cxcr7* promoter activity) was analyzed in sections of VAT from *Cxcr7*^{+/lacZ} and *Cxcr7*^{+/+} mice (n = 3 mice per group). The rectangle delineated by a solid line shows a high magnification view of the area delineated by the dashed rectangle. Scale bars, 200 μm.

3.6 Endothelial-specific deletion of *Cxcr7* and hyperlipidemia

To study whether the expression of *Cxcr7* in ECs plays a role in the regulation of the serum cholesterol levels and circulating monocytes, TMX-inducible, endothelial-specific *Cxcr7* knockout (*VE-Cad-Cre⁺Cxcr7^{fllox}Apoe^{-/-}*) and control mice (*VE-Cad-Cre⁺Cxcr7^{WT}Apoe^{-/-}*) were fed a HCD for 4 wks. No significant differences in the serum cholesterol levels (Fig. 43A), triglyceride levels (Fig. 43B), and peripheral monocyte counts (Fig. 43C) were detectable between TMX-treated *VE-Cad-Cre⁺Cxcr7^{fllox}Apoe^{-/-}* and TMX-treated *VE-Cad-Cre⁺Cxcr7^{WT}Apoe^{-/-}* mice. These findings indicate that the expression of *Cxcr7* in ECs is not involved in the regulation of hyperlipidemia and monocytosis.

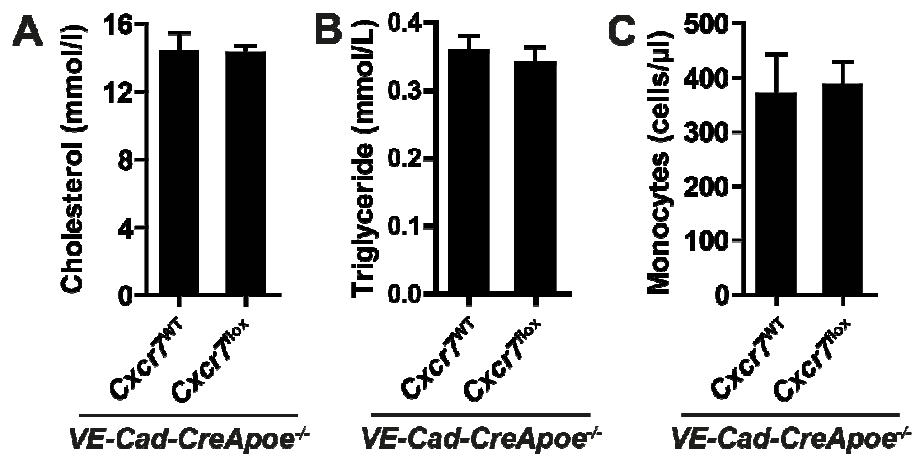


Figure 43. Effects of endothelial-specific *Cxcr7* deletion on hyperlipidemia and hyperlipidemia-induced monocytosis in *Apoe^{-/-}* mice. The serum cholesterol levels (A), triglyceride levels (B), and peripheral monocyte counts (C) in TMX-treated *VE-Cad-Cre⁺Cxcr7^{fllox}Apoe^{-/-}* and *VE-Cad-Cre⁺Cxcr7^{WT}Apoe^{-/-}* mice were determined after 4 wks of a HCD (n = 8 mice per group).

4. DISCUSSION

4.1 Role of Cxcr7 in vascular repair

4.1.1. Cxcr7 and neointima formation

The CXCL12/CXCR4 axis modulates vascular remodeling and the development of atherosclerosis by orchestrating stem cell mobilization and neutrophils homeostasis, respectively (84-88). In contrast to most other chemokines, which bind to various receptors, the only known receptor for CXCL12 that mediates its biological effects was CXCR4 until the discovery that the orphan receptor RCD1 (now called CXCR7) is an alternative receptor for CXCL12 (110, 111). Thus, it needs to be clarified whether CXCR7 plays a role in biological processes that were initially attributed only to CXCR4. Moreover, CXCR7 may also mediate specific effects of CXCL12 independently of CXCR4 in atherosclerotic vascular diseases, which have so far not been described.

Either treatment with a Cxcr4 antagonist or a Cxcl12 antibody reduces neointima formation following vascular injury (84, 85, 88, 89). However, the role of CXCR7 in neointima formation is unclear. In the current study, *Cxcr7* deficiency exacerbated neointimal hyperplasia after vascular injury in *CAG-Cre⁺Cxcr7^{flox}ApoE^{-/-}* mice. The increased neointima formation was associated with an increased accumulation of macrophages, but the relative neointimal SMCs content was not altered. Moreover, the effects of *Cxcr7* were assessed by using a specific synthetic ligand for Cxcr7, CCX771. In contrast to the effects of *Cxcr7* deficiency, CCX771 treatment reduced neointima formation and the macrophage accumulation. Similar to the effects of *Cxcr7* deficiency, the neointimal SMCs area content was not altered by CCX771 treatment. By contrast, either treatment with a Cxcr4 antagonist or a Cxcl12 antibody decreases the neointimal SMC content and mostly does not affect the neointimal macrophage content (84, 85, 87). Only a high dose of the Cxcr4 antagonist POL5551 simultaneously decreases neointimal SMC and macrophage contents (89). These results indicate that the Cxcl12/Cxcr4 axis plays a more important role in neointimal SMC accumulation than in macrophage accumulation. On the other hand, *Cxcr7* mainly regulated the neointimal macrophage accumulation without affecting the relative SMC content. Accordingly, *Cxcr7* is involved in the vascular repair after

injury, but the underlying mechanisms and effects on neointimal hyperplasia differ substantially between *Cxcr7* and *Cxcl12/Cxcr4*.

4.1.2 *Cxcr7* and hyperlipidemia-induced monocytosis

Apoe^{-/-} mice spontaneously develop atherosclerosis accompanied by hyperlipidemia and monocytosis primarily due to an expansion of Ly6C⁺ monocytes (38, 158, 159). High-fat diet feeding further exacerbates the development of atherosclerosis in *Apoe*^{-/-} mice (38, 158-160). During atherosclerosis, the appearance and distribution of atherosclerotic lesion in *Apoe*^{-/-} mice are similar to those observed in humans (160). Vascular injury leads to a pronounced neointima formation in *Apoe*^{-/-} with a B6 genetic background (161). After denudation of the endothelium, exposure of subendothelial components initiates the deposition of platelets and fibrin, leukocyte adhesion and infiltration, SMCs proliferation and migration, progenitor mobilization, and cytokine release (161). Macrophages and SMCs are the major cellular components of the neointima in *Apoe*^{-/-} mice (161). Similarly, exuberant neointimal hyperplasia after coronary stenting in humans is mainly composed of abundant macrophages and SMCs (162). Growing evidence supports a crucial role for monocytes and lipids in lesion formation and vascular remodeling after vascular injury and in the development of atherosclerosis (163-165). In the current study, quantification of lipid levels and peripheral monocyte counts demonstrated that CCX771 administration reduced the serum cholesterol levels, triglyceride levels, and peripheral monocyte counts in *Apoe*^{-/-} mice while the abrogation of *Cxcr7* in *CAG-Cre⁺Cxcr7^{fllox}Apoe^{-/-}* mice caused the opposite outcome. Deficiency of chemokine receptors can cause changes in serum cholesterol levels (166-168). Hyperlipidemia leads to monocytosis by promoting monocyte progenitor cell proliferation and monocyte survival in animal models (38, 40, 169-171). These findings indicate that CCX771 treatment ameliorates hypercholesterolemia and subsequently alleviates hypercholesterolemia-induced peripheral monocytosis, whereas *Cxcr7* deficiency exacerbates hypercholesterolemia and aggravates hypercholesterolemia-induced peripheral monocytosis.

Monocyte subpopulations play a distinct role in different atherosclerotic diseases. Swirski *et al.* reported that Ly6C⁺ rather than Ly6C⁻ monocytes were progressively expanded in an atherosclerosis model in which *Apoe*^{-/-} mice were fed a high-fat diet for 25 wks (38). The expansion of circulating monocytes triggered by

elevated cholesterol levels is linked to an improved survival capacity of monocytes (38). The same group reported a biphasic monocyte response in a murine model of myocardial infarction (35). In phase I, classic monocytes (Ly6C⁺) dominate at the injury sites and are responsible for clearing damaged tissues or cells; in phase II, nonclassic monocytes (Ly6C⁻) monocytes are preferentially recruited to the injury site, attenuate inflammation, and promote wound healing (35). Given the heterogeneity of monocytes and their divergent functions, the current study further tested whether CCX771 differentially regulates the mobilization of the two different monocyte subsets. In the current study, the relative proportions of Gr-1^{high} (corresponding to Ly6C⁺) and Gr-1^{low} (corresponding to Ly6C⁻) monocytes in *Apoe*^{-/-} mice were approximately 65% and 35%, respectively, after 6 d of a HCD. The relative proportions of Gr-1^{high} and Gr-1^{low} monocytes in *Apoe*^{-/-} mice 4 wks after vascular injury were 38% and 62%, respectively. Previous studies reported that the relative proportions of Ly6C⁺ and Ly6C⁻ monocytes in normal C57BL/6 mice were about 15% and 85%, respectively (35). Within the first four days after coronary artery ligation, the relative values of Ly6C⁺ and Ly6C⁻ monocytes change to 75% and 25%, respectively (35). From day 5 on, the percentage of Ly6C⁻ monocytes increases and reaches approximately 85% at day 16 after myocardial infarction (35). The ratio of Gr-1^{high} to Gr-1^{low} monocytes was higher in the current study than that in normal C57BL/6 mice or after myocardial infarction, which might be due to the hypercholesterolemia-induced expansion of Gr-1^{high} monocytes (38). However, CCX771 treatment did not affect the ratio of Gr-1^{high} to Gr-1^{low} monocytes, suggesting that *Cxcr7* affects hyperlipidemia-induced monocytosis, but not monocyte subpopulations.

Clinical findings demonstrate a correlation between the level of peripheral monocytes and vascular diseases. Therefore, monocytosis is considered an independent risk factor for atherosclerosis (38, 172-176). In animal models, the peripheral monocyte count also correlates with lesional macrophage accumulation, the neointimal area, and the size of atherosclerotic lesion (36, 168, 177). Moreover, myocardial infarction increases monocyte recruitment and macrophage accumulation, accelerating the development and exacerbation of atherosclerosis (178). In addition to the SMC migration and proliferation, the neointimal macrophage accumulation is positively related to the neointimal area, supporting a decisive role of the macrophage accumulation in neointima hyperplasia (179). Accordingly, *Cxcr7* might modulate the

circulating monocyte counts through regulating the serum cholesterol levels and may thereby control the accumulation of neointimal macrophage and neointimal growth.

4.1.3 Cxcr7 indirectly modulates the macrophages accumulation in neointima

The results of the current study indicate that *Cxcr7* regulates the peripheral monocyte counts and the accumulation of macrophages by modulating the serum cholesterol levels. However, it remains unclear whether *Cxcr7* might affect monocyte mobilization and lesional macrophage accumulation by alternative mechanisms.

A variety of chemokine/chemokine receptor axes act in a sequential, independent, and complementary manner to achieve macrophage accumulation in the vessels, which is related to the monocyte emigration from the bone marrow to blood, monocytoysis, monocyte survival, the monocyte adhesion cascade, the differentiation from monocytes to macrophages, and the emigration of macrophages from arterial plaques (108, 168, 180, 181). For examples, the *Cxcl12/Cxcr4* axis can mediate the adhesion of monocytes to arteries and affects the neointimal macrophage accumulation (88, 89). Moreover, either the absence of CCL2 (monocyte chemoattractant protein-1, MCP-1) or the lack of the CCL2 receptor CCR2 decreases atherosclerosis and reduces lesional macrophage accumulation (182-184). *Ccr2* deletion leads to an increase of monocytes in the bone marrow, whereas peripheral blood monocytes are decreased, suggesting a crucial role for *Ccr2* in the emigration of monocytes from the bone marrow (185, 186). *Ccr2* also promotes monocyte recruitment to atherosclerotic lesions, monocyte arrest on platelets, and transendothelial migration of monocytes (186-188). Moreover, the homeostasis and infiltration of monocytes, particular of the $Ly6C^+(Gr1^+)$ monocyte subset, is dependent on *Ccr2* (40, 186). By contrast, *Cx3cr1* regulates the monocytoysis of the $Ly6C^-$ monocyte subset (40, 168, 189). In *Cx3cr1^{-/-}Apoe^{-/-}* mice, reduced atherosclerosis due to a decreased lesional macrophage accumulation was observed (190). *Cx3cr1* can also increase the entrance of both monocyte subsets into plaques and promote monocyte survival, suggesting critical functions of *Cx3cr1* in the development of atherosclerosis (40, 168, 189, 191). Moreover, *Ccr5* deficiency ameliorates the development of atherosclerotic lesions, which is associated with diminished macrophage content, and blocking *Ccr5* reduces neointimal hyperplasia following vascular injury by reducing macrophage accumulation (192-194). Interestingly, combined systemic inhibition of *Ccr5*, *Ccl2*, and *Cx3cr1* in *Apoe^{-/-}* mice

almost inhibits the development of atherosclerosis and nearly abolishes the arterial macrophage accumulation. This markedly reduced arterial macrophage accumulation is strongly correlated with a considerable decrease in the peripheral blood monocyte counts (168). LDL-derived LPA induces *Cxcl1* expression, thereby enhancing monocyte adhesion to the vascular endothelium and the accumulation of macrophage (88). Furthermore, lack of the *Cxcl1* receptor *Cxcr2* in bone marrow cells reduces atherosclerosis and lowers the lesional macrophage content, which might be due to the participation of *Cxcl1/Cxcr2* in the integrin-dependent monocyte arrest on ECs (166, 195). Additionally, *Cx₃cr1* is related to the integrin-independent monocytes firm adhesion (196, 197). In contrast, *Ccr7* dominates the emigration of the monocyte-derived cells from arterial plaques (198). Considering the intimate relationship between chemokine/chemokine receptor axes and the macrophage accumulation, the current study explored the participation of *Cxcr7* expressed on bone marrow cells in the lesional macrophage accumulation.

Bone marrow is the major organ for the production and storage of monocytes (199). However, *Cxcr7* deficiency on bone marrow cells did not alter lipid levels, peripheral monocyte counts, macrophage accumulation, and neointima formation. Moreover, *Cxcr7* protein expression was not detectable and *Cxcr7* mRNA expression was low in the bone marrow and peripheral blood cells, which is consistent with a previous study (114). Therefore, *Cxcr7* in bone marrow cells, including monocytes, is unlikely to play a role in the effects of *Cxcr7* on the peripheral monocyte counts.

The current study showed high *Cxcr7* mRNA and protein expression in the spleen, which has also been also identified as a monocyte reservoir (156). Splenic monocytes, rather than bone marrow monocytes, are initially mobilized to the inflamed tissues after injury (156). In line with previous studies, *Cxcr7* expression was detected in cells of the splenic marginal zone (113, 200). Splenic B cells are involved in protective immunity against atherosclerosis (201). However, in the current study, removal of the spleen did not affect the effect of CCX771 on the peripheral blood monocyte counts and neointima formation, suggesting that splenic *Cxcr7* expression does not affect neointima formation via modulating monocyte mobilization.

CXCL12 mediates the migration and recruitment of monocytes, which constitutively express CXCR4 (202, 203). However, no protein expression of *Cxcr7*

was detected on the monocytes, which makes direct effects of *Cxcr7* on monocyte mobilization highly unlikely. Therefore, the current study provides evidence for an indirect role of *Cxcr7* on the peripheral monocyte count.

Moreover, the results of the current study show that *Cxcr7* deficiency increased the serum cholesterol levels in HCD-fed *Apoe*^{-/-} mice. However, the serum cholesterol levels in mildly hyperlipidemic *Cxcr7*^{-/-}*Apoe*^{+/+} mice were not altered. Accordingly, neointima formation and circulating monocyte counts were not changed in *Cxcr7*^{-/-}*Apoe*^{+/+} mice, indicating that the effects of *Cxcr7* on neointimal hyperplasia are dependent on hyperlipidemia.

Similar to *Ccl2*^{-/-}*Cx3cr1*^{-/-}*Apoe*^{-/-} mice (168), weight gain was not related to the alteration of the blood cholesterol levels triggered by *Cxcr7* deletion and CCX771 treatment in the current study. In contrast, *Mcsf*^{-/-} mice exhibit a lower body weight and higher cholesterol levels than those of controls (204). However, the results of the current study do not indicate that *Cxcr7* deletion or CCX771 treatment regulate cholesterol levels through changes in food intake. Moreover, hyperlipidemia not only causes monocytosis, but also enhances lipid deposition in the aortic wall, which in turn increases monocyte recruitment (205). In conclusion, *Cxcr7* indirectly controls the macrophage accumulation through modulating the serum cholesterol levels under hyperlipidemic conditions without affecting the weight gain.

4.1.4 Effects of *Cxcr7* on SPC mobilization and *Cxcl12* levels

Following mechanical vascular injury, increased plasma *Cxcl12* levels trigger the mobilization of SPCs (79, 80). Additionally, apoptotic SMCs induce *Cxcl12* expression in medial SMCs, which mobilizes and recruits SPCs to the injury sites (84, 85, 109). SPCs eventually differentiate into SMCs participating in neointima formation (84, 88, 89, 108). Hence, SPCs are one of the major contributing factors in neointima formation after mechanical vascular injury (84, 85). Disruption of the *Cxcl12*/*Cxcr4* axis reduces neointima formation through inhibiting SPC mobilization and recruitment (84, 85, 88, 89). The role of *Cxcr7* in this process has not been elucidated.

In the current study, neither *Cxcr7* deficiency nor CCX771 treatment interfered with SPC mobilization in response to vascular injury, which is consistent

with the unchanged neointimal SMC content, suggesting that *Cxcr7* is not involved in the injury-induced SPC mobilization.

CXCR7 internalizes and degrades CXCL12 and thereby controls the extracellular availability of CXCL12 (134). In the current study, *Cxcl12* levels were simultaneously elevated in the bone marrow and the circulation of *Cxcr7*^{-/-} mice and after CCX771 treatment. These increased *Cxcl12* levels can be explained by displacement of *Cxcl12* from *Cxcr7* by CCX771 and lack of *Cxcl12* binding to *Cxcr7* in *Cxcr7*^{-/-} mice. In both cases, reduced *Cxcr7*-mediated *Cxcl12* internalization may impair its degradation and thus increase the *Cxcl12* levels.

In the current study, the elevated circulating *Cxcl12* levels did not significantly affect SPC mobilization after vascular. This is in contrast to previous studies, which demonstrated that increased circulating CXCL12 levels after vascular injury or injection of CXCL12 mobilize SPCs (84, 206). However, *Cxcr7* deficiency or CCX771 treatment also increased CXCL12 in the bone marrow and therefore did not change the CXCL12 gradient between the circulation and the bone marrow, which is crucial for the retention of stem cells by high CXCL12 levels in the bone marrow (79, 80, 108). Together, CCX771 treatment or *Cxcr7* deficiency did not disrupt the gradient of *Cxcl12* and therefore increased circulating CXCL12 levels may not enhance SPC mobilization after vascular injury.

4.2 Effects of CCX771 treatment on the development of atherosclerosis

In the current study, CCX771 treatment after vascular injury decreased blood cholesterol levels, which is also a crucial factor in diet-induced atherosclerosis (4). Therefore, the effects of long-term CCX771 treatment on diet-induced atherosclerosis were further investigated. In line with the effects of CCX771 treatment on neointima formation, CCX771 treatment reduced serum cholesterol levels and peripheral monocyte counts, limited atherosclerotic lesion formation, and diminished the lesional accumulation of macrophages. Moreover, CCX771 treatment did not affect the weight gain or impaired hepatic or renal function, suggesting that CCX771 has no major hepatic or renal toxicities even after long-term application in mice.

Furthermore, CCX771 treatment decreased the blood cholesterol levels, ameliorated monocytosis, and limited atherosclerotic plaque formation. The protective

effects of CCX771 treatment in diet-induced atherosclerosis were identical with its effects on neointimal hyperplasia following vascular injury, indicating that CCX771 acts via similar mechanisms. The effects of Cxcr4 on restenosis and diet-induced atherosclerosis are in opposite to those of the treatment with CCX771 (85, 86, 89). Cxcr4 promotes restenosis, because blocking Cxcr4 decreases SPC mobilization and neointimal SMC accumulation leads to reduced neointimal hyperplasia. Moreover, Cxcr4 is protective in diet-induced atherosclerosis, because inhibition of Cxcr4 induces neutrophilia, which increases atherosclerosis (86). Since the effects of Cxcr4 and Cxcr7 appear to be largely independent of each other in atherosclerosis and Cxcr7 appears not, like Cxcr4, to be involved in many important physiological processes (85, 86, 207), targeting Cxcr7 might be more favorable for treating restenosis and atherosclerotic diseases than interfering with Cxcr4.

4.3 Effects of CCX771 treatment on the uptake of VLDL into adipose tissue

The blood cholesterol levels is one of the key risk factors that drive the development of atherosclerosis (4). Cholesterol alone is insoluble in the blood and is carried by different types of lipoproteins in the circulatory system. Lipoproteins are spherical complexes with a hydrophobic lipid core that mainly consists of triglycerides and cholesterol esters. A hydrophilic shell that contains cholesterol, phospholipids, and apolipoproteins encloses the lipid core. Apolipoproteins serve as cofactors for enzymes and are ligands for receptor-mediated processes (208). Lipoproteins can be classified into five major classes according to their size, density and composition: chylomicrons (CMs), very-low-density lipoproteins (VLDLs), intermediate-density lipoproteins (IDLs), low-density lipoproteins (LDLs), and high-density lipoproteins (HDLs). Cholesterol is acquired from the diet and is de novo synthesized through the mevalonate pathway, which is essentially controlled by the rate-limiting enzyme 3-hydroxy-3-methylglutaryl coenzyme A (HMG-CoA) (209). Lipoprotein metabolism is a network including three major interrelated pathways: the exogenous pathway, the endogenous pathway, and the reverse transport pathway. Recent studies showed that several cytokines and/or chemokine receptors could regulate serum cholesterol levels (166-168, 210). For instance, neither Cx₃cr1 nor Ccl2 deficiency in *Apoe*^{-/-} mice changes serum cholesterol levels, whereas simultaneous deletion of Cx₃cr1 and Ccl2

raises serum cholesterol levels (168). Moreover, transplantation of *Cxcr2*^{-/-} bone marrow in *Ldlr*^{-/-} mice decreases VLDL-cholesterol levels and reduces lesional macrophage accumulation (166). In contrast, transplantation of *Ccr5*^{-/-} bone marrow cells in *Ldlr*^{-/-} mice or deletion *Mcsf* in *Apoe*^{-/-} mice increases cholesterol levels (166). Interestingly, transplantation with *Ccr5*^{-/-} bone marrow reduces macrophage content rather than the atherosclerotic plaque size despite the raised cholesterol levels (167). Additionally, *Mcsf*^{-/-}*Apoe*^{-/-} mice develop smaller atherosclerotic lesion despite higher serum cholesterol levels (210).

High blood cholesterol levels accelerate the deposition of lipids and the accumulation of monocytes in lesions, where monocytes differentiate to macrophages and thus promote the development of atherosclerotic lesion. These findings strongly support a positive correlation between the cholesterol levels and the atherosclerotic lesion formation (38, 40, 169-171). The discrepancy between increased cholesterol levels and reduced macrophage content following *Ccr5* deletion in bone marrow could be explained by the double-edged role of *Ccr5*. Absence of *Ccr5* inhibits leukocyte migration and enhances an anti-inflammatory immune response, leading to the reduced macrophage content (193, 194). On the other hand, elevated cholesterol levels in mice with *Ccr5* deficient bone marrow promote excessive cholesterol deposition into the artery wall and the uptake of cholesterol by macrophages (167). These divergent results may explain why *Ccr5* abrogation in the bone marrow does not affect lesion size. In *Mcsf*^{-/-}*Apoe*^{-/-} mice, increased serum cholesterol levels may not increase atherosclerosis due to the lack of the differentiation of monocytes to macrophages in the absence of macrophage colony-stimulating factor (MCSF) (210). Therefore, chemokine receptors can regulate serum cholesterol levels; however, the precise mechanism underlying the chemokine-induced regulation of serum cholesterol levels remains unclear.

To study the role of *Cxcr7* in lipoprotein metabolism, the effect of CCX771 on the lipoprotein profile in *Apoe*^{-/-} mice was determined in the current study. Treatment with CCX771 exclusively decreased the circulating VLDL cholesterol levels in *Apoe*^{-/-} mice without any effect on the levels of LDL and HDL cholesterol. Of note, the lipoprotein profile in *Apoe*^{-/-} mice is characterized by an elevation of the VLDL/IDL-derived cholesterol levels, whereas LDL-cholesterol levels are only mildly increased and HDL-cholesterol levels are reduced (158, 159). Moreover, triglyceride levels in *Apoe*^{-/-} mice are slightly increased compared with those in wild type mice (158, 159).

In the current study, the effect of *Cxcr7* on the regulation of VLDL cholesterol levels was found only under conditions of elevated VLDL concentrations.

Statins are one of the preferred first-line drugs in the clinical therapy of hypercholesterolemia-related diseases (211). Statins inhibit HMG-CoA reductase to lower cholesterol levels, particularly LDL-cholesterol levels, and it also decreases the levels of triglycerides, but increases the levels of HDL (212, 213). Anti-atherogenic HDL transports cholesterol from peripheral tissues to the liver for excretion and is often inversely related to the risk of cardiovascular diseases (214). In comparison to statins, CCX771 treatment reduced VLDL and triglyceride levels, without any effect on LDL and HDL levels. Additionally, the main target organ for statins is the liver (215), where no *Cxcr7* protein expression and a remarkably low expression of *Cxcr7* mRNA were observed. This indicates that the mechanism underlying the regulation of the cholesterol levels by CCX771 treatment is different from stains.

Liver is the major organ for the synthesis of VLDL and increased production of VLDL in the liver causes familial combined hyperlipidemia (FCH), which is the cause for half of all cases of coronary artery disease (216-218). Notably, *Cxcr7* expression was absent in the liver, making the possibility that hepatic *Cxcr7* expression regulates the synthesis of VLDL unlikely. By contrast, abundant *Cxcr7* expression was identified in the spleen, which has been considered to be a site of lipid metabolism (154). However, splenectomy did not change the effects of CCX771 treatment on cholesterol levels. Therefore, the results of the current study suggest that splenic *Cxcr7* expression is not involved in the regulation of cholesterol levels.

The current study demonstrated that CCX771 treatment enhances the uptake of cholesterol from VLDL into VATs, which may explain the reduced serum VLDL levels in CCX771-treated mice. Although *Cxcr7* expression was observed in adipocytes and ECs of adipose tissue, the uptake of VLDL into adipose tissue is likely mediated by the expression of *Cxcr7* on adipocytes, because endothelial cell-specific *Cxcr7* deficiency did not change the serum cholesterol levels. In opposite to the effect of CCX771 treatment, absence of *Cxcr7* increased serum cholesterol levels indicating that activation of *Cxcr7* by CCX771 is mediating the lowering of the VLDL levels. In contrast to the cholesterol levels, *Cxcl12* levels were simultaneously increased in the plasma and bone marrow of both *Cxcr7*^{-/-} and CCX771-treated mice. Therefore, it is unlikely that *Cxcl12* is directly involved in the uptake of VLDL into adipose tissue because the elevated *Cxcl12* levels in *Cxcr7*^{-/-} and CCX771-treated mice cannot

explain the oppositional change of the serum cholesterol concentration. However, these results support the hypothesis that Cxcr7 regulates the uptake of VLDL into the adipose tissue.

Cxcr7 was highly expressed in VATs, which is not only a primary depot of fatty acids stored as triglycerides, but also acts as a large cholesterol reservoir (219). Adipocyte is the main cell type in adipose tissue and orchestrate energy metabolism and glucose homeostasis (219). In adipocytes, almost all cholesterol exists as free unesterified cholesterol due to a lack of acetyl-Coenzyme A acyltransferase (ACAT) (220-222). A dynamic cholesterol equilibrium exists between adipose tissues and peripheral blood, suggesting a potential buffering effect of adipose tissues against hypercholesterolemia (219). Triglyceride-rich lipoproteins (TGRLs), such as CM or VLDL, get access to adipocytes from the peripheral blood through passive exchange or receptor-mediated endocytosis (219). The latter plays a crucial role in lipoprotein metabolism and cholesterol homeostasis (223). For instance, TGRL particles enter cells by LDL receptor (LDLr)-mediated endocytosis and are transferred to lysosomes where TGRL particles are subsequently degraded to intracellular free fatty acid for *de novo* TG biosynthesis (224). In comparison to LDLr, the VLDLr is abundantly expressed in adipose tissue and scarcely detectable in the liver (225-227). VLDLr binds to and mediates the internalization of Apoe-containing lipoproteins, such as VLDL, IDL and CM (225-227). Following the intracellular accumulation of lipoproteins, a negative feedback mechanism including the suppression of HMG-CoA and LDLr occurs to stabilize the cellular cholesterol content (228). VLDLr is not part of a negative feedback mechanism and is upregulated by peroxisome proliferator-activated receptor-gamma (PPAR- γ) agonists in adipocytes (229, 230). PPAR- γ is a crucial transcription factor for lipid metabolism (229). Accordingly, adipose tissues modulate cholesterol homeostasis by orchestrating diverse lipoprotein receptors. In the current study, the mRNA expression of *Ldlr* and *Vldlr* was not changed by CCX771 treatment, suggesting that the enhanced uptake of VLDL into adipocytes after CCX771 treatment is not due to the increased transcriptional expression of *Ldlr* and *Vldlr*. Additionally, β -arrestin-2 increases the endocytosis of LDLr and thus ameliorates hypercholesterolemia (231). Therefore, it seems plausible that binding of CCX771 to Cxcr7 promotes the uptake of VLDL into adipocytes via β -arrestin-2 activation (Fig. 44). However, this proposed mechanism remains to be verified.

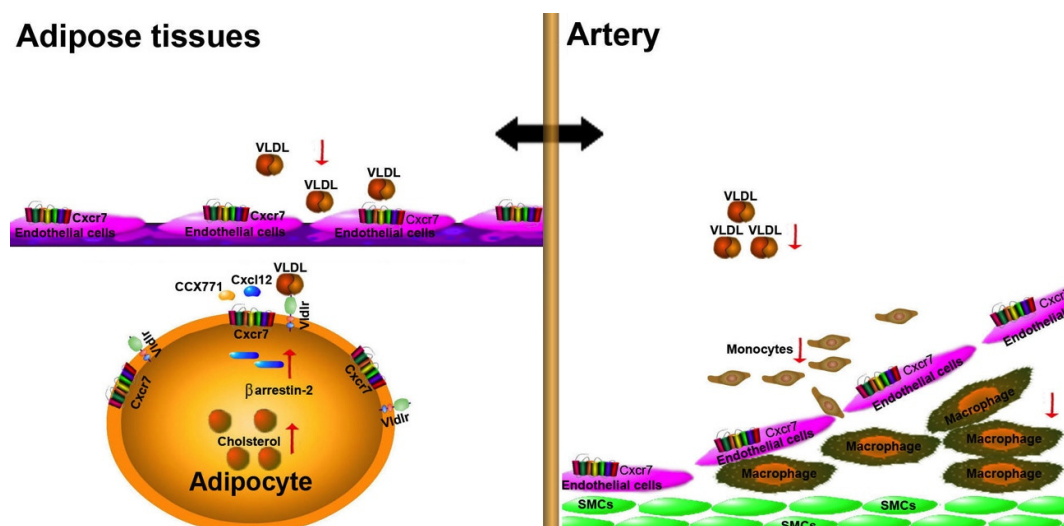


Figure 44. Proposed model of the effects of Cxcr7 on neointima formation and atherosclerosis by controlling VLDL metabolism. After ligand binding, activation of Cxcr7 in adipocytes promotes the uptake of VLDL into the adipocytes and down-regulates the serum cholesterol levels. Then, decreased VLDL levels ameliorate monocytois, decrease the lesional macrophage accumulation, and finally reduce neointimal hyperplasia and the development of atherosclerosis.

The current study demonstrated that *Cxcr7* deficiency aggravates neointima formation, increases peripheral monocyte counts, and elevates cholesterol levels. On the contrary, CCX771 administration exerted opposite effects: it reduced neointimal hyperplasia and atherosclerotic lesion formation. Thus, CCX771 may serve as an agonist that activates Cxcr7, indicating that Cxcr7 is a signaling receptor. Binding of CXCL12 to CXCR7 activates the ERK pathway via β -arrestins (117, 131, 133, 232). β -arrestins are a family of versatile cytosolic adapter or scaffold proteins controlling the signal pathway of seven-transmembrane receptors (233). Either endogenous ligand of CXCR7 (CXCL12 or CXCL11) or Cxcr7-specific synthetic ligands (*e.g.*, CCX771, CCX733 or CCX754) preferentially recruit β -arrestin to CXCR7 (130, 133, 234). Additionally, the CXCR4 antagonist AMD3100 also binds to a allosteric site of CXCR7 and drives β -arrestins recruitment to CXCR7 (232). CCX771 even enhances the CXCL12-mediated β -arrestins recruitment to CXCR7 (133). Therefore, CXCR7 activates signaling events by recruiting β -arrestin. In contrast, G-protein related calcium responses are not triggered by CXCR7 activation, despite it constitutively couples to G proteins (125, 126). Additionally, chemotaxis induced by CXCL12 does not require CXCR7 (110, 129). In sum, CXCR7 is not directly and functionally related to the canonical G protein signaling.

CCX771 is a ligand for Cxcr7 with high affinity and specificity (110, 124). In the current study, elevated Cxcl12 levels induced by CCX771 treatment combined with the opposite results concerning the serum cholesterol levels and monocyte counts observed in *Cxcr7* deficient mice or CCX771-treated mice indicate that CCX771 can act as an agonist of Cxcr7 *in vivo*. However, CCX771 is generally considered to be an antagonist for CXCR7, because it competes with the Cxcr7 ligands CXCL12 and CXCL11, and can limit the role of CXCR7 in integrin activation, leukocyte entry into the central nervous system, transendothelial migration of tumor cells, and pulmonary hypertension (124, 129, 133, 235). These findings are in contrast to the results obtained in the current study. One reason for these contradictory results might rely in the lack of data from direct inactivation of CXCR7 by genetic deletion or CXCR7 siRNA treatment in previous studies. Furthermore, the conclusion from the current study is supported by the finding that CCX771 recruits β -arrestins with more potency than its endogenous ligands leading to an activation of MAP kinases (133). Concordantly, two compounds with similar structure as CCX771 have been proven to be agonists for Cxcr7 (236, 237). Accordingly, CXCR7 is not just a scavenger receptor, and CCX771 might be either an agonist or antagonist in specific physiological processes. Treatment with CCX771 might be a promising therapeutic approach to treat atherogenic dyslipidemia.

5. SUMMARY

Atherosclerosis is a chronic inflammatory disorder of blood vessels and is orchestrated by diverse cytokines, lipoproteins, blood cells, and cellular elements of the arterial wall (3, 4). Chemokine/chemokine receptor axes play a crucial role in the pathogenesis of atherosclerotic vascular diseases. The CXCL12/CXCR4 axis plays a fundamental role in vascular remodeling and the development of atherosclerosis. Most of these effects of CXCL12 have been linked to the interaction with CXCR4. However, the function of the alternative CXCL12 receptor, CXCR7, in the development of atherosclerosis and vascular remodeling remains elusive.

The results of the current study show that the loss of *Cxcr7* expression in *Apoe*^{-/-} mice enhanced neointima formation after vascular injury. Increased neointimal hyperplasia in the absence of *Cxcr7* is associated with increased macrophage accumulation in the neointima. The latter effect can be attributed to elevated serum cholesterol and triglyceride levels, which may promote hyperlipidemia-induced monocytes. However, *Cxcr7* deficiency did not alter the SPC mobilization after vascular injury, suggesting that the Cxcl12 gradient still exists due to the finding that the levels of this chemokine in the bone marrow and blood are simultaneously elevated. Unlike *Cxcr7* deficiency in *Apoe*^{-/-} mice, *Cxcr7* deficiency in *Apoe*^{+/+} mice fed a HCD did not exacerbate neointima formation or affect lipid levels and monocytes after vascular injury, indicating that hyperlipidemia is required for the effects of *Cxcr7* on neointima formation. Moreover, deficiency of *Cxcr7* only in bone marrow cells had no effect on neointima formation, which makes a role of *Cxcr7* on leukocytes in lesion formation unlikely.

In contrast to the effect of *Cxcr7* deficiency, administration of the *Cxcr7* ligand CCX771 in *Apoe*^{-/-} mice inhibited neointima formation. In addition, CCX771 reduced cholesterol and triglyceride levels, and diminished monocytes. Moreover, removal of spleen did not reverse the effects of CCX771 on neointima formation, excluding an important role of splenic *Cxcr7* expression in neointima formation. Given the cholesterol-lowering effect of CCX771, this study further investigated the effect of CCX771 in diet-induced atherosclerosis and found that CCX771 treatment ameliorated lesion formation and hyperlipidemia in diet-induced atherosclerosis. Of note, CCX771 treatment did not result in any obvious toxicity. Lipid profiling

analysis further demonstrated that CCX771 treatment preferentially down-regulates VLDL levels without affecting LDL and HDL levels.

This study showed that CCX771 treatment increased the cholesterol levels and the uptake of VLDL into adipocytes. However, CCX771 treatment did not alter the cholesterol levels and the uptake of VLDL in the liver. Moreover, endothelial-specific *Cxcr7* deficiency failed to increase the cholesterol levels and promote monoytosis. Therefore, the reduced circulating VLDL levels by CCX771 treatment could be attributable to the increased uptake of VLDL into *Cxcr7*-expressing adipocytes. Thus, the data of the current study indicate that *Cxcr7* regulates blood cholesterol levels by promoting its storage in adipocytes.

In conclusion, this study suggests a key role of *Cxcr7* in controlling vascular neointima formation and the development of atherosclerosis. *Cxcr7* activation promotes the uptake of VLDL into adipose tissues and decreases the blood cholesterol levels, especially VLDL cholesterol levels. As a consequence, *Cxcr7* activation ameliorates hyperlipidemia and hyperlipidemia-induced monocytois. The combined down regulation of cholesterol levels and peripheral monocyte counts might not only cause a reduction in the number of monocytes entering into vascular wall, but also reduce the differentiation from monocytes to macrophages. Reduced accumulation of macrophages may reduce the progression of neointimal hyperplasia and the formation of atherosclerotic plaques. CCX771, a *Cxcr7* ligand, could potentiate the athero-protective effects of *Cxcr7*. Accordingly, this unexpected cholesterol-lowering effect of *Cxcr7* may be beneficial in atherosclerotic vascular diseases and can be therapeutically augmented using a synthetic *Cxcr7* ligand, CCX771.

6. REFERENCES

1. Weber, C., and Noels, H. 2011. Atherosclerosis: current pathogenesis and therapeutic options. *Nat Med* 17:1410-1422.
2. Roger, V.L., Go, A.S., Lloyd-Jones, D.M., Benjamin, E.J., Berry, J.D., Borden, W.B., Bravata, D.M., Dai, S., Ford, E.S., Fox, C.S., et al. 2012. Heart disease and stroke statistics--2012 update: a report from the American Heart Association. *Circulation* 125:e2-e220.
3. Weber, C., Zernecke, A., and Libby, P. 2008. The multifaceted contributions of leukocyte subsets to atherosclerosis: lessons from mouse models. *Nat Rev Immunol* 8:802-815.
4. Glass, C.K., and Witztum, J.L. 2001. Atherosclerosis. the road ahead. *Cell* 104:503-516.
5. Ross, R. 1999. Atherosclerosis--an inflammatory disease. *N Engl J Med* 340:115-126.
6. Yamada, Y., Doi, T., Hamakubo, T., and Kodama, T. 1998. Scavenger receptor family proteins: roles for atherosclerosis, host defence and disorders of the central nervous system. *Cell Mol Life Sci* 54:628-640.
7. Carmeliet, P. 2000. Proteinases in cardiovascular aneurysms and rupture: targets for therapy? *J Clin Invest* 105:1519-1520.
8. Vijungco, J., and Eskandari, M.K. 2005. New treatments for cerebrovascular disease. *Perspect Vasc Surg Endovasc Ther* 17:279-287.
9. Lee, M.S., and Nguyen, J. Treatment options for patients with left main coronary artery disease. *Rev Cardiovasc Med* 12:e77-83.
10. Fanggiday, J.C., Stella, P.R., Guyomi, S.H., and Doevendans, P.A. 2008. Safety and efficacy of drug-eluting balloons in percutaneous treatment of bifurcation lesions: the DEBIUT (drug-eluting balloon in bifurcation Utrecht) registry. *Catheter Cardiovasc Interv* 71:629-635.
11. Schillinger, M., and Minar, E. 2005. Restenosis after percutaneous angioplasty: the role of vascular inflammation. *Vasc Health Risk Manag* 1:73-78.
12. Curcio, A., Torella, D., and Indolfi, C. Mechanisms of smooth muscle cell proliferation and endothelial regeneration after vascular injury and stenting: approach to therapy. *Circ J* 75:1287-1296.
13. Ley, K., Laudanna, C., Cybulsky, M.I., and Nourshargh, S. 2007. Getting to the site of inflammation: the leukocyte adhesion cascade updated. *Nat Rev Immunol* 7:678-689.
14. Somers, W.S., Tang, J., Shaw, G.D., and Camphausen, R.T. 2000. Insights into the molecular basis of leukocyte tethering and rolling revealed by structures of P- and E-selectin bound to SLe(X) and PSGL-1. *Cell* 103:467-479.
15. Laudanna, C., Constantin, G., Baron, P., Scarpini, E., Scarlato, G., Cabrini, G., Dehecchi, C., Rossi, F., Cassatella, M.A., and Berton, G. 1994. Sulfatides trigger increase of cytosolic free calcium and enhanced expression of tumor necrosis factor-alpha and interleukin-8 mRNA in human neutrophils. Evidence for a role of L-selectin as a signaling molecule. *J Biol Chem* 269:4021-4026.
16. Yoshida, M., Westlin, W.F., Wang, N., Ingber, D.E., Rosenzweig, A., Resnick, N., and Gimbrone, M.A., Jr. 1996. Leukocyte adhesion to vascular

- endothelium induces E-selectin linkage to the actin cytoskeleton. *J Cell Biol* 133:445-455.
17. Abbal, C., Lambelet, M., Bertaggia, D., Gerbex, C., Martinez, M., Arcaro, A., Schapira, M., and Spertini, O. 2006. Lipid raft adhesion receptors and Syk regulate selectin-dependent rolling under flow conditions. *Blood* 108:3352-3359.
18. Lowell, C.A., and Mayadas, T.N. 2011. Overview: studying integrins in vivo. *Methods Mol Biol* 757:369-397.
19. Campbell, I.D., and Humphries, M.J. 2011. Integrin structure, activation, and interactions. *Cold Spring Harb Perspect Biol* 3.
20. Chan, J.R., Hyduk, S.J., and Cybulsky, M.I. 2001. Chemoattractants induce a rapid and transient upregulation of monocyte alpha4 integrin affinity for vascular cell adhesion molecule 1 which mediates arrest: an early step in the process of emigration. *J Exp Med* 193:1149-1158.
21. Schenkel, A.R., Mamdouh, Z., and Muller, W.A. 2004. Locomotion of monocytes on endothelium is a critical step during extravasation. *Nat Immunol* 5:393-400.
22. Phillipson, M., Heit, B., Colarusso, P., Liu, L., Ballantyne, C.M., and Kubes, P. 2006. Intraluminal crawling of neutrophils to emigration sites: a molecularly distinct process from adhesion in the recruitment cascade. *J Exp Med* 203:2569-2575.
23. Muller, W.A. 2003. Leukocyte-endothelial-cell interactions in leukocyte transmigration and the inflammatory response. *Trends Immunol* 24:327-334.
24. Vestweber, D. 2002. Regulation of endothelial cell contacts during leukocyte extravasation. *Curr Opin Cell Biol* 14:587-593.
25. Nourshargh, S., Krombach, F., and Dejana, E. 2006. The role of JAM-A and PECAM-1 in modulating leukocyte infiltration in inflamed and ischemic tissues. *J Leukoc Biol* 80:714-718.
26. Geissmann, F., Manz, M.G., Jung, S., Sieweke, M.H., Merad, M., and Ley, K. 2010. Development of monocytes, macrophages, and dendritic cells. *Science* 327:656-661.
27. Woollard, K.J., and Geissmann, F. 2010. Monocytes in atherosclerosis: subsets and functions. *Nat Rev Cardiol* 7:77-86.
28. Auffray, C., Sieweke, M.H., and Geissmann, F. 2009. Blood monocytes: development, heterogeneity, and relationship with dendritic cells. *Annu Rev Immunol* 27:669-692.
29. Grage-Griebenow, E., Flad, H.D., and Ernst, M. 2001. Heterogeneity of human peripheral blood monocyte subsets. *J Leukoc Biol* 69:11-20.
30. Ziegler-Heitbrock, H.W. 2000. Definition of human blood monocytes. *J Leukoc Biol* 67:603-606.
31. Passlick, B., Flieger, D., and Ziegler-Heitbrock, H.W. 1989. Identification and characterization of a novel monocyte subpopulation in human peripheral blood. *Blood* 74:2527-2534.
32. Auffray, C., Fogg, D., Garfa, M., Elain, G., Join-Lambert, O., Kayal, S., Sarnacki, S., Cumano, A., Lauvau, G., and Geissmann, F. 2007. Monitoring of blood vessels and tissues by a population of monocytes with patrolling behavior. *Science* 317:666-670.
33. Sasmono, R.T., Oceandy, D., Pollard, J.W., Tong, W., Pavli, P., Wainwright, B.J., Ostrowski, M.C., Himes, S.R., and Hume, D.A. 2003. A macrophage colony-stimulating factor receptor-green fluorescent protein transgene is

- expressed throughout the mononuclear phagocyte system of the mouse. *Blood* 101:1155-1163.
34. Serbina, N.V., Salazar-Mather, T.P., Biron, C.A., Kuziel, W.A., and Pamer, E.G. 2003. TNF/iNOS-producing dendritic cells mediate innate immune defense against bacterial infection. *Immunity* 19:59-70.
 35. Nahrendorf, M., Swirski, F.K., Aikawa, E., Stangenberg, L., Wurdinger, T., Figueiredo, J.L., Libby, P., Weissleder, R., and Pittet, M.J. 2007. The healing myocardium sequentially mobilizes two monocyte subsets with divergent and complementary functions. *J Exp Med* 204:3037-3047.
 36. Danenberg, H.D., Golomb, G., Groothuis, A., Gao, J., Epstein, H., Swaminathan, R.V., Seifert, P., and Edelman, E.R. 2003. Liposomal alendronate inhibits systemic innate immunity and reduces in-stent neointimal hyperplasia in rabbits. *Circulation* 108:2798-2804.
 37. Moreno, P.R., Falk, E., Palacios, I.F., Newell, J.B., Fuster, V., and Fallon, J.T. 1994. Macrophage infiltration in acute coronary syndromes. Implications for plaque rupture. *Circulation* 90:775-778.
 38. Swirski, F.K., Libby, P., Aikawa, E., Alcaide, P., Luscinskas, F.W., Weissleder, R., and Pittet, M.J. 2007. Ly-6Chi monocytes dominate hypercholesterolemia-associated monocytosis and give rise to macrophages in atheromata. *J Clin Invest* 117:195-205.
 39. An, G., Wang, H., Tang, R., Yago, T., McDaniel, J.M., McGee, S., Huo, Y., and Xia, L. 2008. P-selectin glycoprotein ligand-1 is highly expressed on Ly-6Chi monocytes and a major determinant for Ly-6Chi monocyte recruitment to sites of atherosclerosis in mice. *Circulation* 117:3227-3237.
 40. Tacke, F., Alvarez, D., Kaplan, T.J., Jakubzick, C., Spanbroek, R., Llodra, J., Garin, A., Liu, J., Mack, M., van Rooijen, N., et al. 2007. Monocyte subsets differentially employ CCR2, CCR5, and CX3CR1 to accumulate within atherosclerotic plaques. *J Clin Invest* 117:185-194.
 41. Schiopu, A., Nadig, S.N., Cotoi, O.S., Hester, J., van Rooijen, N., and Wood, K.J. 2012. Inflammatory Ly-6C(hi) monocytes play an important role in the development of severe transplant arteriosclerosis in hyperlipidemic recipients. *Atherosclerosis* 223:291-298.
 42. Wu, H., Gower, R.M., Wang, H., Perrard, X.Y., Ma, R., Bullard, D.C., Burns, A.R., Paul, A., Smith, C.W., Simon, S.I., et al. 2009. Functional role of CD11c+ monocytes in atherogenesis associated with hypercholesterolemia. *Circulation* 119:2708-2717.
 43. Goldstein, J.L., Ho, Y.K., Basu, S.K., and Brown, M.S. 1979. Binding site on macrophages that mediates uptake and degradation of acetylated low density lipoprotein, producing massive cholesterol deposition. *Proc Natl Acad Sci U S A* 76:333-337.
 44. Ross, R. 1995. Cell biology of atherosclerosis. *Annu Rev Physiol* 57:791-804.
 45. Ross, R. 1993. The pathogenesis of atherosclerosis: a perspective for the 1990s. *Nature* 362:801-809.
 46. Ferns, G.A., Forster, L., Stewart-Lee, A., Konneh, M., Nourooz-Zadeh, J., and Anggard, E.E. 1992. Probucol inhibits neointimal thickening and macrophage accumulation after balloon injury in the cholesterol-fed rabbit. *Proc Natl Acad Sci U S A* 89:11312-11316.
 47. Schober, A., and Zerneck, A. 2007. Chemokines in vascular remodeling. *Thromb Haemost* 97:730-737.

REFERENCES

48. Zlotnik, A., and Yoshie, O. 2000. Chemokines: a new classification system and their role in immunity. *Immunity* 12:121-127.
49. Vandercappellen, J., Van Damme, J., and Struyf, S. 2008. The role of CXC chemokines and their receptors in cancer. *Cancer Lett* 267:226-244.
50. Strieter, R.M., Polverini, P.J., Kunkel, S.L., Arenberg, D.A., Burdick, M.D., Kasper, J., Dzuiba, J., Van Damme, J., Walz, A., Marriott, D., et al. 1995. The functional role of the ELR motif in CXC chemokine-mediated angiogenesis. *J Biol Chem* 270:27348-27357.
51. Pan, Y., Lloyd, C., Zhou, H., Dolich, S., Deeds, J., Gonzalo, J.A., Vath, J., Gosselin, M., Ma, J., Dussault, B., et al. 1997. Neurotactin, a membrane-anchored chemokine upregulated in brain inflammation. *Nature* 387:611-617.
52. Schulte, A., Schulz, B., Andrzejewski, M.G., Hundhausen, C., Mletzko, S., Achilles, J., Reiss, K., Paliga, K., Weber, C., John, S.R., et al. 2007. Sequential processing of the transmembrane chemokines CX3CL1 and CXCL16 by alpha- and gamma-secretases. *Biochem Biophys Res Commun* 358:233-240.
53. Sun, X., Cheng, G., Hao, M., Zheng, J., Zhou, X., Zhang, J., Taichman, R.S., Pienta, K.J., and Wang, J. 2010. Erratum to: CXCL12 / CXCR4 / CXCR7 chemokine axis and cancer progression. *Cancer Metastasis Rev.*
54. Lappano, R., and Maggiolini, M. 2011. G protein-coupled receptors: novel targets for drug discovery in cancer. *Nat Rev Drug Discov* 10:47-60.
55. Schwartz, T.W., and Sakmar, T.P. 2011. Structural biology: snapshot of a signalling complex. *Nature* 477:540-541.
56. Allen, S.J., Crown, S.E., and Handel, T.M. 2007. Chemokine: receptor structure, interactions, and antagonism. *Annu Rev Immunol* 25:787-820.
57. Rajagopalan, L., and Rajarathnam, K. 2006. Structural basis of chemokine receptor function--a model for binding affinity and ligand selectivity. *Biosci Rep* 26:325-339.
58. Shibata, T., Suzuki, C., Ohnishi, J., Murakami, K., and Miyazaki, H. 1996. Identification of regions in the human angiotensin II receptor type 1 responsible for Gi and Gq coupling by mutagenesis study. *Biochem Biophys Res Commun* 218:383-389.
59. Gaborik, Z., Jagadeesh, G., Zhang, M., Spat, A., Catt, K.J., and Hunyady, L. 2003. The role of a conserved region of the second intracellular loop in AT1 angiotensin receptor activation and signaling. *Endocrinology* 144:2220-2228.
60. Roland, J., Murphy, B.J., Ahr, B., Robert-Hebmann, V., Delauzun, V., Nye, K.E., Devaux, C., and Biard-Piechaczyk, M. 2003. Role of the intracellular domains of CXCR4 in SDF-1-mediated signaling. *Blood* 101:399-406.
61. Breitwieser, G.E. 2004. G protein-coupled receptor oligomerization: implications for G protein activation and cell signaling. *Circ Res* 94:17-27.
62. Milligan, G., Ramsay, D., Pascal, G., and Carrillo, J.J. 2003. GPCR dimerisation. *Life Sci* 74:181-188.
63. Trettel, F., Di Bartolomeo, S., Lauro, C., Catalano, M., Ciotti, M.T., and Limatola, C. 2003. Ligand-independent CXCR2 dimerization. *J Biol Chem* 278:40980-40988.
64. Ceradini, D.J., Kulkarni, A.R., Callaghan, M.J., Tepper, O.M., Bastidas, N., Kleinman, M.E., Capla, J.M., Galiano, R.D., Levine, J.P., and Gurtner, G.C. 2004. Progenitor cell trafficking is regulated by hypoxic gradients through HIF-1 induction of SDF-1. *Nat Med* 10:858-864.

65. Orimo, A., Gupta, P.B., Sgroi, D.C., Arenzana-Seisdedos, F., Delaunay, T., Naeem, R., Carey, V.J., Richardson, A.L., and Weinberg, R.A. 2005. Stromal fibroblasts present in invasive human breast carcinomas promote tumor growth and angiogenesis through elevated SDF-1/CXCL12 secretion. *Cell* 121:335-348.
66. Muller, A., Homey, B., Soto, H., Ge, N., Catron, D., Buchanan, M.E., McClanahan, T., Murphy, E., Yuan, W., Wagner, S.N., et al. 2001. Involvement of chemokine receptors in breast cancer metastasis. *Nature* 410:50-56.
67. Ma, Q., Jones, D., Borghesani, P.R., Segal, R.A., Nagasawa, T., Kishimoto, T., Bronson, R.T., and Springer, T.A. 1998. Impaired B-lymphopoiesis, myelopoiesis, and derailed cerebellar neuron migration in CXCR4- and SDF-1-deficient mice. *Proc Natl Acad Sci U S A* 95:9448-9453.
68. Tachibana, K., Hirota, S., Iizasa, H., Yoshida, H., Kawabata, K., Kataoka, Y., Kitamura, Y., Matsushima, K., Yoshida, N., Nishikawa, S., et al. 1998. The chemokine receptor CXCR4 is essential for vascularization of the gastrointestinal tract. *Nature* 393:591-594.
69. Bleul, C.C., Wu, L., Hoxie, J.A., Springer, T.A., and Mackay, C.R. 1997. The HIV coreceptors CXCR4 and CCR5 are differentially expressed and regulated on human T lymphocytes. *Proc Natl Acad Sci U S A* 94:1925-1930.
70. Bryant, J., Ahern, D.J., and Brennan, F.M. 2012. CXCR4 and vascular cell adhesion molecule 1 are key chemokine/adhesion receptors in the migration of cytokine-activated T cells. *Arthritis Rheum* 64:2137-2146.
71. Schols, D., Struyf, S., Van Damme, J., Este, J.A., Henson, G., and De Clercq, E. 1997. Inhibition of T-tropic HIV strains by selective antagonization of the chemokine receptor CXCR4. *J Exp Med* 186:1383-1388.
72. Bleul, C.C., Farzan, M., Choe, H., Parolin, C., Clark-Lewis, I., Sodroski, J., and Springer, T.A. 1996. The lymphocyte chemoattractant SDF-1 is a ligand for LESTR/fusin and blocks HIV-1 entry. *Nature* 382:829-833.
73. Tashiro, K., Tada, H., Heilker, R., Shirozu, M., Nakano, T., and Honjo, T. 1993. Signal sequence trap: a cloning strategy for secreted proteins and type I membrane proteins. *Science* 261:600-603.
74. Nagasawa, T., Kikutani, H., and Kishimoto, T. 1994. Molecular cloning and structure of a pre-B-cell growth-stimulating factor. *Proc Natl Acad Sci U S A* 91:2305-2309.
75. Janowski, M. 2009. Functional diversity of SDF-1 splicing variants. *Cell Adh Migr* 3:243-249.
76. Shirozu, M., Nakano, T., Inazawa, J., Tashiro, K., Tada, H., Shinohara, T., and Honjo, T. 1995. Structure and chromosomal localization of the human stromal cell-derived factor 1 (SDF1) gene. *Genomics* 28:495-500.
77. Ponomaryov, T., Peled, A., Petit, I., Taichman, R.S., Habler, L., Sandbank, J., Arenzana-Seisdedos, F., Magerus, A., Caruz, A., Fujii, N., et al. 2000. Induction of the chemokine stromal-derived factor-1 following DNA damage improves human stem cell function. *J Clin Invest* 106:1331-1339.
78. De Falco, E., Porcelli, D., Torella, A.R., Straino, S., Iachininoto, M.G., Orlandi, A., Truffa, S., Biglioli, P., Napolitano, M., Capogrossi, M.C., et al. 2004. SDF-1 involvement in endothelial phenotype and ischemia-induced recruitment of bone marrow progenitor cells. *Blood* 104:3472-3482.
79. Sweeney, E.A., Lortat-Jacob, H., Priestley, G.V., Nakamoto, B., and Papayannopoulou, T. 2002. Sulfated polysaccharides increase plasma levels of

- SDF-1 in monkeys and mice: involvement in mobilization of stem/progenitor cells. *Blood* 99:44-51.
80. Hattori, K., Heissig, B., Tashiro, K., Honjo, T., Tateno, M., Shieh, J.H., Hackett, N.R., Quitarano, M.S., Crystal, R.G., Rafii, S., et al. 2001. Plasma elevation of stromal cell-derived factor-1 induces mobilization of mature and immature hematopoietic progenitor and stem cells. *Blood* 97:3354-3360.
81. Petit, I., Szyper-Kravitz, M., Nagler, A., Lahav, M., Peled, A., Habler, L., Ponomaryov, T., Taichman, R.S., Arenzana-Seisdedos, F., Fujii, N., et al. 2002. G-CSF induces stem cell mobilization by decreasing bone marrow SDF-1 and up-regulating CXCR4. *Nat Immunol* 3:687-694.
82. Nagasawa, T., Hirota, S., Tachibana, K., Takakura, N., Nishikawa, S., Kitamura, Y., Yoshida, N., Kikutani, H., and Kishimoto, T. 1996. Defects of B-cell lymphopoiesis and bone-marrow myelopoiesis in mice lacking the CXC chemokine PBSF/SDF-1. *Nature* 382:635-638.
83. Zou, Y.R., Kottmann, A.H., Kuroda, M., Taniuchi, I., and Littman, D.R. 1998. Function of the chemokine receptor CXCR4 in haematopoiesis and in cerebellar development. *Nature* 393:595-599.
84. Schober, A., Knarren, S., Lietz, M., Lin, E.A., and Weber, C. 2003. Crucial role of stromal cell-derived factor-1alpha in neointima formation after vascular injury in apolipoprotein E-deficient mice. *Circulation* 108:2491-2497.
85. Zernecke, A., Schober, A., Bot, I., von Hundelshausen, P., Liehn, E.A., Mopps, B., Mericskay, M., Gierschik, P., Biessen, E.A., and Weber, C. 2005. SDF-1alpha/CXCR4 axis is instrumental in neointimal hyperplasia and recruitment of smooth muscle progenitor cells. *Circ Res* 96:784-791.
86. Zernecke, A., Bot, I., Djalali-Talab, Y., Shagdarsuren, E., Bidzhekov, K., Meiler, S., Krohn, R., Schober, A., Sperandio, M., Soehnlein, O., et al. 2008. Protective role of CXC receptor 4/CXC ligand 12 unveils the importance of neutrophils in atherosclerosis. *Circ Res* 102:209-217.
87. Karshovska, E., Zagorac, D., Zernecke, A., Weber, C., and Schober, A. 2008. A small molecule CXCR4 antagonist inhibits neointima formation and smooth muscle progenitor cell mobilization after arterial injury. *J Thromb Haemost* 6:1812-1815.
88. Subramanian, P., Karshovska, E., Reinhard, P., Megens, R.T., Zhou, Z., Akhtar, S., Schumann, U., Li, X., van Zandvoort, M., Ludin, C., et al. 2010. Lysophosphatidic acid receptors LPA1 and LPA3 promote CXCL12-mediated smooth muscle progenitor cell recruitment in neointima formation. *Circ Res* 107:96-105.
89. Hamesch, K., Subramanian, P., Li, X., Dembowsky, K., Chevalier, E., Weber, C., and Schober, A. 2012. The CXCR4 antagonist POL5551 is equally effective as sirolimus in reducing neointima formation without impairing re-endothelialisation. *Thromb Haemost* 107:356-368.
90. Martin, C., Burdon, P.C., Bridger, G., Gutierrez-Ramos, J.C., Williams, T.J., and Rankin, S.M. 2003. Chemokines acting via CXCR2 and CXCR4 control the release of neutrophils from the bone marrow and their return following senescence. *Immunity* 19:583-593.
91. Zernecke, A., Bidzhekov, K., Noels, H., Shagdarsuren, E., Gan, L., Denecke, B., Hristov, M., Koppel, T., Jahantigh, M.N., Lutgens, E., et al. 2009. Delivery of microRNA-126 by apoptotic bodies induces CXCL12-dependent vascular protection. *Science signaling* 2:ra81.

92. Damas, J.K., Waehre, T., Yndestad, A., Ueland, T., Muller, F., Eiken, H.G., Holm, A.M., Halvorsen, B., Froland, S.S., Gullestad, L., et al. 2002. Stromal cell-derived factor-1 α in unstable angina: potential antiinflammatory and matrix-stabilizing effects. *Circulation* 106:36-42.
93. Stellos, K., Ruf, M., Sopova, K., Kiliass, A., Rahmann, A., Stamatelopoulos, K., Jorbenadze, R., Geisler, T., Gawaz, M., and Bigalke, B. 2011. Plasma levels of stromal cell-derived factor-1 in patients with coronary artery disease: effect of clinical presentation and cardiovascular risk factors. *Atherosclerosis* 219:913-916.
94. Abi-Younes, S., Sauty, A., Mach, F., Sukhova, G.K., Libby, P., and Luster, A.D. 2000. The stromal cell-derived factor-1 chemokine is a potent platelet agonist highly expressed in atherosclerotic plaques. *Circ Res* 86:131-138.
95. Kathiresan, S., Voight, B.F., Purcell, S., Musunuru, K., Ardissino, D., Mannucci, P.M., Anand, S., Engert, J.C., Samani, N.J., Schunkert, H., et al. 2009. Genome-wide association of early-onset myocardial infarction with single nucleotide polymorphisms and copy number variants. *Nat Genet* 41:334-341.
96. Dzau, V.J., Braun-Dullaeus, R.C., and Sedding, D.G. 2002. Vascular proliferation and atherosclerosis: new perspectives and therapeutic strategies. *Nat Med* 8:1249-1256.
97. Sartore, S., Chiavegato, A., Faggini, E., Franch, R., Puato, M., Ausoni, S., and Pauletto, P. 2001. Contribution of adventitial fibroblasts to neointima formation and vascular remodeling: from innocent bystander to active participant. *Circ Res* 89:1111-1121.
98. Scott, N.A., Cipolla, G.D., Ross, C.E., Dunn, B., Martin, F.H., Simonet, L., and Wilcox, J.N. 1996. Identification of a potential role for the adventitia in vascular lesion formation after balloon overstretch injury of porcine coronary arteries. *Circulation* 93:2178-2187.
99. Daniel, J.M., and Sedding, D.G. 2011. Circulating smooth muscle progenitor cells in arterial remodeling. *J Mol Cell Cardiol* 50:273-279.
100. Sata, M., Saiura, A., Kunisato, A., Tojo, A., Okada, S., Tokuhisa, T., Hirai, H., Makuuchi, M., Hirata, Y., and Nagai, R. 2002. Hematopoietic stem cells differentiate into vascular cells that participate in the pathogenesis of atherosclerosis. *Nat Med* 8:403-409.
101. Shimizu, K., Sugiyama, S., Aikawa, M., Fukumoto, Y., Rabkin, E., Libby, P., and Mitchell, R.N. 2001. Host bone-marrow cells are a source of donor intimal smooth-muscle-like cells in murine aortic transplant arteriopathy. *Nat Med* 7:738-741.
102. Hui, D.Y. 2008. Intimal hyperplasia in murine models. *Curr Drug Targets* 9:251-260.
103. Schober, A., Zhou Z, Weber C. 2012. Smooth muscle progenitor cells: A novel target for the treatment of vascular disease? In *Muscle fundamental biology and mechanisms of disease* J. Hill, and Elsevier Science (Firm), editors. S.I.: Academic Press. 1391-1400.
104. Simper, D., Stalboerger, P.G., Panetta, C.J., Wang, S., and Caplice, N.M. 2002. Smooth muscle progenitor cells in human blood. *Circulation* 106:1199-1204.
105. Tanaka, K., Sata, M., Natori, T., Kim-Kaneyama, J.R., Nose, K., Shibamura, M., Hirata, Y., and Nagai, R. 2008. Circulating progenitor cells contribute to neointimal formation in nonirradiated chimeric mice. *Faseb J* 22:428-436.

106. Subramanian, P., Karshovska, E., Reinhard, P., Megens, R.T.A., Zhou, Z., Akhtar, S., Schumann, U., Li, X., van Zandvoort, M., Ludin, C., et al. 2010. Lysophosphatidic acid receptors LPA1 and LPA3 promote CXCL12-mediated smooth muscle progenitor cell recruitment in neointima formation. *Circ Res* 107:96-105.
107. Yu, H., Stoneman, V., Clarke, M., Figg, N., Xin, H.B., Kotlikoff, M., Littlewood, T., and Bennett, M. 2011. Bone marrow-derived smooth muscle-like cells are infrequent in advanced primary atherosclerotic plaques but promote atherosclerosis. *Arterioscler Thromb Vasc Biol* 31:1291-1299.
108. Schober, A. 2008. Chemokines in vascular dysfunction and remodeling. *Arterioscler Thromb Vasc Biol* 28:1950-1959.
109. Massberg, S., Konrad, I., Schurzinger, K., Lorenz, M., Schneider, S., Zohlhoefer, D., Hoppe, K., Schiemann, M., Kennerknecht, E., Sauer, S., et al. 2006. Platelets secrete stromal cell-derived factor 1alpha and recruit bone marrow-derived progenitor cells to arterial thrombi in vivo. *J Exp Med* 203:1221-1233.
110. Burns, J.M., Summers, B.C., Wang, Y., Melikian, A., Berahovich, R., Miao, Z., Penfold, M.E., Sunshine, M.J., Littman, D.R., Kuo, C.J., et al. 2006. A novel chemokine receptor for SDF-1 and I-TAC involved in cell survival, cell adhesion, and tumor development. *J Exp Med* 203:2201-2213.
111. Balabanian, K., Lagane, B., Infantino, S., Chow, K.Y., Harriague, J., Moepps, B., Arenzana-Seisdedos, F., Thelen, M., and Bachelier, F. 2005. The chemokine SDF-1/CXCL12 binds to and signals through the orphan receptor RDC1 in T lymphocytes. *J Biol Chem* 280:35760-35766.
112. Gerrits, H., van Ingen Schenau, D.S., Bakker, N.E., van Disseldorp, A.J., Strik, A., Hermens, L.S., Koenen, T.B., Krajnc-Franken, M.A., and Gossen, J.A. 2008. Early postnatal lethality and cardiovascular defects in CXCR7-deficient mice. *Genesis* 46:235-245.
113. Sierro, F., Biben, C., Martinez-Munoz, L., Mellado, M., Ransohoff, R.M., Li, M., Woehl, B., Leung, H., Groom, J., Batten, M., et al. 2007. Disrupted cardiac development but normal hematopoiesis in mice deficient in the second CXCL12/SDF-1 receptor, CXCR7. *Proc Natl Acad Sci U S A* 104:14759-14764.
114. Berahovich, R.D., Zabel, B.A., Penfold, M.E., Lewen, S., Wang, Y., Miao, Z., Gan, L., Pereda, J., Dias, J., Slukvin, II, et al. 2010. CXCR7 protein is not expressed on human or mouse leukocytes. *J Immunol* 185:5130-5139.
115. Miao, Z., Luker, K.E., Summers, B.C., Berahovich, R., Bhojani, M.S., Rehemtulla, A., Kleer, C.G., Essner, J.J., Nasevicius, A., Luker, G.D., et al. 2007. CXCR7 (RDC1) promotes breast and lung tumor growth in vivo and is expressed on tumor-associated vasculature. *Proc Natl Acad Sci U S A* 104:15735-15740.
116. Tarnowski, M., Grymula, K., Reca, R., Jankowski, K., Maksym, R., Tarnowska, J., Przybylski, G., Barr, F.G., Kucia, M., and Ratajczak, M.Z. 2010. Regulation of expression of stromal-derived factor-1 receptors: CXCR4 and CXCR7 in human rhabdomyosarcomas. *Mol Cancer Res* 8:1-14.
117. Wang, J., Shiozawa, Y., Wang, J., Wang, Y., Jung, Y., Pienta, K.J., Mehra, R., Loberg, R., and Taichman, R.S. 2008. The role of CXCR7/RDC1 as a chemokine receptor for CXCL12/SDF-1 in prostate cancer. *J Biol Chem* 283:4283-4294.

118. Tarnowski, M., Liu, R., Wysoczynski, M., Ratajczak, J., Kucia, M., and Ratajczak, M.Z. 2010. CXCR7: a new SDF-1-binding receptor in contrast to normal CD34(+) progenitors is functional and is expressed at higher level in human malignant hematopoietic cells. *Eur J Haematol* 85:472-483.
119. Van Rechem, C., Rood, B.R., Touka, M., Pinte, S., Jenal, M., Guerardel, C., Ramsey, K., Monte, D., Begue, A., Tschan, M.P., et al. 2009. Scavenger chemokine (CXC motif) receptor 7 (CXCR7) is a direct target gene of HIC1 (hypermethylated in cancer 1). *J Biol Chem* 284:20927-20935.
120. Boudot, A., Kerdivel, G., Habauzit, D., Eeckhoutte, J., Le Dily, F., Flouriot, G., Samson, M., and Pakdel, F. 2011. Differential estrogen-regulation of CXCL12 chemokine receptors, CXCR4 and CXCR7, contributes to the growth effect of estrogens in breast cancer cells. *PLoS One* 6:e20898.
121. Liu, H., Xue, W., Ge, G., Luo, X., Li, Y., Xiang, H., Ding, X., Tian, P., and Tian, X. 2010. Hypoxic preconditioning advances CXCR4 and CXCR7 expression by activating HIF-1alpha in MSCs. *Biochem Biophys Res Commun* 401:509-515.
122. Marechal, R., Demetter, P., Nagy, N., Berton, A., Decaestecker, C., Polus, M., Closset, J., Deviere, J., Salmon, I., and Van Laethem, J.L. 2009. High expression of CXCR4 may predict poor survival in resected pancreatic adenocarcinoma. *Br J Cancer* 100:1444-1451.
123. Jin, Z., Nagakubo, D., Shirakawa, A.K., Nakayama, T., Shigeta, A., Hieshima, K., Yamada, Y., and Yoshie, O. 2009. CXCR7 is inducible by HTLV-1 Tax and promotes growth and survival of HTLV-1-infected T cells. *Int J Cancer* 125:2229-2235.
124. Cruz-Orengo, L., Holman, D.W., Dorsey, D., Zhou, L., Zhang, P., Wright, M., McCandless, E.E., Patel, J.R., Luker, G.D., Littman, D.R., et al. 2011. CXCR7 influences leukocyte entry into the CNS parenchyma by controlling abluminal CXCL12 abundance during autoimmunity. *J Exp Med* 208:327-339.
125. Libert, F., Parmentier, M., Lefort, A., Dumont, J.E., and Vassart, G. 1990. Complete nucleotide sequence of a putative G protein coupled receptor: RDC1. *Nucleic Acids Res* 18:1917.
126. Levoye, A., Balabanian, K., Baleux, F., Bachelierie, F., and Lagane, B. 2009. CXCR7 heterodimerizes with CXCR4 and regulates CXCL12-mediated G protein signaling. *Blood* 113:6085-6093.
127. Damaj, B.B., McColl, S.R., Neote, K., Songqing, N., Ogborn, K.T., Hebert, C.A., and Naccache, P.H. 1996. Identification of G-protein binding sites of the human interleukin-8 receptors by functional mapping of the intracellular loops. *Faseb J* 10:1426-1434.
128. Naumann, U., Cameroni, E., Pruenster, M., Mahabaleshwar, H., Raz, E., Zerwes, H.G., Rot, A., and Thelen, M. 2010 Feb CXCR7 functions as a scavenger for CXCL12 and CXCL11. *PLoS One* 5:e9175.
129. Hartmann, T.N., Grabovsky, V., Pasvolsky, R., Shulman, Z., Buss, E.C., Spiegel, A., Nagler, A., Lapidot, T., Thelen, M., and Alon, R. 2008. A crosstalk between intracellular CXCR7 and CXCR4 involved in rapid CXCL12-triggered integrin activation but not in chemokine-triggered motility of human T lymphocytes and CD34+ cells. *J Leukoc Biol* 84:1130-1140.
130. Rajagopal, S., Kim, J., Ahn, S., Craig, S., Lam, C.M., Gerard, N.P., Gerard, C., and Lefkowitz, R.J. 2010. Beta-arrestin- but not G protein-mediated signaling by the "decoy" receptor CXCR7. *Proc Natl Acad Sci U S A* 107:628-632.

131. Decaillot, F.M., Kazmi, M.A., Lin, Y., Ray-Saha, S., Sakmar, T.P., and Sachdev, P. 2011. CXCR7/CXCR4 heterodimer constitutively recruits beta-arrestin to enhance cell migration. *J Biol Chem* 286:32188-32197.
132. Boldajipour, B., Mahabaleshwar, H., Kardash, E., Reichman-Fried, M., Blaser, H., Minina, S., Wilson, D., Xu, Q., and Raz, E. 2008. Control of chemokine-guided cell migration by ligand sequestration. *Cell* 132:463-473.
133. Zabel, B.A., Wang, Y., Lewen, S., Berahovich, R.D., Penfold, M.E., Zhang, P., Powers, J., Summers, B.C., Miao, Z., Zhao, B., et al. 2009. Elucidation of CXCR7-mediated signaling events and inhibition of CXCR4-mediated tumor cell transendothelial migration by CXCR7 ligands. *J Immunol* 183:3204-3211.
134. Luker, K.E., Steele, J.M., Mihalko, L.A., Ray, P., and Luker, G.D. 2010. Constitutive and chemokine-dependent internalization and recycling of CXCR7 in breast cancer cells to degrade chemokine ligands. *Oncogene* 29:4599-4610.
135. Maksym, R.B., Tarnowski, M., Grymula, K., Tarnowska, J., Wysoczynski, M., Liu, R., Czerny, B., Ratajczak, J., Kucia, M., and Ratajczak, M.Z. 2009. The role of stromal-derived factor-1 - CXCR7 axis in development and cancer. *Eur J Pharmacol*.
136. Berahovich, R.D., Zabel, B.A., Penfold, M.E., Lewen, S., Wang, Y., Miao, Z., Gan, L., Pereda, J., Dias, J., Slukvin, II, et al. 2010. CXCR7 protein is not expressed on human or mouse leukocytes. *J Immunol* 185:5130-5139.
137. Hayashi, S., and McMahon, A.P. 2002. Efficient recombination in diverse tissues by a tamoxifen-inducible form of Cre: a tool for temporally regulated gene activation/inactivation in the mouse. *Dev Biol* 244:305-318.
138. Monvoisin, A., Alva, J.A., Hofmann, J.J., Zovein, A.C., Lane, T.F., and Iruela-Arispe, M.L. 2006. VE-cadherin-CreERT2 transgenic mouse: a model for inducible recombination in the endothelium. *Dev Dyn* 235:3413-3422.
139. Lindner, V., Fingerle, J., and Reidy, M.A. 1993. Mouse model of arterial injury. *Circ Res* 73:792-796.
140. Zhang, S.H., Reddick, R.L., Burkey, B., and Maeda, N. 1994. Diet-induced atherosclerosis in mice heterozygous and homozygous for apolipoprotein E gene disruption. *J Clin Invest* 94:937-945.
141. Meir, K.S., and Leitersdorf, E. 2004. Atherosclerosis in the apolipoprotein-E-deficient mouse: a decade of progress. *Arterioscler Thromb Vasc Biol* 24:1006-1014.
142. Huston, J.M., Ochani, M., Rosas-Ballina, M., Liao, H., Ochani, K., Pavlov, V.A., Gallowitsch-Puerta, M., Ashok, M., Czura, C.J., Foxwell, B., et al. 2006. Splenectomy inactivates the cholinergic antiinflammatory pathway during lethal endotoxemia and polymicrobial sepsis. *J Exp Med* 203:1623-1628.
143. Abdelrahman, M., Collin, M., and Thiemermann, C. 2004. The peroxisome proliferator-activated receptor-gamma ligand 15-deoxyDelta12,14 prostaglandin J2 reduces the organ injury in hemorrhagic shock. *Shock* 22:555-561.
144. Garber, D.W., Kulkarni, K.R., and Anantharamaiah, G.M. 2000. A sensitive and convenient method for lipoprotein profile analysis of individual mouse plasma samples. *J Lipid Res* 41:1020-1026.
145. Hellems, J., Mortier, G., De Paepe, A., Speleman, F., and Vandesompele, J. 2007. qBase relative quantification framework and software for management

- and automated analysis of real-time quantitative PCR data. *Genome Biol* 8:R19.
146. Russell, H.K., Jr. 1972. A modification of Movat's pentachrome stain. *Arch Pathol* 94:187-191.
 147. Otto, C.M., Kuusisto, J., Reichenbach, D.D., Gown, A.M., and O'Brien, K.D. 1994. Characterization of the early lesion of 'degenerative' valvular aortic stenosis. Histological and immunohistochemical studies. *Circulation* 90:844-853.
 148. Nunnari, J.J., Zand, T., Joris, I., and Majno, G. 1989. Quantitation of oil red O staining of the aorta in hypercholesterolemic rats. *Exp Mol Pathol* 51:1-8.
 149. Bell, P., Limberis, M., Gao, G., Wu, D., Bove, M.S., Sanmiguel, J.C., and Wilson, J.M. 2005. An optimized protocol for detection of E. coli beta-galactosidase in lung tissue following gene transfer. *Histochem Cell Biol* 124:77-85.
 150. So, P.T., Dong, C.Y., Masters, B.R., and Berland, K.M. 2000. Two-photon excitation fluorescence microscopy. *Annu Rev Biomed Eng* 2:399-429.
 151. Megens, R.T., Reitsma, S., Schiffers, P.H., Hilgers, R.H., De Mey, J.G., Slaaf, D.W., oude Egbrink, M.G., and van Zandvoort, M.A. 2007. Two-photon microscopy of vital murine elastic and muscular arteries. Combined structural and functional imaging with subcellular resolution. *J Vasc Res* 44:87-98.
 152. O'Connell, K.A., and Edidin, M. 1990. A mouse lymphoid endothelial cell line immortalized by simian virus 40 binds lymphocytes and retains functional characteristics of normal endothelial cells. *J Immunol* 144:521-525.
 153. Schober, A., Karshovska, E., Zerneck, A., and Weber, C. 2006. SDF-1alpha-mediated tissue repair by stem cells: a promising tool in cardiovascular medicine? *Trends Cardiovasc Med* 16:103-108.
 154. Fatouros, M., Bourantas, K., Bairaktari, E., Elisaf, M., Tsolas, O., and Cassiouis, D. 1995. Role of the spleen in lipid metabolism. *Br J Surg* 82:1675-1677.
 155. Aviram, M., Brook, J.G., Tatarsky, I., Levy, Y., and Carter, A. 1986. Increased low-density lipoprotein levels after splenectomy: a role for the spleen in cholesterol metabolism in myeloproliferative disorders. *Am J Med Sci* 291:25-28.
 156. Swirski, F.K., Nahrendorf, M., Etzrodt, M., Wildgruber, M., Cortez-Retamozo, V., Panizzi, P., Figueiredo, J.L., Kohler, R.H., Chudnovskiy, A., Waterman, P., et al. 2009. Identification of splenic reservoir monocytes and their deployment to inflammatory sites. *Science* 325:612-616.
 157. Jeon, H., and Blacklow, S.C. 2005. Structure and physiologic function of the low-density lipoprotein receptor. *Annu Rev Biochem* 74:535-562.
 158. Plump, A.S., Smith, J.D., Hayek, T., Aalto-Setälä, K., Walsh, A., Verstuyft, J.G., Rubin, E.M., and Breslow, J.L. 1992. Severe hypercholesterolemia and atherosclerosis in apolipoprotein E-deficient mice created by homologous recombination in ES cells. *Cell* 71:343-353.
 159. Zhang, S.H., Reddick, R.L., Piedrahita, J.A., and Maeda, N. 1992. Spontaneous hypercholesterolemia and arterial lesions in mice lacking apolipoprotein E. *Science* 258:468-471.
 160. Nakashima, Y., Plump, A.S., Raines, E.W., Breslow, J.L., and Ross, R. 1994. ApoE-deficient mice develop lesions of all phases of atherosclerosis throughout the arterial tree. *Arterioscler Thromb* 14:133-140.

REFERENCES

161. Shi, W., Pei, H., Fischer, J.J., James, J.C., Angle, J.F., Matsumoto, A.H., Helm, G.A., and Sarembock, I.J. 2004. Neointimal formation in two apolipoprotein E-deficient mouse strains with different atherosclerosis susceptibility. *J Lipid Res* 45:2008-2014.
162. Komatsu, R., Ueda, M., Naruko, T., Kojima, A., and Becker, A.E. 1998. Neointimal tissue response at sites of coronary stenting in humans: macroscopic, histological, and immunohistochemical analyses. *Circulation* 98:224-233.
163. Libby, P. 2002. Inflammation in atherosclerosis. *Nature* 420:868-874.
164. Hansson, G.K., and Libby, P. 2006. The immune response in atherosclerosis: a double-edged sword. *Nat Rev Immunol* 6:508-519.
165. Schober, A., and Weber, C. 2005. Mechanisms of monocyte recruitment in vascular repair after injury. *Antioxid Redox Signal* 7:1249-1257.
166. Boisvert, W.A., Santiago, R., Curtiss, L.K., and Terkeltaub, R.A. 1998. A leukocyte homologue of the IL-8 receptor CXCR-2 mediates the accumulation of macrophages in atherosclerotic lesions of LDL receptor-deficient mice. *J Clin Invest* 101:353-363.
167. Potteaux, S., Combadiere, C., Esposito, B., Lecureuil, C., Ait-Oufella, H., Merval, R., Ardouin, P., Tedgui, A., and Mallat, Z. 2006. Role of bone marrow-derived CC-chemokine receptor 5 in the development of atherosclerosis of low-density lipoprotein receptor knockout mice. *Arterioscler Thromb Vasc Biol* 26:1858-1863.
168. Combadiere, C., Potteaux, S., Rodero, M., Simon, T., Pezard, A., Esposito, B., Merval, R., Proudfoot, A., Tedgui, A., and Mallat, Z. 2008. Combined inhibition of CCL2, CX3CR1, and CCR5 abrogates Ly6C(hi) and Ly6C(lo) monocytosis and almost abolishes atherosclerosis in hypercholesterolemic mice. *Circulation* 117:1649-1657.
169. Averill, L.E., Meagher, R.C., and Gerrity, R.G. 1989. Enhanced monocyte progenitor cell proliferation in bone marrow of hyperlipemic swine. *Am J Pathol* 135:369-377.
170. Feldman, D.L., Mogelesky, T.C., Liptak, B.F., and Gerrity, R.G. 1991. Leukocytosis in rabbits with diet-induced atherosclerosis. *Arterioscler Thromb* 11:985-994.
171. Murphy, A.J., Akhtari, M., Tolani, S., Pagler, T., Bijl, N., Kuo, C.L., Wang, M., Sanson, M., Abramowicz, S., Welch, C., et al. 2011. ApoE regulates hematopoietic stem cell proliferation, monocytosis, and monocyte accumulation in atherosclerotic lesions in mice. *J Clin Invest* 121:4138-4149.
172. Barron, H.V., Cannon, C.P., Murphy, S.A., Braunwald, E., and Gibson, C.M. 2000. Association between white blood cell count, epicardial blood flow, myocardial perfusion, and clinical outcomes in the setting of acute myocardial infarction: a thrombolysis in myocardial infarction 10 substudy. *Circulation* 102:2329-2334.
173. Cannon, C.P., McCabe, C.H., Wilcox, R.G., Bentley, J.H., and Braunwald, E. 2001. Association of white blood cell count with increased mortality in acute myocardial infarction and unstable angina pectoris. OPUS-TIMI 16 Investigators. *Am J Cardiol* 87:636-639, A610.
174. Chapman, C.M., Beilby, J.P., McQuillan, B.M., Thompson, P.L., and Hung, J. 2004. Monocyte count, but not C-reactive protein or interleukin-6, is an independent risk marker for subclinical carotid atherosclerosis. *Stroke* 35:1619-1624.

175. Nasir, K., Guallar, E., Navas-Acien, A., Criqui, M.H., and Lima, J.A. 2005. Relationship of monocyte count and peripheral arterial disease: results from the National Health and Nutrition Examination Survey 1999-2002. *Arterioscler Thromb Vasc Biol* 25:1966-1971.
176. Johnsen, S.H., Fosse, E., Joakimsen, O., Mathiesen, E.B., Stensland-Bugge, E., Njolstad, I., and Arnesen, E. 2005. Monocyte count is a predictor of novel plaque formation: a 7-year follow-up study of 2610 persons without carotid plaque at baseline the Tromso Study. *Stroke* 36:715-719.
177. Danenberg, H.D., Fishbein, I., Gao, J., Monkkonen, J., Reich, R., Gati, I., Moerman, E., and Golomb, G. 2002. Macrophage depletion by clodronate-containing liposomes reduces neointimal formation after balloon injury in rats and rabbits. *Circulation* 106:599-605.
178. Dutta, P., Courties, G., Wei, Y., Leuschner, F., Gorbato, R., Robbins, C.S., Iwamoto, Y., Thompson, B., Carlson, A.L., Heidt, T., et al. 2012. Myocardial infarction accelerates atherosclerosis. *Nature* 487:325-329.
179. Costa, M.A., and Simon, D.I. 2005. Molecular basis of restenosis and drug-eluting stents. *Circulation* 111:2257-2273.
180. Poteaux, S., Combadiere, C., Esposito, B., Casanova, S., Merval, R., Ardouin, P., Gao, J.L., Murphy, P.M., Tedgui, A., and Mallat, Z. 2005. Chemokine receptor CCR1 disruption in bone marrow cells enhances atherosclerotic lesion development and inflammation in mice. *Mol Med* 11:16-20.
181. Gautier, E.L., Jakubzick, C., and Randolph, G.J. 2009. Regulation of the migration and survival of monocyte subsets by chemokine receptors and its relevance to atherosclerosis. *Arterioscler Thromb Vasc Biol* 29:1412-1418.
182. Boring, L., Gosling, J., Cleary, M., and Charo, I.F. 1998. Decreased lesion formation in CCR2^{-/-} mice reveals a role for chemokines in the initiation of atherosclerosis. *Nature* 394:894-897.
183. Gu, L., Okada, Y., Clinton, S.K., Gerard, C., Sukhova, G.K., Libby, P., and Rollins, B.J. 1998. Absence of monocyte chemoattractant protein-1 reduces atherosclerosis in low density lipoprotein receptor-deficient mice. *Mol Cell* 2:275-281.
184. Dawson, T.C., Kuziel, W.A., Osahar, T.A., and Maeda, N. 1999. Absence of CC chemokine receptor-2 reduces atherosclerosis in apolipoprotein E-deficient mice. *Atherosclerosis* 143:205-211.
185. Serbina, N.V., and Pamer, E.G. 2006. Monocyte emigration from bone marrow during bacterial infection requires signals mediated by chemokine receptor CCR2. *Nat Immunol* 7:311-317.
186. Tsou, C.L., Peters, W., Si, Y., Slaymaker, S., Aslanian, A.M., Weisberg, S.P., Mack, M., and Charo, I.F. 2007. Critical roles for CCR2 and MCP-3 in monocyte mobilization from bone marrow and recruitment to inflammatory sites. *J Clin Invest* 117:902-909.
187. Weber, K.S., von Hundelshausen, P., Clark-Lewis, I., Weber, P.C., and Weber, C. 1999. Differential immobilization and hierarchical involvement of chemokines in monocyte arrest and transmigration on inflamed endothelium in shear flow. *Eur J Immunol* 29:700-712.
188. Schober, A., Zernecke, A., Liehn, E.A., von Hundelshausen, P., Knarren, S., Kuziel, W.A., and Weber, C. 2004. Crucial role of the CCL2/CCR2 axis in neointimal hyperplasia after arterial injury in hyperlipidemic mice involves early monocyte recruitment and CCL2 presentation on platelets. *Circ Res* 95:1125-1133.

REFERENCES

189. Geissmann, F., Jung, S., and Littman, D.R. 2003. Blood monocytes consist of two principal subsets with distinct migratory properties. *Immunity* 19:71-82.
190. Combadiere, C., Poteaux, S., Gao, J.L., Esposito, B., Casanova, S., Lee, E.J., Debre, P., Tedgui, A., Murphy, P.M., and Mallat, Z. 2003. Decreased atherosclerotic lesion formation in CX3CR1/apolipoprotein E double knockout mice. *Circulation* 107:1009-1016.
191. Landsman, L., Bar-On, L., Zernecke, A., Kim, K.W., Krauthgamer, R., Shagdarsuren, E., Lira, S.A., Weissman, I.L., Weber, C., and Jung, S. 2009. CX3CR1 is required for monocyte homeostasis and atherogenesis by promoting cell survival. *Blood* 113:963-972.
192. Schober, A., Manka, D., von Hundelshausen, P., Huo, Y., Hanrath, P., Sarembock, I.J., Ley, K., and Weber, C. 2002. Deposition of platelet RANTES triggering monocyte recruitment requires P-selectin and is involved in neointima formation after arterial injury. *Circulation* 106:1523-1529.
193. Zernecke, A., Liehn, E.A., Gao, J.L., Kuziel, W.A., Murphy, P.M., and Weber, C. 2006. Deficiency in CCR5 but not CCR1 protects against neointima formation in atherosclerosis-prone mice: involvement of IL-10. *Blood* 107:4240-4243.
194. Braunersreuther, V., Zernecke, A., Arnaud, C., Liehn, E.A., Steffens, S., Shagdarsuren, E., Bidzhekov, K., Burger, F., Pelli, G., Luckow, B., et al. 2007. Ccr5 but not Ccr1 deficiency reduces development of diet-induced atherosclerosis in mice. *Arterioscler Thromb Vasc Biol* 27:373-379.
195. Huo, Y., Weber, C., Forlow, S.B., Sperandio, M., Thatté, J., Mack, M., Jung, S., Littman, D.R., and Ley, K. 2001. The chemokine KC, but not monocyte chemoattractant protein-1, triggers monocyte arrest on early atherosclerotic endothelium. *J Clin Invest* 108:1307-1314.
196. Imai, T., Hieshima, K., Haskell, C., Baba, M., Nagira, M., Nishimura, M., Kakizaki, M., Takagi, S., Nomiyama, H., Schall, T.J., et al. 1997. Identification and molecular characterization of fractalkine receptor CX3CR1, which mediates both leukocyte migration and adhesion. *Cell* 91:521-530.
197. Fong, A.M., Robinson, L.A., Steeber, D.A., Tedder, T.F., Yoshie, O., Imai, T., and Patel, D.D. 1998. Fractalkine and CX3CR1 mediate a novel mechanism of leukocyte capture, firm adhesion, and activation under physiologic flow. *J Exp Med* 188:1413-1419.
198. Feig, J.E., Pineda-Torra, I., Sanson, M., Bradley, M.N., Vengrenyuk, Y., Bogunovic, D., Gautier, E.L., Rubinstein, D., Hong, C., Liu, J., et al. 2010. LXR promotes the maximal egress of monocyte-derived cells from mouse aortic plaques during atherosclerosis regression. *J Clin Invest* 120:4415-4424.
199. van Furth, R., and Cohn, Z.A. 1968. The origin and kinetics of mononuclear phagocytes. *J Exp Med* 128:415-435.
200. Wang, H., Beaty, N., Chen, S., Qi, C.F., Masiuk, M., Shin, D.M., and Morse, H.C., 3rd. 2012. The CXCR7 chemokine receptor promotes B-cell retention in the splenic marginal zone and serves as a sink for CXCL12. *Blood* 119:465-468.
201. Caligiuri, G. 2002. Protective immunity against atherosclerosis carried by B cells of hypercholesterolemic mice. *Journal of Clinical Investigation* 109:745-753.
202. Loetscher, M., Geiser, T., O'Reilly, T., Zwahlen, R., Baggiolini, M., and Moser, B. 1994. Cloning of a human seven-transmembrane domain receptor, LESTR, that is highly expressed in leukocytes. *J Biol Chem* 269:232-237.

203. Bleul, C.C., Fuhlbrigge, R.C., Casasnovas, J.M., Aiuti, A., and Springer, T.A. 1996. A highly efficacious lymphocyte chemoattractant, stromal cell-derived factor 1 (SDF-1). *J Exp Med* 184:1101-1109.
204. Smith, J.D., Trogan, E., Ginsberg, M., Grigaux, C., Tian, J., and Miyata, M. 1995. Decreased atherosclerosis in mice deficient in both macrophage colony-stimulating factor (op) and apolipoprotein E. *Proc Natl Acad Sci U S A* 92:8264-8268.
205. Potteaux, S., Gautier, E.L., Hutchison, S.B., van Rooijen, N., Rader, D.J., Thomas, M.J., Sorci-Thomas, M.G., and Randolph, G.J. 2011. Suppressed monocyte recruitment drives macrophage removal from atherosclerotic plaques of Apoe^{-/-} mice during disease regression. *J Clin Invest* 121:2025-2036.
206. Akhtar, S., Gremse, F., Kiessling, F., Weber, C., and Schober, A. 2013. CXCL12 Promotes the Stabilization of Atherosclerotic Lesions Mediated by Smooth Muscle Progenitor Cells in Apoe-Deficient Mice. *Arterioscler Thromb Vasc Biol* 33:679-686.
207. Kucia, M., Jankowski, K., Reca, R., Wysoczynski, M., Bandura, L., Allendorf, D.J., Zhang, J., Ratajczak, J., and Ratajczak, M.Z. 2004. CXCR4-SDF-1 signalling, locomotion, chemotaxis and adhesion. *J Mol Histol* 35:233-245.
208. Kwiterovich, P.O., Jr. 2000. The metabolic pathways of high-density lipoprotein, low-density lipoprotein, and triglycerides: a current review. *Am J Cardiol* 86:5L-10L.
209. Goedeke, L., and Fernandez-Hernando, C. 2011. Regulation of cholesterol homeostasis. *Cell Mol Life Sci* 69:915-930.
210. Clinton, S.K., Underwood, R., Hayes, L., Sherman, M.L., Kufe, D.W., and Libby, P. 1992. Macrophage colony-stimulating factor gene expression in vascular cells and in experimental and human atherosclerosis. *Am J Pathol* 140:301-316.
211. McKenney, J.M. 2001. Lipid management: tools for getting to the goal. *Am J Manag Care* 7:S299-306.
212. Malinowski, J.M. 1998. Atorvastatin: a hydroxymethylglutaryl-coenzyme A reductase inhibitor. *Am J Health Syst Pharm* 55:2253-2267; quiz 2302-2253.
213. Asztalos, B.F., Horvath, K.V., McNamara, J.R., Roheim, P.S., Rubinstein, J.J., and Schaefer, E.J. 2002. Comparing the effects of five different statins on the HDL subpopulation profiles of coronary heart disease patients. *Atherosclerosis* 164:361-369.
214. Baliga, R.R. 2012. HDL-cholesterol: perfection is the enemy of good? *Med Clin North Am* 96:27-37.
215. Lennernas, H., and Fager, G. 1997. Pharmacodynamics and pharmacokinetics of the HMG-CoA reductase inhibitors. Similarities and differences. *Clin Pharmacokinet* 32:403-425.
216. Williams, R.R., Hopkins, P.N., Hunt, S.C., Wu, L.L., Hasstedt, S.J., Lalouel, J.M., Ash, K.O., Stults, B.M., and Kuida, H. 1990. Population-based frequency of dyslipidemia syndromes in coronary-prone families in Utah. *Arch Intern Med* 150:582-588.
217. Venkatesan, S., Cullen, P., Pacy, P., Halliday, D., and Scott, J. 1993. Stable isotopes show a direct relation between VLDL apoB overproduction and serum triglyceride levels and indicate a metabolically and biochemically coherent basis for familial combined hyperlipidemia. *Arteriosclerosis and Thrombosis* 13:1110-1118.

REFERENCES

218. Lusis, A.J., Fogelman, A.M., and Fonarow, G.C. 2004. Genetic basis of atherosclerosis: part I: new genes and pathways. *Circulation* 110:1868-1873.
219. Krause, B.R., and Hartman, A.D. 1984. Adipose tissue and cholesterol metabolism. *J Lipid Res* 25:97-110.
220. Schreibman, P.H., and Dell, R.B. 1975. Human adipocyte cholesterol. Concentration, localization, synthesis, and turnover. *J Clin Invest* 55:986-993.
221. Prattes, S., Horl, G., Hammer, A., Blaschitz, A., Graier, W.F., Sattler, W., Zechner, R., and Steyrer, E. 2000. Intracellular distribution and mobilization of unesterified cholesterol in adipocytes: triglyceride droplets are surrounded by cholesterol-rich ER-like surface layer structures. *J Cell Sci* 113 (Pt 17):2977-2989.
222. Chung, S., Sawyer, J.K., Gebre, A.K., Maeda, N., and Parks, J.S. 2011. Adipose Tissue ATP Binding Cassette Transporter A1 Contributes to High-Density Lipoprotein Biogenesis In Vivo. *Circulation* 124:1663-1672.
223. Brown, M.S., and Goldstein, J.L. 1986. A receptor-mediated pathway for cholesterol homeostasis. *Science* 232:34-47.
224. Huang, Z.H., Minshall, R.D., and Mazzone, T. 2009. Mechanism for endogenously expressed ApoE modulation of adipocyte very low density lipoprotein metabolism: role in endocytic and lipase-mediated metabolic pathways. *J Biol Chem* 284:31512-31522.
225. Takahashi, S., Suzuki, J., Kohno, M., Oida, K., Tamai, T., Miyabo, S., Yamamoto, T., and Nakai, T. 1995. Enhancement of the binding of triglyceride-rich lipoproteins to the very low density lipoprotein receptor by apolipoprotein E and lipoprotein lipase. *J Biol Chem* 270:15747-15754.
226. Goudriaan, J.R., Tacke, P.J., Dahlmans, V.E., Gijbels, M.J., van Dijk, K.W., Havekes, L.M., and Jong, M.C. 2001. Protection from obesity in mice lacking the VLDL receptor. *Arterioscler Thromb Vasc Biol* 21:1488-1493.
227. Goudriaan, J.R., Espirito Santo, S.M., Voshol, P.J., Teusink, B., van Dijk, K.W., van Vlijmen, B.J., Romijn, J.A., Havekes, L.M., and Rensen, P.C. 2004. The VLDL receptor plays a major role in chylomicron metabolism by enhancing LPL-mediated triglyceride hydrolysis. *J Lipid Res* 45:1475-1481.
228. Takahashi, S., Sakai, J., Fujino, T., Hattori, H., Zenimaru, Y., Suzuki, J., Miyamori, I., and Yamamoto, T.T. 2004. The very low-density lipoprotein (VLDL) receptor: characterization and functions as a peripheral lipoprotein receptor. *J Atheroscler Thromb* 11:200-208.
229. Tao, H., Aakula, S., Abumrad, N.N., and Hajri, T. 2010. Peroxisome proliferator-activated receptor-gamma regulates the expression and function of very-low-density lipoprotein receptor. *Am J Physiol Endocrinol Metab* 298:E68-79.
230. Go, G.W., and Mani, A. 2012. Low-density lipoprotein receptor (LDLR) family orchestrates cholesterol homeostasis. *Yale J Biol Med* 85:19-28.
231. Wu, J.H., Peppel, K., Nelson, C.D., Lin, F.T., Kohout, T.A., Miller, W.E., Exum, S.T., and Freedman, N.J. 2003. The adaptor protein beta-arrestin2 enhances endocytosis of the low density lipoprotein receptor. *J Biol Chem* 278:44238-44245.
232. Kalatskaya, I., Berchiche, Y.A., Gravel, S., Limberg, B.J., Rosenbaum, J.S., and Heveker, N. 2009. AMD3100 is a CXCR7 ligand with allosteric agonist properties. *Mol Pharmacol* 75:1240-1247.

-
233. Luttrell, L.M., and Lefkowitz, R.J. 2002. The role of beta-arrestins in the termination and transduction of G-protein-coupled receptor signals. *J Cell Sci* 115:455-465.
234. Luker, K.E., Gupta, M., Steele, J.M., Foerster, B.R., and Luker, G.D. 2009. Imaging ligand-dependent activation of CXCR7. *Neoplasia* 11:1022-1035.
235. Gambaryan, N., Perros, F., Montani, D., Cohen-Kaminsky, S., Mazmanian, M., Renaud, J.F., Simonneau, G., Lombet, A., and Humbert, M. 2011. Targeting of c-kit+ haematopoietic progenitor cells prevents hypoxic pulmonary hypertension. *Eur Respir J* 37:1392-1399.
236. Uto-Konomi, A., McKibben, B., Wirtz, J., Sato, Y., Takano, A., Nanki, T., and Suzuki, S. 2013. CXCR7 agonists inhibit the function of CXCL12 by down-regulation of CXCR4. *Biochem Biophys Res Commun* 431:772-776.
237. Wijtmans, M., Maussang, D., Sirici, F., Scholten, D.J., Canals, M., Mujic-Delic, A., Chong, M., Chatalic, K.L., Custers, H., Janssen, E., et al. 2012. Synthesis, modeling and functional activity of substituted styrene-amides as small-molecule CXCR7 agonists. *Eur J Med Chem* 51:184-192.

7. ACKNOWLEDGEMENT

At the end of my thesis, I could not help recalling all those people who helped me to make this thesis possible. It is my greatest pleasure to express my sincerest appreciation to all of them.

I firstly offer my foremost and sincerest gratitude to my esteemed supervisor, Professor Andreas Schober. This thesis would not have been possible without his guidance, support and unflagging encouragement. Professor Andreas Schober provided me this extraordinary opportunity/privilege to start my Ph.D in IMCAR and supported me to proceed to the doctoral projects and thesis with patience, knowledge, and insightful ideas. His enthusiasm, vigorous, and knowledgeable will ever inspire me in the future research career.

I gratefully acknowledge Professor Christine Weber for the academic support and the facilities provided to operate the research work.

My thanks are due to Dr. Rory Koenen for conducting my second-round interview before entering into IMCAR and for useful guidance and instructions.

Dr. Elisa Liehn gave me useful comments on mouse operation during training and examination. She deserves my sincere appreciation.

I would like to thank Professor Marc van Zandvoort for his critical advises and comments

I take this opportunity to say heartfelt thanks to Dr. Remco T.A. Megens, who helped me performing TPLSM experiment and provided me experimental hands-on training.

I am thankful to Dr. Heidi Noels for her helpful suggestions and insight comments.

I would like to thank Professor Jürgen Bernhagen and Dr. Nikolaus L. Schlaich as my examiners and their valuable comments and suggestions on my thesis.

I appreciate the support of the core facility “Two-photon image” of IZKF and the financial support from the Deutsche Forschungsgemeinschaft (DFG FOR809, WE1913/11-2, IRTG1508-EuCAR) and the Interdisciplinary Center for Clinical Research within the Faculty of Medicine at the RWTH Aachen University.

The research and thesis would not come to a successful and smooth completion without excellent technical assistance, efficient organization, and kindly help.

I would like express my gratitude to Anni Mayer for providing assistance with various problems all the time even outside the lab.

Lots of thanks also to Sandra Knarren for kindly helping me and making the lab run smoothly and safely.

My special and deep gratitude is due to Kathrin Heyll, Anna, Thiemann, Yuan Kong, Yvonne Jansen and Judit Corbalan Campos for their excellent assistance and friendly help.

I am also highly indebted to Melanie Garbe and Stephanie, who taught me a lot about mouse surgical techniques, which helped me a lot.

I would like to express my deepest gratitude to Roya Soltan, your contagious laughing made the lab atmosphere more relaxed.

Leon Decker and Sabine Winkler deserve a lot of appreciation not only because of their kindly help and suggestions, but also for the arrangement of several things of PCR and cell culture in the lab.

The IMCAR collects a group of talented, enthusiastic and friendly colleagues, forming a stimulating and fun-filled environment. It was an enjoyable experience to learn and grow here.

I would like to acknowledge Shamina Akhtar, who helped with my experiments whenever required and provided critical tips for my English presentations and experiments. The numerous discussions with her helped me to improve my knowledge.

My sincere appreciation also goes to Mengyu Zhu, who helped me do the *in vitro* assay of adipocytes for the revision.

I am deeply grateful to Yuanyuan Wei, who gave me a lot of useful suggestions on my experiments and life, kindness friendship and support.

My sincere appreciation also goes to Pallavi Subramanian, Maliheh Nazari-Jahantigh, Zhou Zhe and Karim Hamesch for their suggestions and help in the lab.

I also thankful to Seena Koyadan and Zhuojun Wu, who helped me perform the TPLSM experiment. Wu also really gave me a big hand in life.

I would like to thank Wendy Theelen for product and mice ordering.

ACKNOWLEDGEMENT

Lots of thanks to Santosh Vijayan for giving me suggestions on the thesis writing and job hunting.

To my dear colleagues, Baixue Zhou, Pathricia Tilstam, Adelina Curaj, Sakine Simsekyilmaz, Lukas Pawig, Asare Yaw, Franziska Cordes, Martin Schmitt, I am grateful for your generous comments, support and advices.

I would like to thank all my friends.

I am very much indebted to my family for their unconditional love and constant support.

8. CURRICULUM VITAE

PERSONAL INFORMATION

Name	Xiaofeng Li
Date of Birth	28 th May, 1981
Place of birth	Henan, China
Nationality	Chinese

ACADEMIC EDUCATION

Nov 2008 – Now	Ph.D. in molecular cardiovascular research. Institute for Molecular Cardiovascular Research (IMCAR) of the RWTH Aachen University, Germany.
Sept 2005 - Jun 2008	Masters in biochemistry and molecular Biology. Huazhong Agricultural University, Wuhan, China.
Sept 2001 - Jun 2005	Bachelors in biological technology. Henan Agricultural University, Zhengzhou, China.

PUBLICATIONS

Li X, Penfold ME, Koenen RR, Thiemann A, Heyll K, Akhtar S, Koyadan S, Wu Z, van Zandvoort M, Weber C, Schober A. Activation of CXCR7 limits atherosclerosis and improves hyperlipidemia by increasing cholesterol storage in adipose tissue. *Circulation*, 2013 (under revision).

Li X, Lei T, Xia T, Chen X, Feng S, Chen H, Chen Z, Peng Y, Yang Z. Molecular characterization, chromosomal and expression patterns of three aquaglyceroporins (AQP3, 7, 9) from pig. *Comp Biochem Physiol B Biochem Mol Biol* 149: 468-76 (2008).

Hamesch K, Subramanian P, **Li X**, Dembowsky K, Chevalier E, Weber C, Schober A. The CXCR4 antagonist POL5551 is equally effective as sirolimus in reducing neointima formation without impairing re-endothelialisation. *Thromb Haemost.*107(2):356-368 (2012).

Subramanian P, Karshovska E, Reinhard P, Megens RT, Zhou Z, Akhtar S, Schumann U, **Li X**, van Zandvoort M, Ludin C, Weber C, Schober A. Lysophosphatidic acid receptors LPA1 and LPA3 promote CXCL12-mediated smooth muscle progenitor cell recruitment in neointima formation. *Circ Res* 107: 96-105. (2010).

CONFERENCES

- Jun 2010 Oral presentation
IVBM (The International Vascular Biology Meeting, Los Angeles, America)
Title: Protective role of the CXCR7 ligand CCX771 in neointima formation after vascular injury and atherosclerosis in mice
- Jul 2010 Poster presentation
FCVB (Frontiers in Cardiovascular Biology, Berlin, Germany)
Title: The CXCR7 ligand CCX771 reduces neointima formation after vascular injury and atherosclerosis in *Apoe*^{-/-} mice
- Oct 2011 Poster presentation
ESM (the European society for microcirculation, Munich, Germany)
Title: The CXCR7 ligand CCX771 reduces neointima formation after vascular injury and atherosclerosis in *Apoe*^{-/-} mice
- Dec 2012 Poster presentation
5th German Atherosclerosis Congress (Munich, Germany)
Title: Activation of Cxcr7 improves hyperlipidemia by increasing cholesterol storage in adipose tissue and limits atherosclerosis